INVESTIGATION OF STRENGHTHENING TECHNIQUES USING PSEUDO-DYNAMIC TESTING

A THESIS SUBMITTED TO
THE GRADUATE SCHOOL OF NATURAL AND APPLIED SCIENCES
OF
MIDDLE EAST TECHNICAL UNIVERSITY

BY

EFE GÖKÇE KURT

IN PARTIAL FULFILLMENT OF THE REQUIREMENTS
FOR
THE DEGREE OF MASTER OF SCIENCE
IN
CIVIL ENGINEERING

JUNE 2010

Approval of the thesis:

INVESTIGATION OF STRENGHTHENING TECHNIQUES USING PSEUDO-DYNAMIC TESTING

submitted by **EFE GÖKÇE KURT** in partial fulfillment of the requirements for the degree of **Master of Science in Civil Engineering Department, Middle East Technical University** by,

Prof. Dr. Canan Özgen
Dean, Graduate School of **Natural and Applied Sciences** _____

Prof. Dr. Güney Özcebe
Head of Department, **Civil Engineering** _____

Prof. Dr. Güney Özcebe
Supervisor, **Civil Engineering Dept., METU** _____

Examining Committee Members:

Prof. Dr. Uğur Ersoy
Civil Engineering Dept., BU _____

Prof. Dr. Güney Özcebe
Civil Engineering Dept., METU _____

Prof. Dr. Haluk Sucuoğlu
Civil Engineering Dept., METU _____

Assoc. Prof. Dr. Barış Binici
Civil Engineering Dept., METU _____

Assoc. Prof. Dr. Erdem Canbay
Civil Engineering Dept., METU _____

Date: 17.06.2010

I hereby declare that all information in this document has been obtained and presented in accordance with academic rules and ethical conduct. I also declare that, as required by these rules and conduct, I have fully cited and referenced all material and results that are not original to this work.

Name, Last name : Efe Gökçe Kurt

Signature :

ABSTRACT

INVESTIGATION OF STRENGHTHENING TECHNIQUES USING PSEUDO-DYNAMIC TESTING

Kurt, Efe Gökçe

M.S., Department of Civil Engineering

Supervisor: Prof. Dr. Güney Özcebe

June 2010, 120 pages

Pseudo-dynamic testing was employed to observe the seismic performance of three different retrofit methods on two story three bay reinforced concrete frame structures. The three test frames have hollow clay tile (HCT) infills in the central bay. All of the test frames represent the seismic deficiencies of the Turkish construction practice such as use of plain reinforcing bars, low strength concrete and insufficient confining steel. Two non-invasive and occupant friendly retrofit schemes suggested in the Turkish Earthquake Code, namely use of Fiber Reinforced Polymers and precast concrete panels integrated on the HCT infills and traditional approach of adding concrete infill wall were employed. Specimens were subjected to three different scale levels of North-South component of Duzce ground motion. Reference specimen experienced severe damage at 100% scale level and reached collapse stage due to the loss of integrity of the infill wall and significant damage on the boundary columns. The retrofitted test structures were able to survive the highest level 140% Duzce ground motion. Test results confirmed the success of the retrofit methods for simulated earthquake loads.

Keywords: Pseudo-Dynamic Testing, Seismic Strengthening, Hollow Clay Tile Infills, Fiber Reinforced Polymers, Precast Concrete Panels, Concrete Infill Walls

ÖZ

DİNAMİK-BENZERİ DENEYLERLE YAPI GÜÇLENDİRME TEKNİKLERİNİN İRDELENMESİ

Kurt, Efe Gökçe

Yüksek Lisans, İnşaat Mühendisliği Bölümü

Tez Yöneticisi: Prof. Dr. Güney Özcebe

Haziran 2010, 120 sayfa

Üç farklı güçlendirme yönteminin iki katlı üç açıklıklı betonarme çerçeveler üzerindeki sismik performansı dinamik-benzeri deney yöntemi uygulanarak gözlemlenmiştir. Üç deney elemanın orta açıklığında delikli tuğla duvar bulunmaktadır. Bütün deney elemanları Türkiye'deki inşaat uygulamalarında bulunan düz donatı, düşük beton dayanımı ve yetersiz sargı donatısı gibi sismik yetersizlikler göstermektedir. Türk deprem kodunda bulunan bina sakinleri için uygun olan delikli tuğla duvarlara monte edilen Lifli Polimerler ve ön üretimli beton paneller ile geleneksel yaklaşım olan betonarme duvar yöntemleri uygulanmıştır. Deney elemanları Duzce yer hareketinin Kuzey-Güney bileşenin üç farklı ölçeğine maruz bırakılmıştır. Referans deney elemanı %100 ölçekte ağır hasar görmüş, tuğla duvarın bütünlüğünü koruyamamasından ve tuğla duvarı çevreleyen kolonların ciddi hasar görmesinden dolayı çökme aşamasına gelmiştir. Güçlendirilen çerçeveler en yüksek seviye olan %140 Duzce yer hareketinde sağ kalmayı başarabilmiştir. Deney sonuçları, uygulanan deprem yükleri için güçlendirme yöntemlerinin başarısını onaylamıştır.

Anahtar Kelimeler: Dinamik-Benzeri Deney, Sismik Güçlendirme, Delikli Tuğla Duvarlar, Lifli Polimerler, Ön Üretimli Beton Paneller, Betonarme Dolgu Duvar

To my family.

ACKNOWLEDGEMENTS

This thesis is the outcome of over 5000 laboratory man-hours that were invested in order to construct large-scale experimental setups at Structural Mechanics Laboratory at Middle East Technical University. All this work has been completed under the supervision of Prof. Dr. Güney Özcebe. To me, he is more than a supervisor. His strong personality and reliable suggestions has affected the way of my life.

This research would have been impossible without the aid of Assoc. Prof. Dr. Erdem Canbay. His support and patience brought me to the end of all of the challenging tasks.

I am also grateful to Assoc. Prof. Dr. Barış Binici. Through his guidance and exceptional teaching abilities, I have become a much more confident and technically sound engineer.

I would also like to thank Asst. Prof. Dr. Özgür Kurç for helping in experiments and data processing.

Many thanks to İrfan Bahadır Önder for being with me not only at good times but also at hard and exhausting times.

I am also grateful to my colleagues M. Emrah Eryaşar, M. Emre Özkök, R. Tarık Oksay, Arda Erdem, Can Karageyik, A. Güney Özcebe, Engin B. Oğuz and Alper Aldemir.

I owe special thanks to METU Structural Mechanics Laboratory staff; Murat Demirel, Hasan Metin, Osman Keskin and Barış Esen.

The financial supports from the Scientific and Technical Research Council of Turkey (TUBITAK – 106M451) is gratefully acknowledged.

Last but not lesat, I thank my father, my mother and my brother, Gökmen Kurt, for their endless support and love. Thanks for giving me the best prize I will ever have: the chance of living in this world. However far away and however long I stay, my heart will always be with them.

TABLE OF CONTENTS

LIST OF TABLES

TABLES

LIST OF FIGURES

FIGURES

CHAPTER 1

INTRODUCTION

1.1. GENERAL

The experimental investigation on the dynamic behavior of structures under earthquake loading is a challenging task. The experimental research in earthquake engineering has been mostly focused on quasi-static testing of components or sub-assemblies. In these tests, specimens are generally subjected to slowly changing prescribed forces or deformations applied by hydraulic actuators. Due to slow application of prescribed monotonically increasing deformations that represent the seismic demand, inertial forces within the structure cannot be taken into account. The purpose with quasi-static cyclic testing is to observe the behavior of structural elements when they are subjected to loading and unloading cycles irrespective of actual earthquake loading.

Experiments conducted by the use of shaking tables or pseudo-dynamic testing approach are more realistic for earthquake loading simulations. Shaking table tests are capable of accounting for the inertial effects, time and frequency content of ground motion, as it is possible to employ actual ground motions in a dynamic manner. However, shaking tables are extremely expensive due to their technology and maintenance. Furthermore, size and mass limitations of shaking tables render it difficult to test multistory large scale structures.

In pseudo-dynamic testing method, part of the structural properties (mass, damping) or response is mathematically modeled and the rest of the structure which cannot be mathematically modeled is physically tested in parallel with computations. Pseudo- dynamic testing is performed using well-established step by step time integration methods. At a given time step, deformations imposed by a specified ground motion are applied on the test specimen and resisting forces are measured. Using actuator feedback forces and proceeding in the computational

time interval, new displacements are computed from the discrete parameter model. The main advantages in pseudo-dynamic testing method are including the earthquake demand in quasi-static tests, slow application of forces (allows observing the damage at a given time during the ground motion) and testing larger scale specimens. Downsides of the pseudo-dynamic testing are exclusion of time dependent effects (since velocity of actuators is neglected in the computations) and measurement errors that can corrupt the response. Advancements on mitigation of measurement errors, feasibility of quasi-static actuators, and attractive features of pseudo-dynamic testing as it incorporates seismic demand have led to its widespread use worldwide in the last ten years. In addition, its verification with shaking table tests proved its success in simulating earthquake response.

Seismic assessment, evaluation and rehabilitation procedures have gained increasing popularity in order to mitigate the seismic damage expected as a result of an earthquake in Marmara Region of Turkey. For this purpose, a number of studies on seismic evaluation and strengthening have been conducted in the Middle East Technical University Structural Mechanics Laboratory in the last thirty five years. Addition of reinforced concrete infill walls to an existing deficient structural system has been tested and applied successfully in the past years all over the country. Recently, two new non-invasive strengthening techniques, namely fiber reinforced polymers (FRP) and precast panels (PCP) applications were developed at METU Structural Mechanics Laboratory. Effectiveness and feasibility of these methods have been comparatively studied in some analytical studies. However, direct comparisons of the seismic behavior of retrofitted structures employing different rehabilitation techniques have not been presented in the literature yet.

Aforementioned rehabilitation procedures have been tested using quasi-static procedures disregarding the actual earthquake demand on the structures and results on strength and ductility enhancements are reported. Turkish Earthquake Code 2007 has a section on performance based seismic assessment and rehabilitation procedures. This requires not only the knowledge of the structural strength (before and after rehabilitation) but also the accurate prediction of deformations and damage levels as a result of an expected uncertain ground motion. Hence, reliable experiments that can simulate the seismic demand are

deemed essential to verify the effectiveness of the rehabilitation and assessment procedures.

1.2. OBJECT AND SCOPE OF THE STUDY

Seismic strengthening and repair of damaged structures is one of the top priority topics of countries prone to earthquakes. Intensive researches have been conducted on this topic. Structural Mechanics Laboratory at Middle East Technical University (METU) is the pioneer institution on research and application of this topic in Turkey.

Seismic strengthening of deficient and occupied buildings is among the most important problems in Turkey. The traditional approach of adding reinforced concrete infill walls is the most commonly chosen alternative for current seismic retrofit applications in Turkey. However, the construction work involved for this retrofit scheme is extremely demanding. Furthermore, it results in lengthened retrofit time and necessitates relocating the occupants. 75,000 buildings in Istanbul are estimated as collapse or near collapse at a possible earthquake in Marmara Region of Turkey (JICA, IBB, 2002). Strengthening of this huge building stock, including Istanbul and other metropolis cities, is a challenging engineering problem and is only possible by rapid, ease and economic solutions. Evacuating numerous buildings and relocating occupants with owned belongings to other residences is an unpractical solution. In addition, this will cause a chaotic and an uneconomic situation.

Retrofitting with new generation materials become possible by extensive experimental and analytical researches (Ehsani et al., 1998; Ozcebe et al., 2003; Frosch et al., 2003; Tankut et al., 2005; Binici et al., 2007). Strengthening the hollow clay infill walls of existing concrete structural systems to resist earthquake loadings has been aimed. Two strengthening approaches have been adopted:

- Strengthening with carbon fiber reinforced polymers (Ehsani et al., 1999; Ozcebe et. al, 2003).

- Strengthening with high strength precast concrete panels (Tankut et. al, 2005).

Integration of the two aforementioned strengthening techniques to hallow clay infill walls is satisfied in order to enhance the insufficient lateral rigidity and

strength of the structures. The aim is to prevent collapse of the concrete structures under a severe earthquake.

Research on these non-invasive strengthening techniques has been conducted with rational use of the existing resources. Although studies with quasi-static methods have been worldwide used at the second time period of 20th century, it does not necessarily answer modern earthquake engineering demands. Despite strength and displacement capacities of the structures may be obtained by quasi-static experiments, it is not sufficiently possible to obtain structural system demands under an implemented ground motion. As structural demands under earthquake loading is not provided by a quasi-static experiment, engineering approach remains on the conservative side. However, it is vital to use limited resources in a rational and an economic way.

In this study the aim is to explore the "true" seismic performance of aforementioned retrofit methods by pseudo-dynamic testing and critically examine their possible use. Four ½ scaled three bay-two story concrete frames representing the deficiencies as low concrete compressive strength, insufficient lateral reinforcement, weak beam-column joints, use of plain bars as longitudinal reinforcement, in Turkish building stock are constructed. A reference frame without strengthening is tested with only hollow clay brick infill and plaster. The other three experiments are conducted as:

i) Fiber reinforced polymers retrofitted specimen

ii) Precast concrete panels retrofitted specimen

iii) Reinforced concrete infill wall retrofitted specimen

Reinforced concrete infill wall retrofitted specimen may be considered as a representative upper most strengthening level for existing concrete structures and it can be treated as another 'reference' specimen.

NS component of the 7.1 moment magnitude Duzce ground motion was employed for the tests. Tests were conducted by applying the Duzce motion in three increments (i.e. 50%, 100% and 140%) by scaling the acceleration record. Such a scaling was employed based on the preliminary dynamic analysis of the reference frame to investigate the response at three different hazard levels applied simultaneously.

CHAPTER 2

PSEUDO-DYNAMIC (PsD) TESTING

In this chapter, information about Pseudo-dynamic testing technique and its background are presented briefly. In the literature, there are hundreds of experiments reported in this area. This chapter, however, summarizes the most important contributions.

2.1. PSEUDO-DYNAMIC METHOD

Pseudo-dynamic testing technique is as an on-line computer controlled procedure that combines the simplicity of quasi-static testing with the reliability of shaking table tests. PsD method emerged as an alternative to shaking table tests some thirty years ago (Takanashi et al., 1975). In this testing method, part of the structural properties (mass, damping) or response (sub-structure whose response is known to remain elastic) is mathematically modeled and the rest of the structure which cannot be mathematically modeled is physically tested in parallel with computations. Pseudo-dynamic testing is performed using well-established step by step time integration methods. At a given time step, deformations imposed by a specified ground motion are applied on the test specimen and resisting forces are measured. Using actuator feedback forces and proceeding in the computational time interval, new displacements are computed from the discrete parameter model.

Displacement computations are based on the actually measured state of damage in the test specimen for the reliability of the test. Mass, damping and the ground motion properties are assumed and restoring forces are obtained directly from the experimental specimen. Pre-calibrated load cells are used to measure the restoring forces as in a quasi-static experiment. These measured forces are then used in the numerical integration of the governing second order differential

equations of motion of the test specimen to implement nodal displacement history for further steps.

The time-discretized equation of motion for time step "i" may be simply written as:

$$M \cdot a_i + C \cdot v_i + R_i + K \cdot d_i = - M \cdot a_{gi} \qquad \textit{(Eq. 2.1)}$$

where;

M: Mass matrix

C: Viscous damping matrix

R_i: Nodal restoring forces at time "i"

K: Geometric stiffness matrix

a_i, v_i, d_i: Nodal accelerations, velocities and displacements, respectively, at time i

a_{gi}: Ground acceleration at time "i"

Equation of motion (Eq. 2.1) is solved numerically in a stepwise manner where R_i is the restoring force measured from the test specimen. Result of the numerical integration is the displacement which shall be applied to the specimen at each node by servo controlled actuators. Both implicit and explicit integration algorithms may be employed for solving equation of motion during a PsD test. Explicit methods use the state of the structure at the beginning of each step to assess the response of the structure at the end of that step. Implicit methods compute the response of the test specimen by using the knowledge of the response at the target displacement. The displacement is affected by other response parameters resulted at the end of the given step. Advantage of using implicit algorithms is improved stability conditions and use of larger integration time steps. On the other hand, explicit methods are easier to implement and preferred when stability conditions are satisfied for the test specimen.

Pseudo-dynamic testing may be divided into two sections: calculation and loading sections. Calculation section contains the required software and hardware to solve the equation of motion of the system and loading section includes

application of the calculated displacements by using servo controlled actuators. Figure 2.1 summarizes the calculation and loading sections.

Pseudo-dynamic method may be compared with two testing methods: quasi-static test technique and shake table tests. There are some advantages of pseudo-dynamic method over these two testing techniques (Mahin *et* al, 1989) . PsD method overcomes the problem, which is observed in a quasi-static test, of introducing the imposed response of large scale specimens during an actual earthquake. Moreover, PsD method is applicable for large and heavy specimens which are not suitable for shake table test. Besides, PsD experiments are more prone to observe the damage states of the test specimen when compared to a shake table test as the test is conducted slower and step by step manner. Nevertheless, PsD method has also some drawbacks as all testing methods possess. According to the study conducted by Mahin *et* al. (1989):

"Like all experimental techniques, the pseudodynamic method has inherent limitation and errors and these limitations must be fully recognized in developing a structural test program. In particular, the need for high performance displacement control equipment and measurement instrumentation must be taken into account."

Downsides of the pseudo-dynamic testing are exclusion of time dependent effects (since velocity of actuators is neglected in the computations and measurement errors that can corrupt the observed response. Control of the errors during a PsD test should be satisfied, if not, non-divergence of the calculation algorithm may occur and thus leads to critical issues like unexpected large forces applied by the actuators during a PsD test.

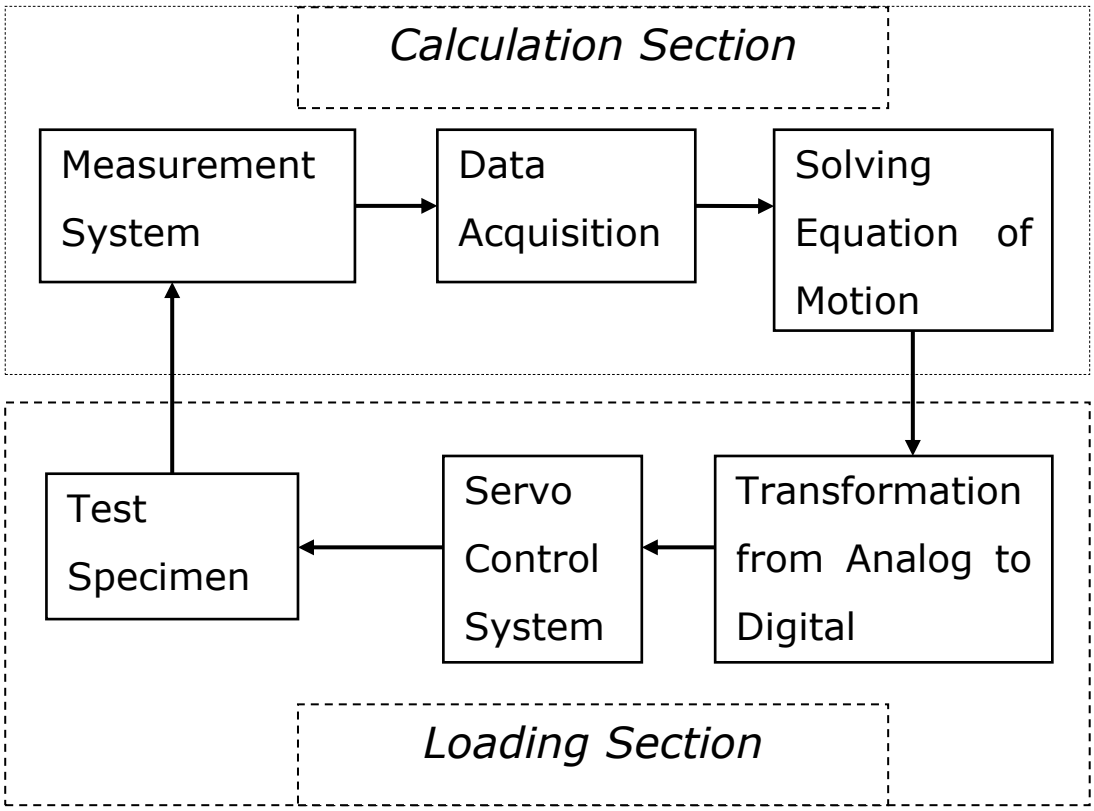

Figure 2.1 Loading and calculation sections of PsD testing

2.2. BACKGROUND

Takanashi et al.were the pioneers of the pseudo-dynamic testing technique. They have conducted first pseudo-dynamic experiments in Japan by the mid 1970s. Following these initial researches, other Japanese researchers have executed pseudo-dynamic experiments . In pseudo-dynamic testing technique, results of the experiments can be very sensitive to measurement and control errors. This drawback made several researchers to focus on the issue of error analysis.

Mahin and Shing (1985) published a report representing the pseudo-dynamic testing technique step by step. They verified the practicability of pseudo-

dynamic testing technique by testing a simple cantilever column having single degree of freedom. They later tested a strengthened steel structure, which was previously investigated on a shake table, by using pseudo-dynamic testing. The tested structure was a 5/48 scale prototype of an open sea platform. This study showed that pseudo-dynamic testing could be carried out in structural dynamics by well defined analytical techniques combined with quasi-static loadings. Both numerical and experimental errors affected test result. It was stated that experimental errors might accumulate because of using step by step integration. Importance of using precise experimental equipments and proper acquisition setup was emphasized.

Nakashima (1985a) investigated the relation between the stability of the structure and time interval integration. It was stated that integration time interval came into question when explicit integration technique was conducted. It was mentioned that choosing the right time interval was the fundamental condition for both stability and precise solution.

Nakashima (1985b) studied the effect of integration time step over the displacement, velocity and acceleration of the structure. He made some suggestions to minimize the errors in experiments.

Aktan (1986) conducted an experiment of a 1/5 scaled seven storey concrete frame by using pseudo-dynamic testing technique. He proposed a control procedure benefiting from previous experiences and problems. He used this control procedure during the experiment and investigated the test results. The control procedure presented in this study provided versatile and accurate means of testing large scale structures under simulated earthquake loadings through the use of pseudo-dynamic testing.

Shing and Mahin (1987) investigated the accumulation of experimental errors and their end results. Experimental errors were divided into two: systematic errors and accidental errors. It was concluded that systematic errors were more critical than accidental ones. Some systematic errors might cause energy increase or energy consumption. In former conditions, numerical solutions might increase infinitely and in latter conditions, structural behavior might be over damped. Consequently, multi degree of freedom systems were more prone to error accumulation in higher modes. Natural frequency was dominant in structures

tested using pseudo-dynamic technique; however aforementioned experimental errors might cause a higher mode excitation.

Size of the test specimen was limited by laboratory capacity. It was suitable to test a substructure of a large scaled structure. This approach also provides economy. One of the first studies of testing substructures is done by Nakashima *et al.* (1990). In this study a new integration technique is proposed.

In literature, use of implicit integration was studied in addition to explicit integration in pseudo-dynamic testing (Peek and Yi, 1990; Shing and Vannan, 1991; Bursi and Shing, 1996). Most of these studies provided information about minimizing error in implicit integration. Studies showed that implicit integration techniques do not lead to errors as much as explicit integration techniques.

Pseudo-dynamic test might be conducted as quasi-static and might also be conducted in real time by using dynamic actuators. One of the first examples of real time experiments is the work of Nakashima, Kato and Takaoka (1992). In these real time experiments, feedback to the system in 2 milliseconds is achieved by using digital displacement meters and a digital servo mechanism.

Darby et al. (1999) described a new type of real-time substructuring method for testing systems under dynamic loading. The method involved separating a system into a linear subsystem, modeled numerically, and a possible nonlinear subsystem, to be tested physically at full or large scale. Researchers stated that the purposed method overcomed problems of scaling and timedependent effects associated with shaking tables and pseudo-dynamic testing methods.

Chang (2002) implemented successfully a practical application of an unconditionally stable explicit method to solve the momentum equations of motion and verified in performing an on-line dynamic test. Since this algorithm was unconditionally stable and explicit it was very suitable to perform the on-line dynamic test with high frequency modes and its implementation could be as simple as the commonly used explicit on-line dynamic test algorithm.

CHAPTER 3

STRUCTURAL STRENGTHENING

Strengthening of structures has been a popular research area since there are a number of structures (buildings, bridges, etc.) that are vulnerable to earthquake and wind loadings. This chapter briefly summarizes about strengthening of structures weak against earthquake loading and mentions the development of strengthening techniques worldwide and in Turkey.

3.1. STRENGTHENING OF STRUCTURES

Common deficiencies observed in structures are insufficient lateral load carrying capacity, insufficient transverse reinforcement amount, use of strong beams – weak columns, lack of sufficient lap splice length, low concrete compressive strength, lack of transverse reinforcement detailing at potential plastic hinge regions and beam-column joints.

Seismic strengthening of structures may be categorized into two major topics. The first one is strengthening of entire structure members (columns, beams) and the other is strengthening of structural systems. Main objective is usually to increase lateral load capacity, rigidity and ductility of the structures. Not all of the techniques used in strengthening are shown, but most common ways of strengthening are presented in Figure 3.1.

One of the methods in member strengthening is jacketing of structural elements. Jacketing of reinforced concrete columns is usually achieved by concrete or steel jacketing. Wrapping of fiber reinforced polymers (FRP) around columns yields increase of ductility and provides a confinement effect (Pantelides et al., 1999; Shan et al., 2006 ; Ozcan *et* al., 2008). Wrapping of FRP at critical locations

of a beam advances the moment carrying capacity of the section; however it leads to an increase in design shear of the wrapped beam. Hereby, precautions should be taken to increase the shear capacity of the wrapped beam section.

Julio et al. (2005) tested seven full-scale column-footings strengthened by reinforced concrete (RC) jacketing after their surface had been prepared considering different techniques. With this study, it was confirmed that RC jacketing is a very effective strengthening technique, leading to values of resistance and stiffness of the strengthened column considerably higher than those of the original column. For RC short columns and deteriorated or damaged RC columns, the purposed conclusions may not apply.

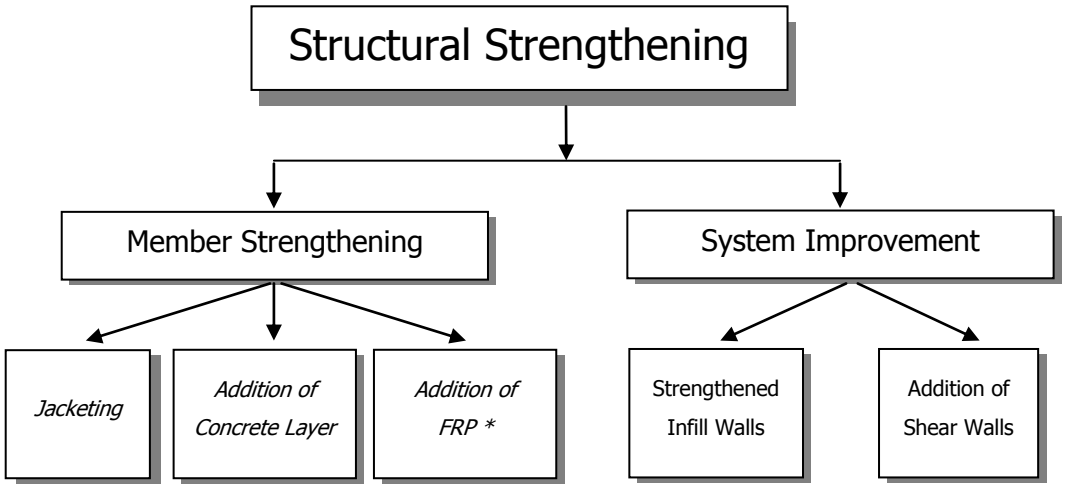

Figure 3.1 A brief scheme of structural strengthening

*FRP: Fiber Reinforced Polymers

It is usually more desirable to strengthen the structural system rather than strengthening structural members. Three procedures are discussed in this chapter: strengthening of infill walls and adding shear walls. Strengthening of infill walls may be achieved by FRP or precast concrete panels. Successful implementation of FRP or precast concrete panels increase the rigidity and lateral load carrying capacity of the system. Adding of shear walls is another way of strengthening structural systems. Shear walls should be designed in order to carry the most of the lateral load (~90%) during an earthquake excitation.

3.2. BACKGROUND

There are numerous researches on the topics of CFRP, precast concrete panels and shear walls. However, proceeding parts focus on key researches worldwide and in Turkey.

3.2.1. FRP (Fiber Reinforced Polymers)

FRP is widely used for strengthening of unreinforced masonry walls. Observations have shown that strengthening walls with FRP enhances the shear capacity of the walls significantly. In addition, the strengthened walls show a more ductile behavior (Schwegler, 1995; Laursen et al., 1995). Other investigations have proven that walls strengthened with FRP have an increased flexural capacity (Ehsani et al., 1999; Hamilton et al. 1999; Velazquez et al. 2000). Some studies have resulted that masonry walls strengthened with FRP fails from debonding of FRP from the wall (Hamilton et al. 1999; Velazquez et al. 2000). Thirteen tests were conducted by Albert et. al (2001) ; some of the tests were conducted without FRP and other tests were strengthened with FRP. The tests showed that FRP retrofitting increased lateral strength of the specimens significantly. FRP application for strengthening of masonry structures is highly dependent on the proper anchorage to the surrounding structural members (Tumilian *et* al., 2001) .

Biskinis and Fardis (2009) explained the rules for flexural and shear strength calculations, the secant stiffness to yield point and the cyclic deformation capacity of concrete members retrofitted with FRP. Their proposals are adopted in Annex A of Part 3 of Eurocode 8.

Ozcebe et. al (2003) conducted experiments on seven identical one bay and two story infilled concrete frames. One frame tested as a reference frame and other six frames were strengthened by FRP sheets. First experiment was conducted by bonding two diagonal FRP sheets to the masonry wall with epoxy based glue and no additional anchorage was implemented. FRP sheets debond from the infill wall at the early phases of the experiment. As a result, no remarkable increase in the lateral strength of the specimen was observed. In the third experiment, FRP sheets were extended to frame members of the test specimen and FRP anchorages

were applied. Still, there was no anchorage to the infill wall of the test specimen. FRP sheets lost bonding to the infill wall alike in the second experiment. To prevent debonding from infill wall, more anchorages were used and ends of the columns were wrapped by two layers of FRP in the fourth experiment. The fourth specimen showed an increased ductility and increase in the strength about 2.3 times relative to the reference frame. 200 mm wide FRP sheets were used along each diagonal of the test specimen in the fifth experiment. The fifth specimen showed also increased ductility and strength of the specimen was around 2.1 times the reference frame. In the sixth experiment, FRP wrapped regions were extended to potential plastic hinge regions. In this experiment, increase in strength was around 1.9 compared to the times the reference frame.

A compressive study was conducted by Erdem *et* al. (2003) Two 1/3 scale three bay and two story reinforced frames were tested. One of the frames was strengthened with reinforced reinforced concrete infill wall and the other one was strengthened with carbon FRP in the existing infill wall in the mid bay. Both strengthening techniques increased the stiffness and strength significantly. The lateral strength increase was approximately 500%.

Akin *et* al. (2009) tested eight 1/3 scale 1 bay 2 story reinforced concrete frames. The aim of this study was to strengthen the masonry infill walls by using FRP sheets. Some of the observed results were:

-It is possible to convert non structural masonry infill walls into structural walls by FRP sheets and strips.

-Strengthening with FRP increased the strength of all specimens considerably.

-Improvement in the drift characteristics of the tested specimens was observed.

-Strengthening with FRP provides a feasible and economic solution.

3.2.2. Precast Concrete Panel

Concrete frames strengthened with precast concrete panels have considerable increases in their initial stiffness, lateral load carrying capacity and

strength. It was observed that failure of the precast panels occurs at higher displacements than the monolithically cast panels (Kaldjian and Yuzugullu, 1983) . Precast infill wall systems not only increase the strength, also increases the ductility of the systems (Higashi et. al, 1984). Shapes of the precast panels placed in concrete frames do not have an considerable effect (Duvarci, 2003) .

Frosch *et*. *al* (1996) tested three model structures to evaluate the system behavior of the precast infill wall system. Researcher stated that strengthening by means of precast concrete panels is an option to strengthen and stiffen many existing reinforced concrete moment-resisting frames lacking strength and ductility. Precast infill wall eliminates costly and time consuming procedures related to cast-in-place infill wall.

Baran *et. al* (2005) tested 1/3 scaled three one bay two story reinforced concrete frames. The bay of the test specimens were filled with bricks. A test was conducted as a reference test and no strengthening techniques were applied in this test. In the other two tests different arrangements of precast concrete panels were implemented. Panels were assembled to the existing frame by using epoxy based glues. The specimens tested under reversed cyclic loading revealed that precast concrete panels improved the seismic performance.

Tankut *et* al. (2005) studied precast panel applications. They stated that precast panels glued to masonry walls with epoxy based glue turned masonry walls into strong and rigid infill walls capable of carrying lateral loads and energy dissipation. Advantages of precast panels were listed as speed in construction and minimum disturbance to building occupants.

Series of full-scale pseudo-dynamic tests had been carried out at the ELSA Laboratory of Joint Research Centre. Tests were conducted on 'as built' and FRP retrofitted full-scale frames. More ductile and energy dissipating global performance were targeted in these series of experiments. Experiments revealed that introducing FRP retrofitting supplied extra ductility with respect to non-strengthened frame. Frame without retrofitting was almost lacking the appropriate capacity to resist even 0.20g PGA level of excitation. Effectiveness of FRP strengthening was highlighted in terms of ductility and energy dissipation. (Di Ludovico *et* al., 2008) .

3.2.3. Reinforced concrete infill walls

First implementation of reinforced concrete infill wall in Turkey was applied to a one story industrial building in 1968 by U. Ersoy and Ş. Uzsoy at Bartın (Ersoy and Uzsoy, 1971) .

Aoyama et. al (1984) studied the behavior of RC frames strengthened with reinforced concrete infill walls. Implementing reinforced concrete infill walls resulted in increase of strength and decrease in deformation capacity.

Jirsa and Kreger (1989) tested four one-bay, one-story specimens with reinforced concrete infill wall. Adding of infill walls increased the lateral strength of the test specimens; however the failure mode of the entire three specimens was brittle. Failure occurred in the columns at regions where column bars were spliced.

Altin et. al (1992) conducted experiments of fourteen 1/3 scale, one-bay and two-story specimens to investigate the behavior of reinforced concrete frames strengthened by reinforced concrete infills. The frames were tested under reversed cyclic loading. The infills properly connected to the frame increased both the strength and the stiffness of the test specimens considerably.

Miller and Reaveley (1996) proposed that the economic way of strengthening between addition of steel braces and addition of RC infill walls to an existing structural frame was addition of RC infill walls. The most expensive way was reported as base isolation.

Turk (1998) conducted nine experiments to observe the effect of strengthening with cast-in-place reinforced concrete infills to the damaged frames. Tested frames were 1/3 scale, one bay two story specimens. The researcher concluded that connection between the added infill and the existing frame played an important role for the efficiency of the strengthening. The researcher also pointed out that the level of damage of the existing frames did not considerably changed the behavior of the added infill walls.

Sonuvar et. al(2001) tested five 1/3 scale, two-story and one-bay reinforced concrete frames under reversed cyclic loading in order to investigate the behavior of repaired frames. Addition of infill walls to the damaged frames significantly increased the stiffness and lateral strength of the test frames.

Canbay et al. (2003) tested 1/3 scale, three-bay and two story concrete frame to damaging lateral drift reversals and was then strengthened with the addition of reinforced concrete infill to mid bay. Researches concluded that the lateral load carrying capacity of the frame increased approximately 4 times with the introduction of infill wall to the damaged bare frame.

CHAPTER 4

EXPERIMENTAL SETUP

4.1. GENERAL

Four ½-scaled three-bay and two-story lightly reinforced concrete frames were prepared for this study at Middle East Technical University Structural Mechanics Laboratory. Previously, 1/3 scaled three-bay and two-story lightly reinforced concrete frame was tested by Canbay *et. al.* All experiments were conducted using pseudo-dynamic testing technique. Three different strengthening methodologies, namely Fiber Reinforced Polymers (FRP), precast concrete panels and reinforced reinforced concrete infill walls were examined to highlight the efficiencies and behaviors of the methodologies. Three test frames had masonry infill wall at the middle bay. The first frame tested was reference frame without any strengthening practice. Other two of these frames were strengthened with FRP and precast concrete panels, respectively. Last experiment was conducted strengthening the experimental frame by cast-in-place reinforced reinforced concrete infill wall. Experimental setup and applications of strengthening techniques used for this study are examined in proceeding sections in depth.

4.2. TEST FRAME

All of the specimens were cast in place and vertically by using steel molds. The steel formwork was manufactured from 3 mm thick steel plates. Special care was taken in manufacturing of the molds to have possibly precise dimensions. Steel plates were assembled with bolts, forming the formwork. The dimensions of the test specimen are given in Figure 4.1. The outer bays of the test frame have a width of 2500 mm. The middle bay is 1300 mm in width. The clear height of the first story is 2000 mm and the second story 1500 mm. The columns are 150 x 150

mm and T-shaped beams are 150 x 200 mm. T-shaped beams have a 600 mm width and 60 mm thickness.

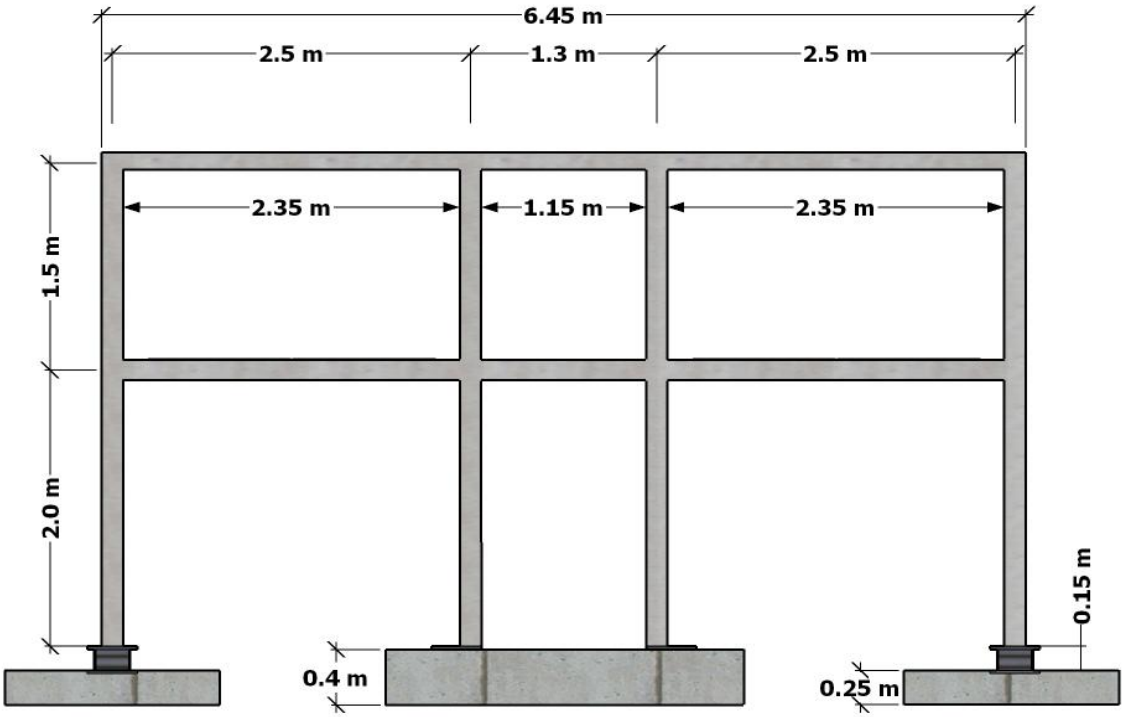

Figure 4.1 Dimensions of the test specimen

4.2.1. Details of the Test Specimens

Properties and detailing of the reinforcement were chosen to represent the common deficiencies encountered in building stock in Turkey.

4Φ8 plain bars were used as longitudinal reinforcement in both columns and beams. Reinforcement details of the columns and beams are shown in Figure 4.2. The longitudinal reinforcements of the columns were arranged to be continous. At the top of the columns of 2 mm thick plates were welded to have a fine compression by the mass blocks placed over the beams. The column longitudinal reinforcement is welded to the thick plate of 25mm at the bases and battened with L-shaped same plain bars of 50 mm height. Strengthening was done by welding of these bars with 50 mm weld length. The beam longitudinal reinforcement was not spliced but welded. Top beam longitudinal reinforcements are welded 15 mm at the mid span and bottom beam longitudinal reinforcements are welded 15 mm at

the third columns. At exterior columns, force transducers were placed at the foundation level in order to measure the column end forces (Canbay et al., 2004). The top surface of the force transducer was roughened to provide better bonding between steel plate and concrete. No splice problem was encountered during the experiments at those locations. The reinforcement pattern of the specimens is illustrated in Figure 4.2.

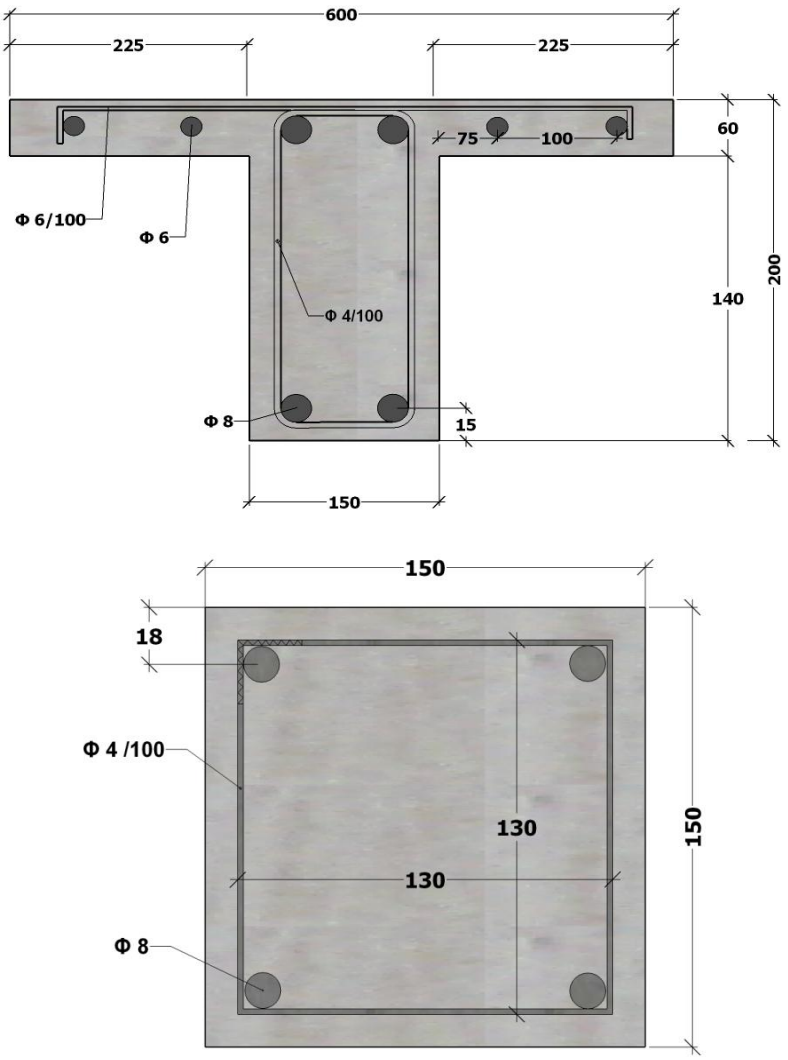

Figure 4.2 Reinforcement details of columns and beams (All dimensions in mm)

The same lateral reinforcement was provided in columns and beams. Plain bars with a diameter of 4 mm were used as transverse reinfrocement. The tie

spacing was 100 mm both for columns and beams. The ends of the ties had 90° hooks. The straight portion of the hook was extended ten bar diameters.

4.2.2. Foundation of the Test Specimens

Three single foundations are poured on the strong floor. Middle foundation has larger dimensions compared to the corner foundations. The two small square foundations have 1.5 m size in length and width. The other foundation has a size of 3.5 m in length and 1.5 m in width. The two small foundations have a height of 250 mm and the other foundation has a height of 400 mm. This design is intended to have equal level of all foundations when the force transducers are placed on the exterior foundations. Details of the foundation are given in Figure 4.3.

There are holes on the strong floor at the Structural Mechanics Laboratory of METU. These holes exist at 1 m away from each other and have 70 cm deep. The foundations are fixed to the strong floor by means of steel bolts that have diameter of 50 mm. Eight 5/8" high strength bolts are placed into the foundation for each force transducer. Force transducers are bolted and fixed to the foundation by means of these bolts. A general view of these bolts is shown in Figure 4.4.

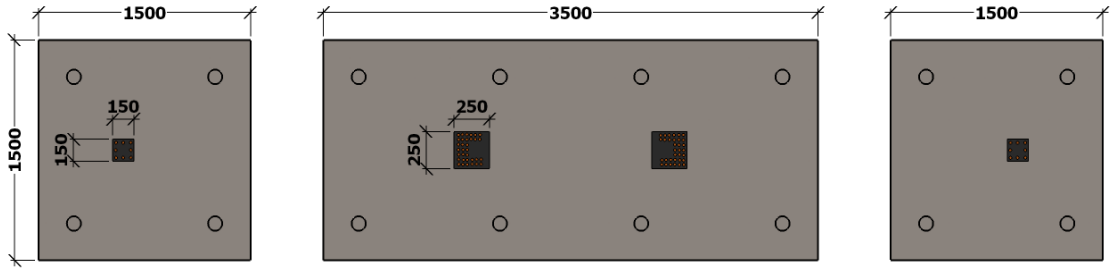

Figure 4.3 Plan View of the Foundation (All dimensions are in mm)

For foundation concrete, steel forms were assembled. Ready mixed concrete was ordered from a ready mixed concrete company. All the forms were cleaned and greased from inside in order to remove the steel forms easily. Approximately 3.5 m^3 concrete was poured to the foundation. Mechanical vibration was used to set the concrete compactly. Cylinder specimens were taken to test the

quality of the concrete. General views of the foundation before and after pouring of concrete are shown in Figure 4.5.

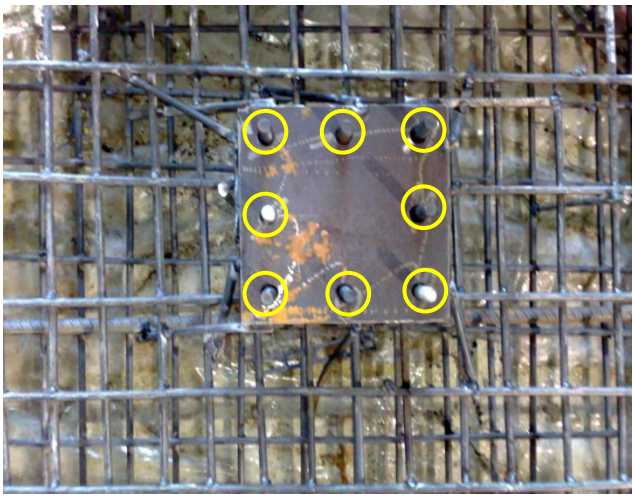

Figure 4.4 A general view of the bolts welded to the foundation for the transducers

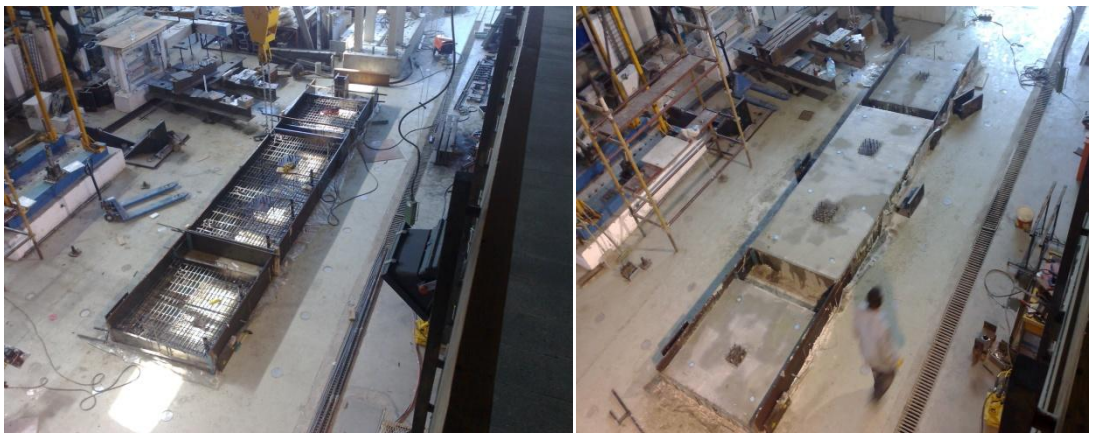

Figure 4.5 General views of the foundation before and after pouring of concrete

The grade of the ordered ready mixed concrete was C25, which has a uniaxial compressive strength of 25 MPa at 28 days. According to the standard cylinder tests, the concrete of the foundation had a 28 day uniaxial compressive strength of 29 MPa.

4.2.3. Materials

In the experiments, low unixaxial compressive strength for concrete was targeted for the tested. Concrete of the frames and panels was produced at the Structural Mechanics Laboratory of METU. The target compressive cylinder strength of the frames was 7.5 MPa. Table 3.1 gives the mix proportions of concrete for frames. Materials used in the mix are presented by weight for a unit cubic concrete.

Table 4.1 Mix Design of the frames (weight for 1 m^3 of concrete)

Mixture component	***Weight (kg)***	***Proportions by weight (%)***
Cement	254	11.14
0-3 mm Aggregate	658	28.86
3-7 mm Aggregate	608	26.67
7-12 mm Aggregate	506	22.19
Water	254	11.14
Total	2280	100.00

Several cylinders were taken and tested to verify the compressive strength of the specimens. Table 3.2 gives the values of the uniaxial compressive strength of the cylinders at the test days. The test cylinders were 150 mm in diameter and 300 mm in height.

Table 4.2 Uniaxial compressive strength of the cylinders at the test days

Test Name	***Compressive Cylinder Strength (MPa)***
Reference Frame	7.4
Frame with FRP	7.8
Frame with Precast Panels	7.3
Frame with Shear Wall	7.5

Aim of the curing of the specimens was to prevent cracking of the concrete. Same curing conditions were applied to the specimens and the cylinders taken from the concrete batch of the specimens.

Four longitudinal plain bars were used in all columns and beams. All longitudinal reinforcement had a bar diameter of 8 mm. Three samples having a length of 40 cm were taken from the reinforcing steel batch. These samples were tested to obtain stress-strain relationships of the steel used. Transverse reinforcement used had a diameter of 4 mm. Three samples were taken from 4 mm steel bars and they were tested too. Properties of reinforcing bars used are shown in Table 4.3.

Table 4.3 Mechanical Properties of Reinforcing Bars

Steel No	**f_y (MPa)**	**f_{ult} (MPa)**	**Properties**
Φ4	290	320	Plain
Φ8	330	365	Plain
Φ10	510	570	Deformed

4.2.4. Instrumentation

In the experiments, several LVDTs (Linear Variable Displacement Transducer) and electrical dial gages were used to obtain displacement measurements and load cells were used to have load measurements. Column curvatures at the bases were measured by using 2 LVDTs for each column.. To measure each floor tip displacement 2 LVDTs were used which makes a total of 4 LVDTs for floor displacement readings. Averages of the 2 LVDT readings at each floor were taken to measure each floor's displacement. There were 2 special transducers manufactured by Canbay *et* al. (2004). These transducers were placed under the exterior columns and 6 channels were used to acquire moment, shear and axial forces under these columns. To get load measurements at each floor 500 kN compression-tension load cells were used at each floor. Details of the test setup, loading system and instrumentation are given in Figure 4.6.

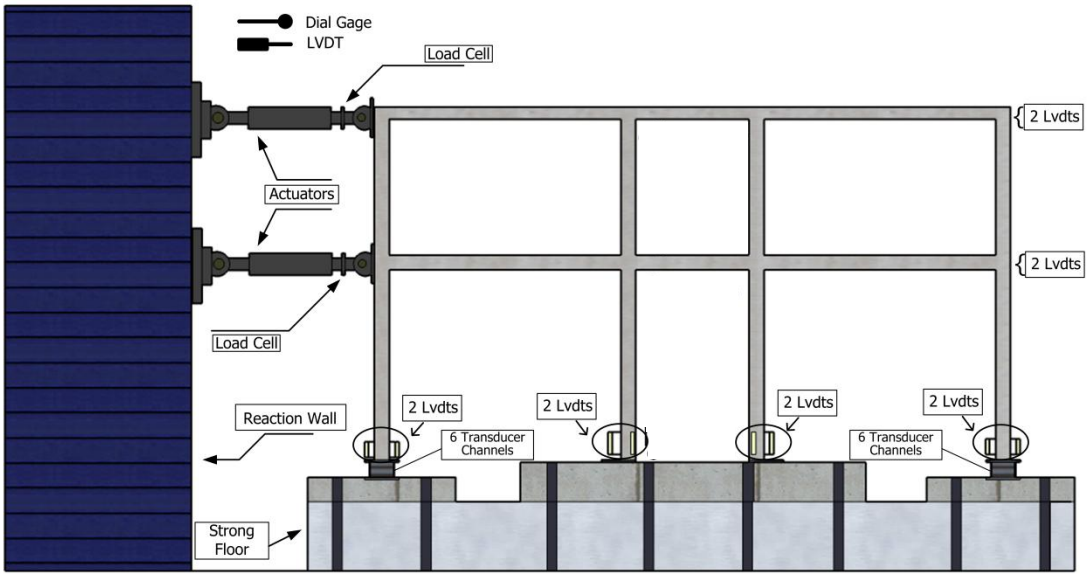

Figure 4.6 Details of the test setup, loading system and instrumentation.

Internal forces at the exterior column ends were measured by means of force transducers. Each force transducer consists of six minor load cells. Four of these small load cells were placed vertically for axial force computation and two of them were placed diagonally for shear and moment force computations. Voltage outputs were taken from these small load cells by means of data acquisition system. Afterwards, a special S matrix, that transforms obtained mV/V values to force readings, is used. A general view of the force transducers are presented in Figure 4.7.

Figure 4.7 General view of the force transducers.

Curvatures were measured by means of two LVDTs at the column bases. The LVDTs used were 50 mm stroke and measurement was taken between 30 mm and 180 mm above the base of the columns. A general view of the LVDTs at the column bases is shown in Figure 4.8.

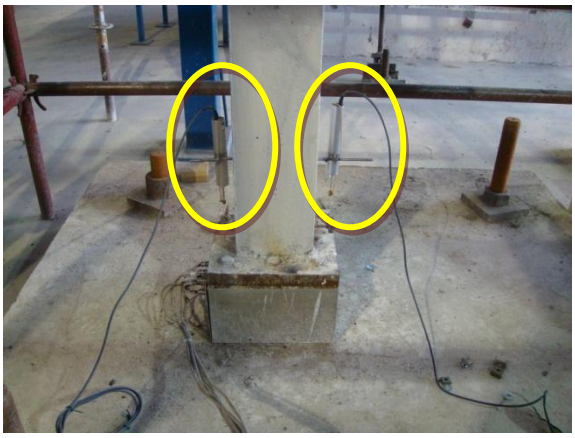

Figure 4.8 A general view of the curvature measurement at a column base

Two LVDTs were used at each floor end to measure tip displacements of the frame. A heidenheim was placed at each floor end to feedback the tip displacements for the computer system. A general view of the LVDTs and heidenheim at floor end is shown in Figure 4.9.

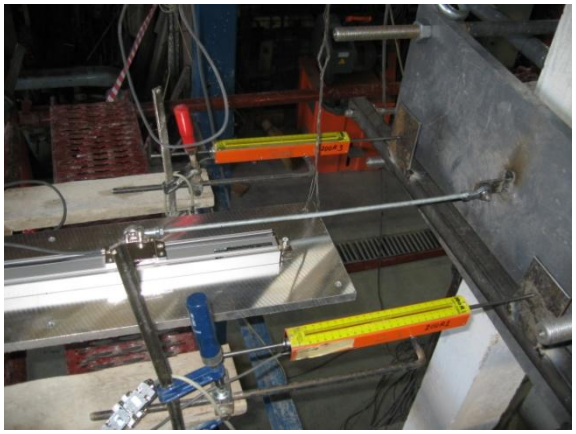

Figure 4.9 A general view of the LVDTs and Heidenheim at a floor end.

4.3. TEST SETUP AND LOADING SYSTEM

General information of the test frame and loading system will be discussed in this section.

The testing system consisted of strong floor, reaction wall, computer controlled actuators, loading equipment, instrumentation and data acquisition system. Foundations of the test frame were fixed to the strong floor by means of 50 mm diameter high strength bolts. Holes had a spacing of 1 m on the strong floor which has a depth of 700 mm. Under the strong floor there existed a gallery. The bolts were both fixed over the foundations and above the gallery. For the exterior foundations, 4 bolts were used. For the middle foundation, 8 bolts were used.

Vertical testing of the specimens was possible by means of the reaction wall. Lateral loading system was fixed to the reaction wall properly. This loading system should be exactly aligned to the gross center of the beams. For accurate positioning of the system and the actuators, a movable design was provided. This movable design allowed movements of the actuators. A general view of the movable loading system parts is given in Figure 4.10. Two I-300 steel sections of three meter height were fixed to the reaction wall. On these I sections three U-200 sections were fixed with high strength steel bolts. Specially designed adaptors were placed on these U sections. The adaptors compromised of two 25 mm thick steel plates and had holes on it to anchor the actuators. The steel plates on the adaptors had slots allowing it to move vertically and the adaptors were allowed to move horizontally on the U sections. The total loading system was fixed to the reaction wall through the holes on the I sections.

The lateral displacement was applied by using computer controlled actuators. The actuators was fixed to the adaptors and supported by specially designed table system. The table system consisted of 70 x 70 square steel sections, bolts having 42 mm diameter, 1 m x 1 m x 20 mm steel plates and steel tubes. Four 42 mm bolts were welded to the square steel sections. Steel plate was placed through the bolts and anchored with counter nuts. Steel tubes were placed over the bolts. Nuts were welded at the ends of the steel tubes to allow the movement of bolts throughout the steel tubes. Over the steel tubes 42 mm bolts were placed again and steel plate was placed

Figure 4.10 A general view of the movable loading system.

over these bolts by means of counter nuts. The actuators of each floor were supported by the square plates. Counter weight system was designed to align the actuators vertically. The counter weight system was assured by means of pulley systems. 200 kg of weight was used to have a balanced positioning of the actuators. The table and the actuators are shown in Figure 4.11.

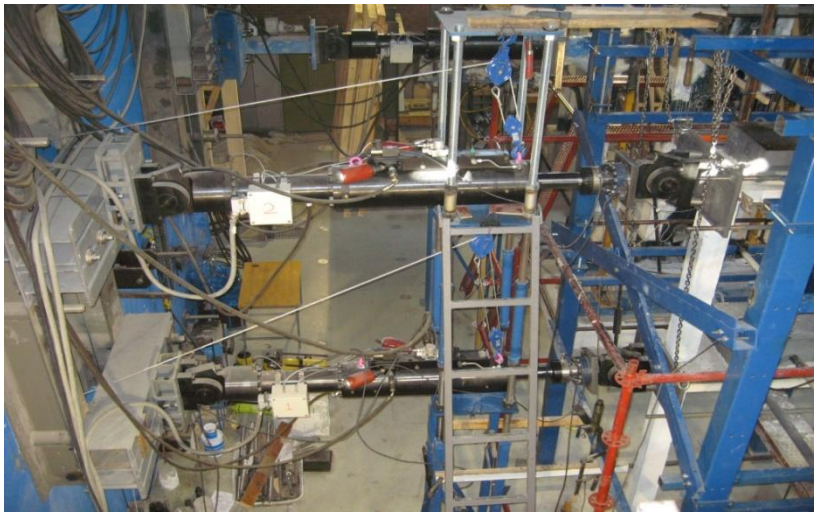

Figure 4.11 A general view of the table system and actuators.

The axial load on the columns was provided by means of steel blocks. Two different sizes of steel blocks were employed because of the geometry of the test specimen. One type of the steel blocks had a length of 1000 mm, width of 450 mm and a height of 100 mm. The other type had a length of 1550 mm, width of 450 mm and a height of 100 mm. Smaller mass blocks, blocks with 1000 mm length, were placed on the first floor and blocks having 1550 mm length were placed on the second floor. One small mass block had a weight of 330 kg. Infill wall limited the positioning of mass blocks to the middle bay. Therefore mass blocks were placed to the first and third bay on the first floor. Three small mass blocks were welded to each other and one piece three level mass blocks having a weight of 1 ton was obtained. Six smaller mass blocks which had a weight of 2 tons were put on each bay on the first floor. 2 tons were put with same geometry on the first and third bay. As a result, a total of 4 tons was put on the first floor. On the second floor, mass blocks were laid to the all floor. Two levels of 1550 mm length mass blocks were put. On these blocks three mass blocks were put at the mid span. One 1500 mm length mass block had a weight of 511 kg. As a result a total of 6 tons were placed on the second floor. A general view of the mass blocks on the first and second floor is shown in Figure 4.12.

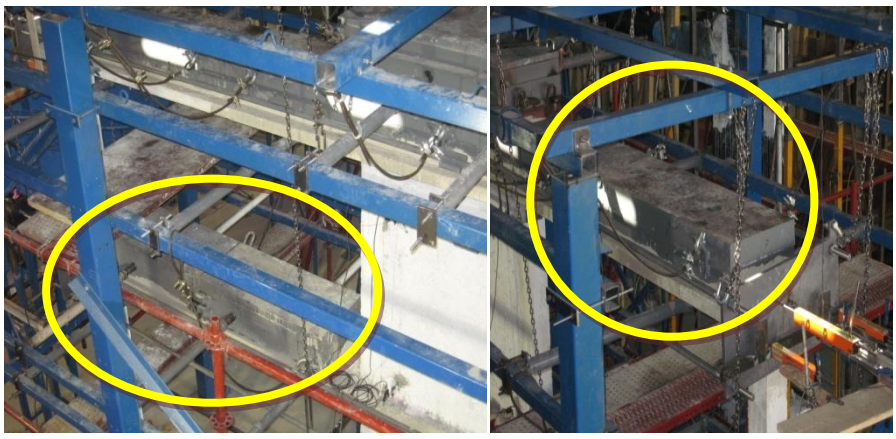

Figure 4.12 A general view of the mass blocks on the first and second floor.

Actuators were connected to the frame by means of 20 mm rectangular thick steel plates.. 25 mm steel plate had the geometry of the beam between the 20 mm steel plate and the concrete frame. It had a T-shaped cross section and there

was a pin at the gross center of the steel plate. The gross center of the steel plate was exactly coinciding with the gross center of the T-shaped beam. T-shaped steel plate was welded to the concrete by a 10 mm diameter of bolt that existed before pouring the concrete of the frame. Transfer of compression was applied to the frame directly by this system. However pushing from the other side of the frame was not possible as there were no actuators. Steel plates that the actuators were connected had 4 holes. From these holes 7 m steels that had 30 mm circular cross section were passed to the other side of the frame. At the other side of the frame there was the same application that was done at the actuator's side of the frame. The 25 mm steel plates had also 4 holes and 7 m anchorages were passed through them. 7 m anchorages were tightened by nuts at both sides of the frame.

4.4. TEST SPECIMENS

4.4.1. Reference Frame

General

Test frames used in this study represent the interior frame of the prototype structure shown in Figure 4.13. Red color is used to indicate the location of non-structural infill walls.

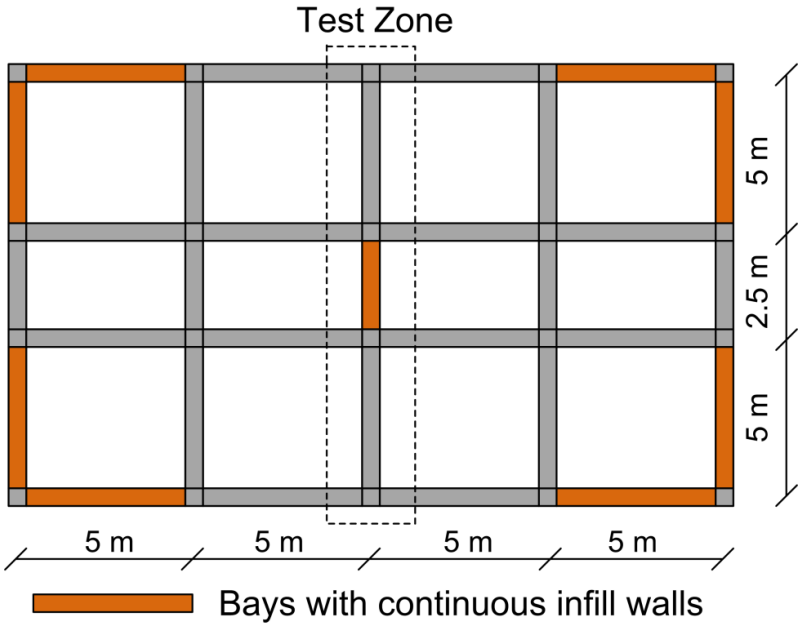

Figure 4.13 Plan view of prototype building.

The reference test specimen shown in Figure 4.14 is the scaled model of the interior frame marked on Figure 4.13.

The building floor plan has approximately 1% infill wall area that is commonly encountered in Turkey. The central frame of the building is investigated by physical testing. ½ scale model of the selected frame having overall dimensions of 3.6 m x 6.45 m is manufactured in the Middle East Technical University (METU) Structural Mechanics Laboratory owing to the limitations of the facility. The building has uniform distributed dead and live loads of 300kg/m^2 and 250kg/m^2 which are independent from scale factors. Preliminary analysis results show that such magnitude distributed loads produce axial load ratios (axial load divided by the axial load carrying capacity) of 0.13 and 0.23 in the first story exterior and interior columns, respectively. The gravity axial load ratios for the second story exterior and interior columns are estimated as 0.08 and 0.15, respectively.

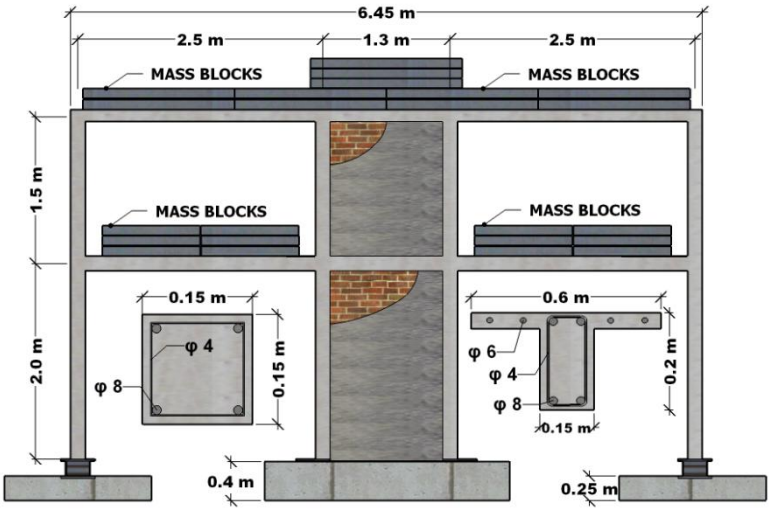

Figure 4.14 Illustration of Reference Frame

After placing the steel blocks to simulate the permanent load on the structure, infill walls from hollow clay brick (Figure 4.15) was laid in the central bay and centric to the column faces. Remaining 20 mm on each face of the wall was covered with plaster to make the infill wall flush to column sides. Columns of the frame were 150 mm x 150 mm with a longitudinal reinforcement ratio of 1.14% and had 4 mm diameter ties with 90 degree hooks spaced at 100 mm. According to

Turkish Earthquake Code 2007 (TEC 2007), the required volumetric ratio of the confining steel reinforcement for the plastic hinge regions is about 0.25% which has to be connected with 135 degree hooks. On the other hand, the test frame had 0.16% volumetric ratio of transverse reinforcement with 90 degree hooks at the potential plastic hinge regions of the columns. Other deficiencies of the test structure are the lack of transverse reinforcement at beam-column joints and violation of the strong column weak beam concept required by modern earthquake resistant design methods (TEC 2007).

Inelastic pushover analysis of the frame using the first mode shape lateral load profile was conducted (Figure 4.15). Lateral capacity of the reference frame was estimated around 65 kN. Hinging at first storey columns was formed. After failure of the strut at first storey, sudden drop at lateral force was observed.

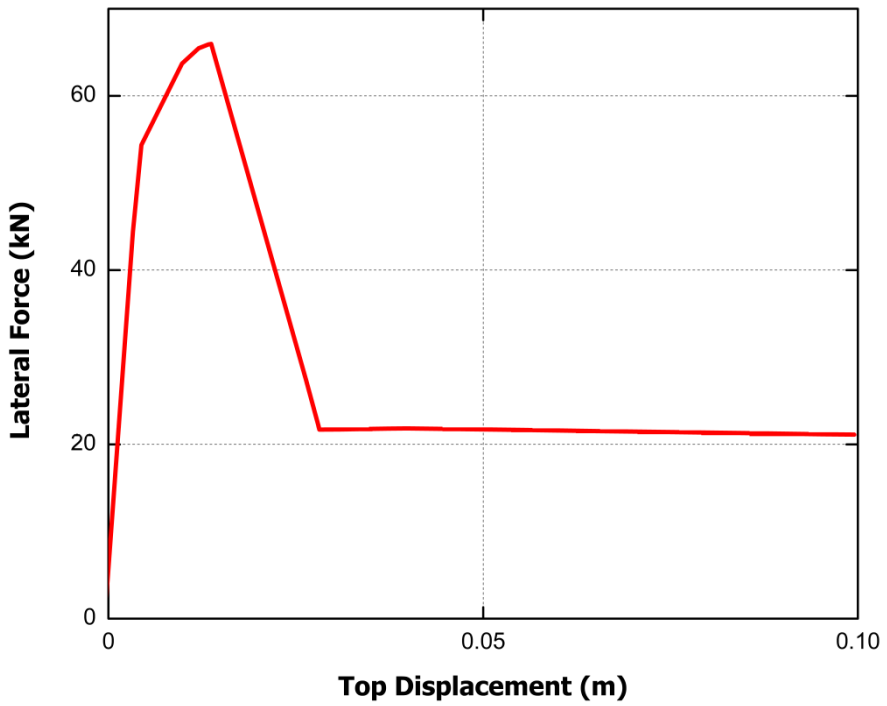

Figure 4.15 Pushover Curve for Reference Frame

Material Properties

Hollow clay tile infill units having dimensions shown in Figure 4.16 had a uniaxial compressive strength of 14 MPa in the direction along voids. The uniaxial compressive strength of brick laying mortar and plaster were 12 MPa. Uniaxial tensile strength of 8 mm diameter plain bars used in columns and beams longitudinal reinforcement had a yield strength of 330MPa and an ultimate strength of 365 MPa. Plain bars with a diameter of 4 mm having yield strength of 290MPa were used as ties in all frame members constituting beams and columns. These member details along with low strength concrete having an average uniaxial compressive strength of 7.4 MPa resemble the properties of the deficient building stock encountered in Turkey.

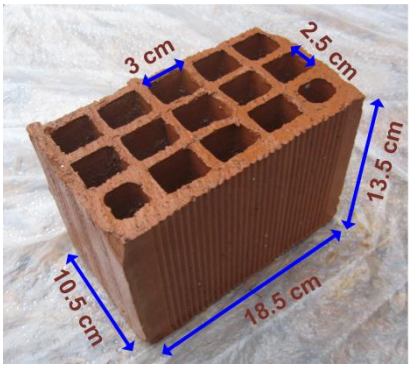

Figure 4.16 Hollow clay brick used in experiments

4.4.2. Fiber Reinforced Polymer (FRP) Retrofitted Specimen

General

The FRP retrofitted structure was identical to the reference frame with the only difference being the strengthening method used in the central bay on infill walls (Figure 4.17). Strengthened specimen was designed according to the Turkish Earthquake Code 2007 to achieve a base shear capacity of about 80% larger than the capacity of the reference frame. For this purpose, lateral strength contribution was computed using an FRP strain limit of 0.003. For such a lateral strength enhancement, the ductility and performance state of the retrofitted structure was aimed to be examined experimentally.

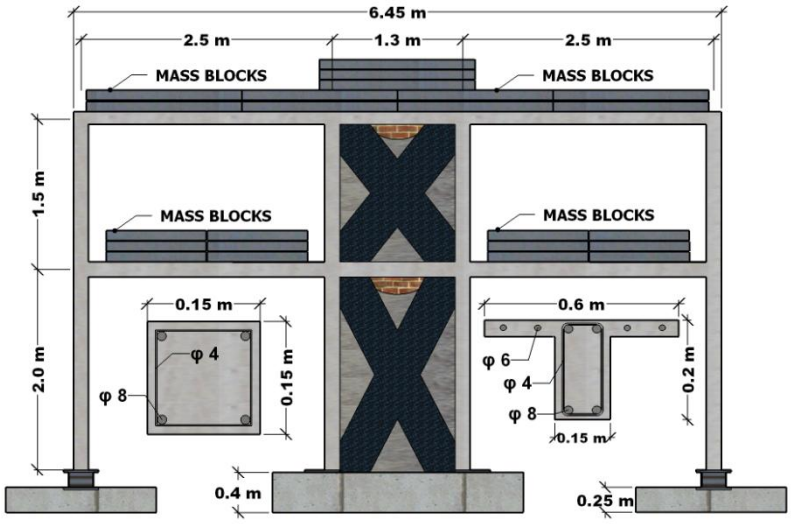

Figure 4.17 FRP Retrofitted Specimen

This retrofit method targets limiting the inter-story deformations and increasing the base shear capacity of the existing weak frame with the FRP tensile strength contribution working as a diagonal strut. In addition, FRP helps in keeping the infill walls intact, hence delaying out of plane collapse possibility.

Shear strength contribution to the test specimen of applying two FRP sheets was calculated by means of the proposed equation in TEC 2007.

$$T_f = 0.003 \times E_f \times w_f \times t_f$$

where;

T_f : Tensile strength of one FRP strut

E_f : Elasticity Modulus of FRP sheets

w_f : Width of FRP sheets

t_f : Thickness of FRP sheets

$$T_f = 0.003 \times 230000 \times 450 \times 0.166$$

$$T_f = 51.5\ kN$$

Shear strength contribution to the frame of two FRP sheets is the horizontal component of FRP struts.

$\alpha \approx 58^{\circ}$; $\cos\alpha = 0.52$

Therefore, shear strength contribution is:

$V_{FRP} = 2 \times 51.5 \times 0.52$

$V_{FRP} = 54\ kN$

Existing shear capacity of the system was 65 kN as obtained from pushover analysis. The contribution of strengthening was $V_{\%} = \frac{54}{65} \times 100$

$V_{\%} = 83\%$

Material Properties

A custom made FRP sheet having a uniaxial strength of 4,900 MPa with the modulus of elasticity of 230,000 MPa and the thickness of 0.16 mm was used in the design of the FRP diagonals. The FRP diagonal braces are integrated to the boundary frame by FRP anchors embedded in holes drilled through the foundation, columns and slabs.

FRP Application

FRP retrofitting was employed by placing two FRP (fiber reinforced polymer) strips along the diagonal of the hollow clay tile (HCT) infills on both surfaces. The integrity of the FRP and the infill wall-plaster composite was provided by using FRP dowels passing through the walls. These dowels were fanned out on both faces of the infill wall. In this way it was aimed to delay FRP debonding from the plastered infill wall surface. The FRP diagonal braces were integrated to the boundary frame by FRP anchors embedded in holes drilled through the foundation, columns and slabs. Anchor dowels were obtained by wrapping FRP sheets (Figure 4.18). The depth of the anchor dowels was selected as 75 mm i.e. ½-scaled values of the code prescribed embedment depths.

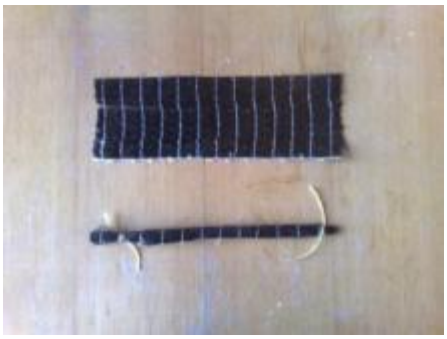

Figure 4.18 General views of FRP anchorage and the wrapped FRP sheet.

First, several 8 mm diameter anchorage holes were drilled throughout the infill wall, columns and beams on both stories. These holes were first washed and then cleared by pressurized air in order to get rid of small particles in the holes. Anchorage holes at the foundation were dig inclined in the direction of cross FRP sheets. Anchorage holes at the foundation were also cleared by pressurized air.

Premier was used to clear the dust on the infill wall and smoothen the surface of the infill wall. Afterwards, high strength mortar was applied on the surface of the infill wall as shown in Figure 4.19. Following these, 450 mm thick cross strips and 600 mm x 600 mm square FRP sheets were glued to the infill wall on both floors by using epoxy-based glue (Figure 4.19).

Figure 4.19 General view of the infill wall before and after placing FRP sheets.

A representative view of FRP sheets, anchorages and dowels are shown in Figure 4.20.

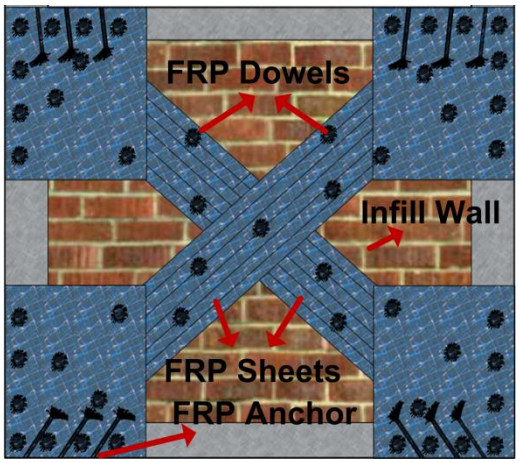

Figure 4.20 A representative view of FRP sheets, anchorages and dowels. (Plaster is not shown)

4.4.3. Precast Concrete Panel (PCP) Retrofitted Specimen

General

The precast concrete panel (PCP) retrofitted structure was identical to the reference frame with the only difference being the strengthening method used in the central bay on infill walls (Figure 4.21). Strengthened specimen was designed according to the Turkish Earthquake Code 2007 (TEC07) to achieve a base shear capacity of about 35% larger than the capacity of the reference frame. For this purpose, lateral strength contribution of precast concrete panels was computed using proposed equations by TEC07. For such a strength enhancement, the ductility and performance state of the retrofitted structure was aimed to be examined experimentally.

Columns had a shear capacity of around 6 kN. Additional base shear by adding precast concrete panels was estimated according to Turkish Earthquake Code 2007:

$V_{pcp} = A_{dp} \times \tau_{dp}$

$A_{dp} = 25 \times 1150 = 28750\ mm^2$

$\tau_{dp} \approx 2.20\ \text{MPa}$

$V_{pcp} \approx 64\ \text{kN}$

Where;

V_{pcp} : Shear force capacity of precast concrete panels

A_{dp} : Horizontal cross-section area of the precast concrete panels

τ_{dp} : Sliding shear strength

Four columns with a shear capacity around 6 kN;

$V_{total} = 64 + 4 \times 6$

$V_{total} \approx 88$ kN

Base shear was estimated as 88kN according to the preliminary studies.

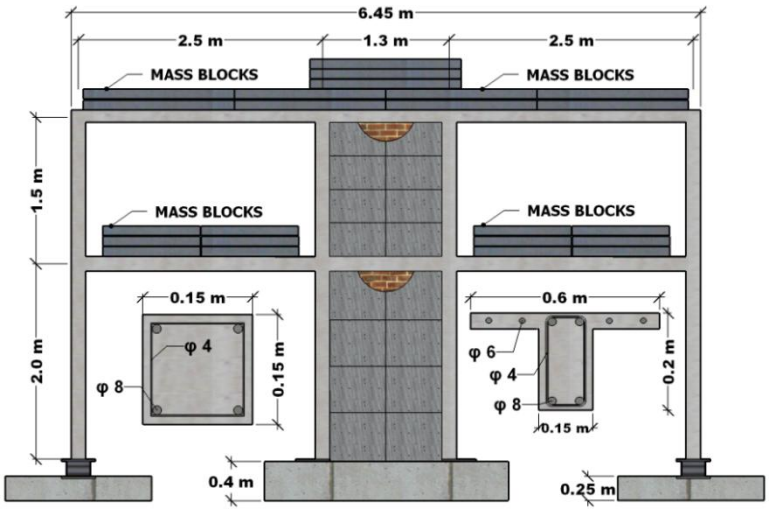

Figure 4.20 PCP Retrofitted Specimen

The main advantage of using precast concrete panels (over in situ cast concrete shear wall) is the convenience of transporting lighter concrete elements and achieving the connections easily without any disturbance to the occupants.

Material Properties

For each story, eight precast concrete panels with a thickness of 25 mm was bonded on the infill walls from one side. Uniaxial compressive strength of the PCPs was 40MPa on the test day. Mix Design of concrete panels is presented in Table 4.4. Panels had about 0.3% longitudinal mesh reinforcement in both directions for handling purposes.

Table 4.4 Mix Design of the concrete panels (weight for 1 m^3 of concrete)

Mixture component	***Weight (kg)***	***Proportions by weight (%)***
Cement	439	19.25
0-3 mm Aggregate	864	37.90
3-7 mm Aggregate	750	32.89
Water	227	9.96
Admixture*	*4.39*	*1*
Total	2280	100.00

*Admixture weight ratio is given as the percentage of cement used.

PCP Application

General view of the precast concrete panels is shown in Figure 4.22.

Figure 4.21 General view of the precast concrete panels.

Eight precast concrete panels (PCPs) with a thickness of 25 mm were bonded on the infill walls from one side at each floor. Dimensions of the precast concrete panels are shown in Figure 4.23.

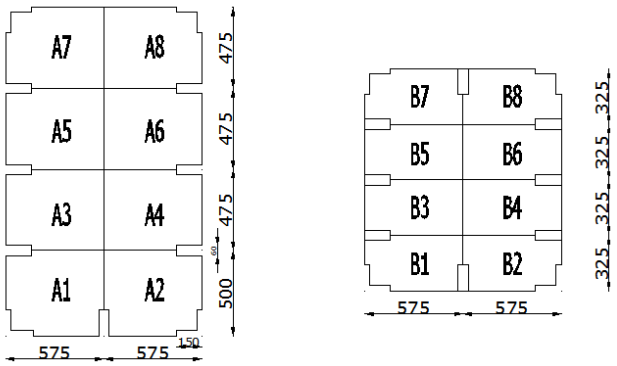

Figure 4.22 Dimensions (in mm) of the precast concrete panels for both floors.

PCPs were produced with shear keys with steel reinforcement (10 mm diameter) that were connected to the columns, beam, and foundation. 10 mm diameter deformed bar anchorages had a length of 240 mm of which penetrates 120 mm to the surrounding columns, beam and foundation.

Shear keys were filled with high strength mortar (uniaxial compressive strength of 50 MPa) to provide force transfer between the panels and the boundary elements. Representative view of PCP application is shown in Figure 4.24.

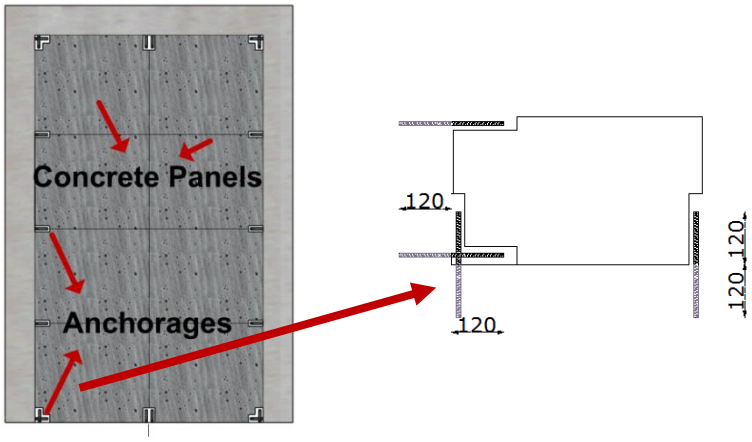

Figure 4.23 Representative view of PCP application.

4.4.4. Reinforced Concrete Infill Wall Application

General

The reinforced concrete infill wall retrofitted structure was identical to the reference frame with the only difference being the strengthening method used in the central bay (Figures 4.25). Strengthened specimen was designed according to the Turkish Earthquake Code 2007 (TEC07) to achieve a base shear capacity of about %70 larger than the capacity of the reference frame. For this purpose, lateral strength contribution of reinforced concrete infill walls was computed using pushover analysis. For such a strength enhancement, the ductility and performance state of the retrofitted structure was aimed to be examined experimentally.

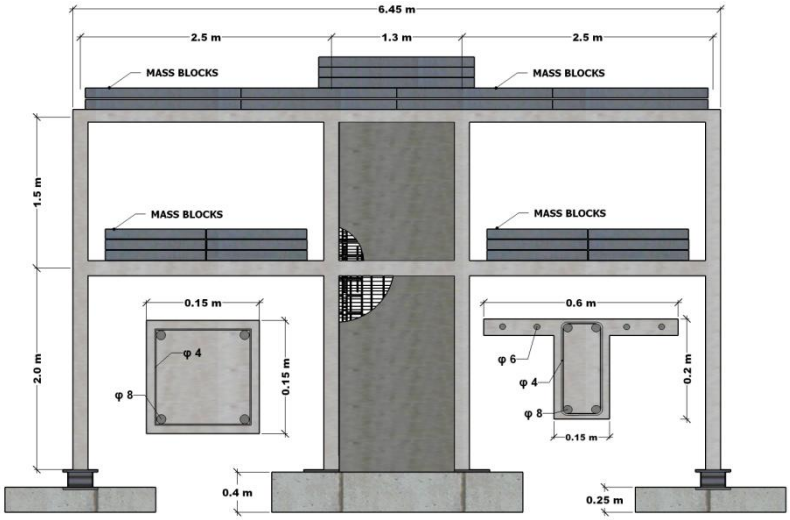

Figure 4.24 Reinforced Concrete Infill Wall Retrofitted Specimen

Pushover analysis of reinforced concrete infill wall retrofitted specimen indicated a base shear of around 115 kN (Figure 4.25).

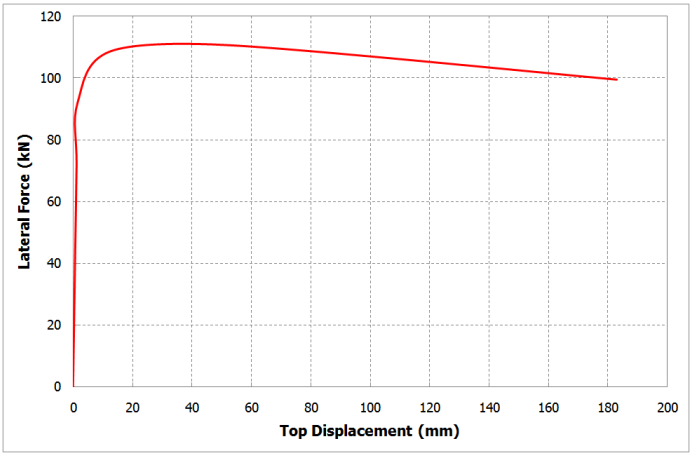

Figure 4.25 Pushover Curve for Reinforced Concrete Infill Wall Retrofitted Specimen

Material Properties

Cast in place reinforced concrete infill wall was designed with a thickness of 10 cm. Uniaxial compressive strength of the concrete of the reinforced concrete infill wall was 22.4 MPa for the first floor and 21.2 MPa for the second floor on the test day. Reinforced concrete infill wall had about 0.48% longitudinal reinforcement and 0.25% transverse reinforcement. Anchorages of the reinforced concrete infill wall were designed according to Turkish Earthquake Code 2007. Reinforced concrete infill wall was anchored to existing foundation and beams by 10 mm diameter deformed bars and to existing columns by 8 mm deformed bars.

Concrete of the infill wall was prepared at the Structural Mechanics Laboratory at METU. Proportions of the materials used for concrete of the infill wall are presented in Table 4.5. Uniaxial compressive strength of the concrete cylinders of the reinforced concrete infill wall had an average of 22 MPa for the first and second floors at the test day, respectively.

Table 4.5 Mix design of concrete of the infill wall (weight for 1 m^3 of concrete)

Mixture component	***Weight (kg)***	***Proportions by weight (%)***
Cement	260	11.37
0-3 mm Aggregate	1052	46.15
3-7 mm Aggregate	190	8.36
7-12 mm Aggregate	564	24.75
Water	214	9.37
Total	2280	100.00

Reinforced concrete infill wall Application

15 Φ10 deformed reinforcements were used as base anchorages. Base anchorages penetrates 150 mm and 225 mm trough the foundation and reinforced concrete infill wall, respectively. Total length of the base anchorages were 375 mm. Side columns were constructed in the reinforced concrete infill wall because of low concrete quality and poor reinforcement detailing of existing columns. 4 Φ8 deformed bars were used as longitudinal reinforcement in constructing the site columns. 3 Φ10 deformed bars were anchored to the foundation inside the side columns. Thus, total area of the anchorages exceeded the total area of the longitudinal reinforcements of the side columns. This provided transfer of forces to the foundation properly. Plain bars used as transverse reinforcement of side columns were Φ4/50.

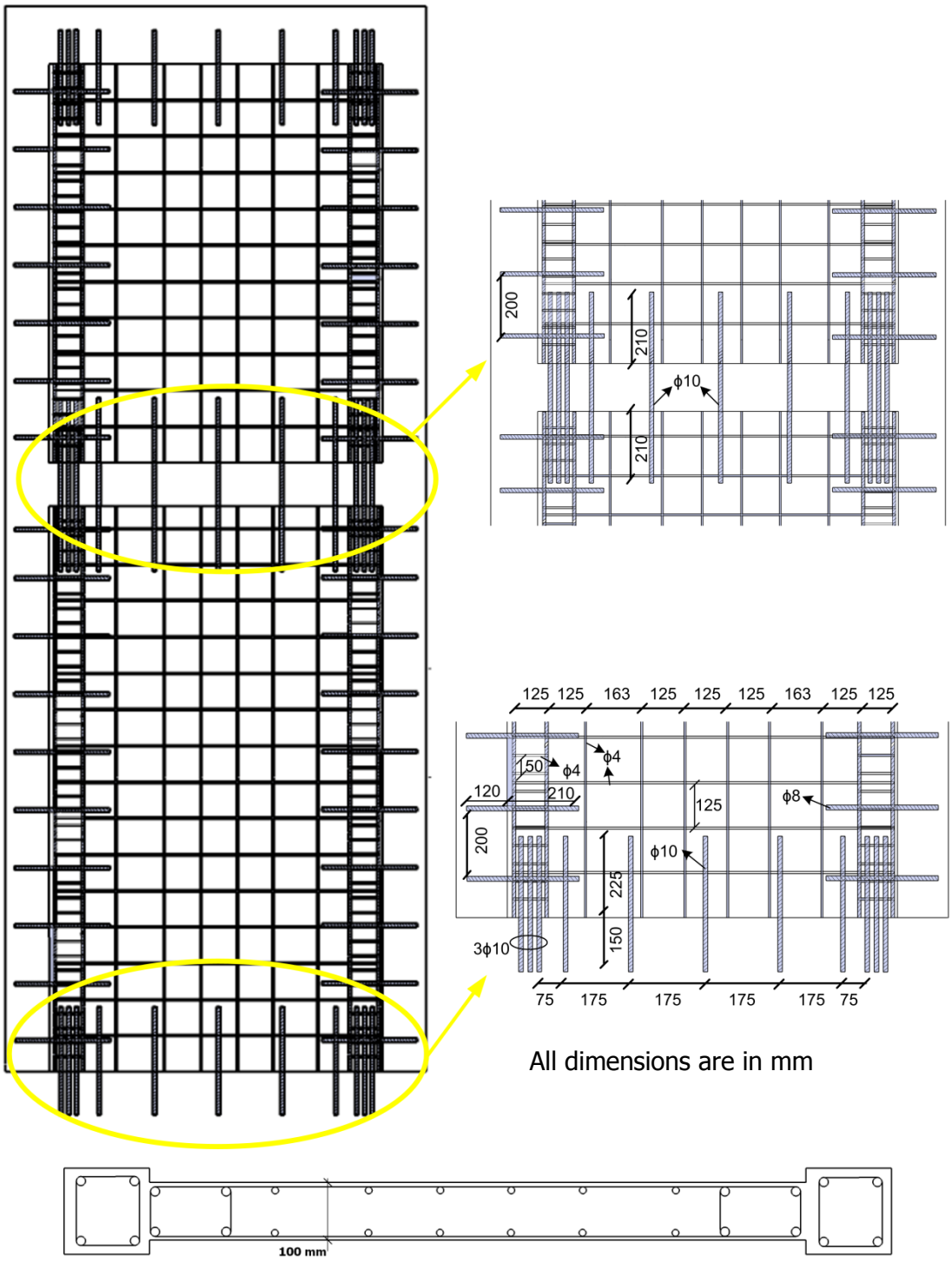

Figure 4.26 Representative views of reinforced concrete infill wall reinforcements, anchorages and cross-section

Transverse reinforcements of the concrete infill were Φ4/125. 12 Φ4 plain bars were used as longitudinal reinforcement of reinforced concrete infill wall.

Reinforced concrete infill wall was anchoraged to the existing columns by deformed Φ8 bars with a spacing of 200 mm. Length, diameter and spacing of all reinforcements and anchorages are presented in Figure 4.26.

4.5. TESTING PROCEDURE

PSD experiments were conducted using the continuous pseudo dynamic testing method (Molina et al., 1999). Integration process was executed continuously to eliminate possible relaxation errors. The mass matrix used for the numerical integration was a 2×2 lumped mass matrix consistent with the actual mass of the test structure (i.e. first story mass = 7000 kg, second story mass = 5000 kg). Use of an actual ground motion was found to be more appropriate to mimic the hazard level that could be expected for the prototype building. North-South component of 7.1 moment magnitude 1999 Duzce ground motion with three different scale factors was employed for the test. Acceleration time series of the motion and pseudo acceleration spectrum of the motion are shown in Figure 4.27 and Figure 4.28, respectively. Tests were conducted about 1000 times slower compared to the real time motion. Modification of the ground motion to obtain various damage states was conducted by scaling the acceleration time series by 50%, 100% and 140%. Such a scaling was employed to investigate the response at three different hazard levels:

a) 50% Duzce: Spectral acceleration value for 50% Duzce is approximately similar to the base shear capacity ratio (base shear capacity divided by structure weight) of the bare frame at the structure's fundamental period. Hence, it is expected that structure will remain near or below yielding considering the presence of infill walls. It can be stated that this level should produce immediate occupancy compatible damage levels.

b) 100% Duzce: Use of the actual Duzce ground motion recorded in 1999 Adapazari earthquake can represent the hazard level realistically for less frequent events.

c) 140% Duzce: This hazard level will correspond to a severe and rare earthquake and has approximately similar Sa value with the Turkish Earthquake Design Spectrum for Zone 1 on firm soil conditions at the pre-test estimated fundamental period of the structure.

It should be kept in mind that recent studies on the seismicity of the region state that Turkish Earthquake Design Spectrum can give design S_a values well above those estimated by using realistic attenuation relationships (Kalkan and Gulkan,2004)

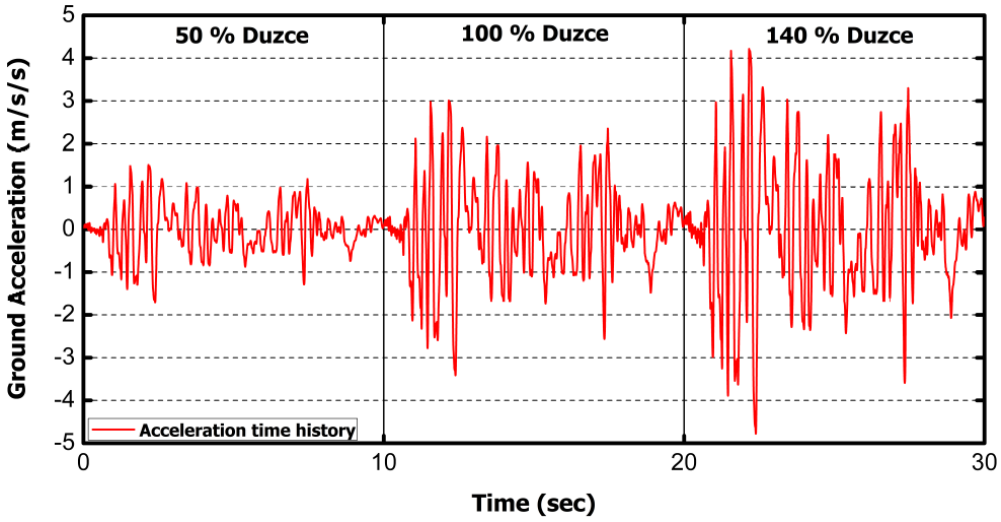

Figure 4.27 Ground acceleration time history.

Consequently, 100 and 140% ground motion tests were conducted on damaged specimens. It is believed that as long as the structure remained below minimum and moderate damage states for these two levels, respectively, the results of experiments could serve the purpose of relating damage with the displacement demand. The original ground motion is compressed in time by a factor of $1/\sqrt{2}$ to incorporate scale effects according to similitude law (Bertero et al., 1984; Elkhoraibi and Mosalam, 2007).

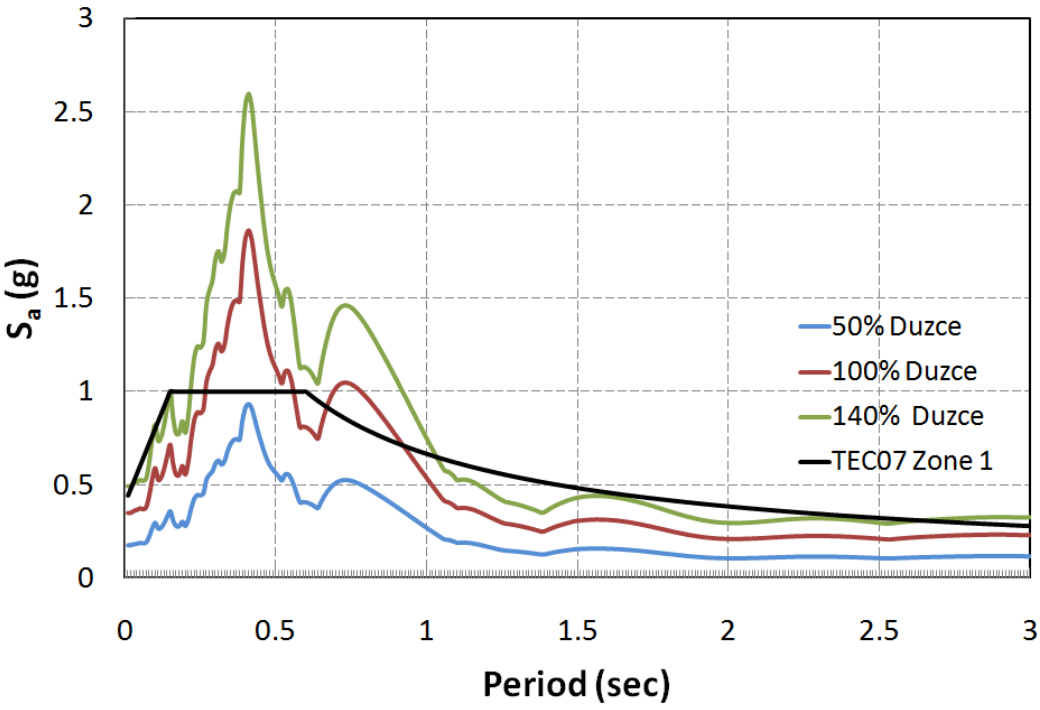

Figure 4.28 Spectrum of scaled ground motions

CHAPTER 5

REFERENCE FRAME

5.1. TEST RESULTS

In this chapter, test results and experimental observations are presented in detail. The time histories of ground motion used during the experiments, floor displacements, inter-story drift ratios, base shear, axial, shear and moment forces, curvatures at column bases, floor accelerations, identified damping ratio and initial periods of the test specimen are given. In addition, force deformation response of the specimen, moment-curvature response and moment interaction response of exterior columns are presented.

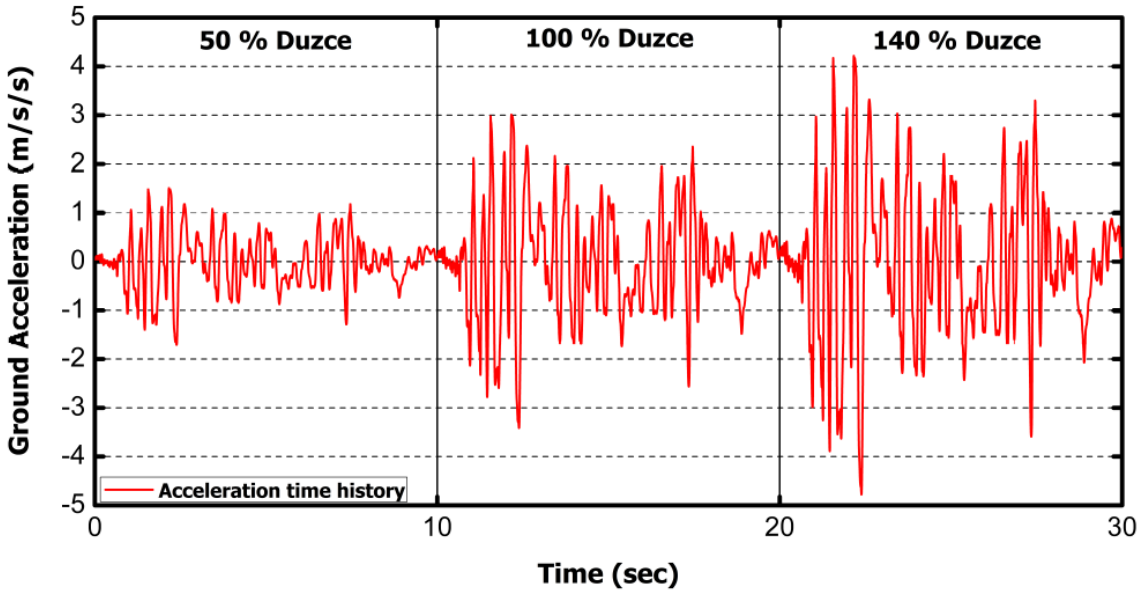

Figure 5.1 Ground acceleration time history.

Time histories of ground accelerations used in the experiments are shown in Figure 5.1. Three scaled, namely 50%, 100% and 140%, Duzce North-South component is implemented consecutively for the experiments.

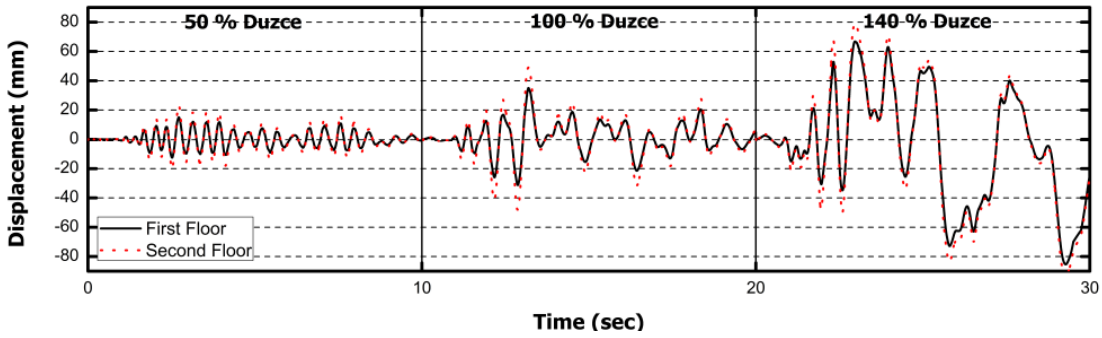

Figure 5.2 Time history of floor displacements.

At 50% scaled test tip displacement reached up to 23mm which results 0.7% drift ratio for first floor and 0.6% for second floor. In full scale ground motion experiment tip displacement was around 49 mm. In this test, drift ratio was around 1.8% for first floor and 1.1% for second floor. Maximum displacement values are reached at 140% scaled experiment (Figure 5.2). Peak displacement at 140% scaled experiment for first floor was around 85 mm for second floor and 94 mm for second floor.

Inter-story drift ratio is a considerable criterion for estimating damage states of a structure. Figure 5.3 shows time history of inter story drift ratios for first and second floors of the test frame. At 50% scaled experiment inter-story drift ratios are under 1% for both first and second floors. No significant damage was observed at interior and exterior columns. Interface cracks occurred on the infill wall. On the other hand, at 100% scaled experiment maximum inter-story drift ratios are around 2% for first floor and 1% for second floor. Plastic hinging at the bases of interior columns was observed and diagonal cracks were observed on the infill wall. At 140% scaled experiment inter-story drift ratio increased up to 4% for first floor.

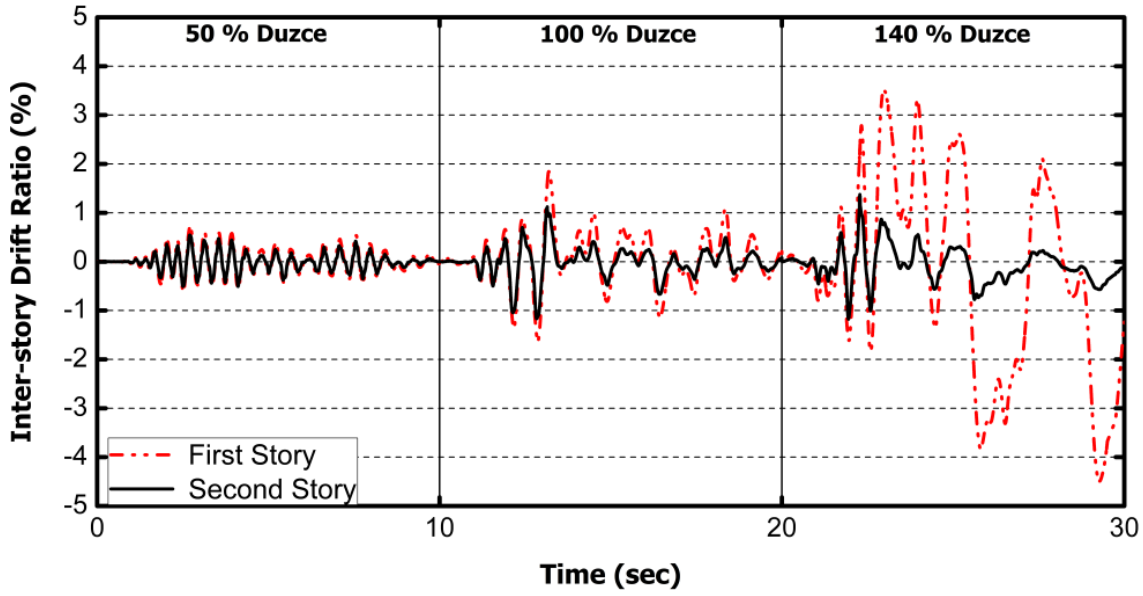

Figure 5.3 Time history of inter-story drift ratios.

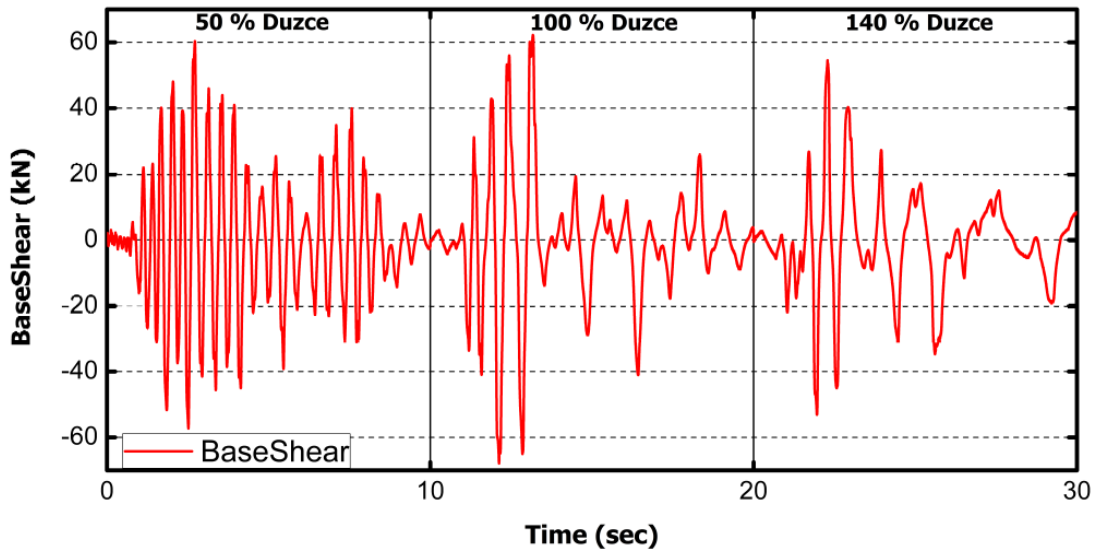

Figure 5.4 Time history of base shear.

Based on Figure 5.4, maximum base shear of the test specimen was around 60 kN at 50% scaled experiment. Test frame reached to its capacity; ~67 kN at 100% scaled experiment. After significant damage on the infill wall, decrease in the

base shear is observed at 140% scaled experiment. Maximum base shear at 140% scaled test was around 55 kN.

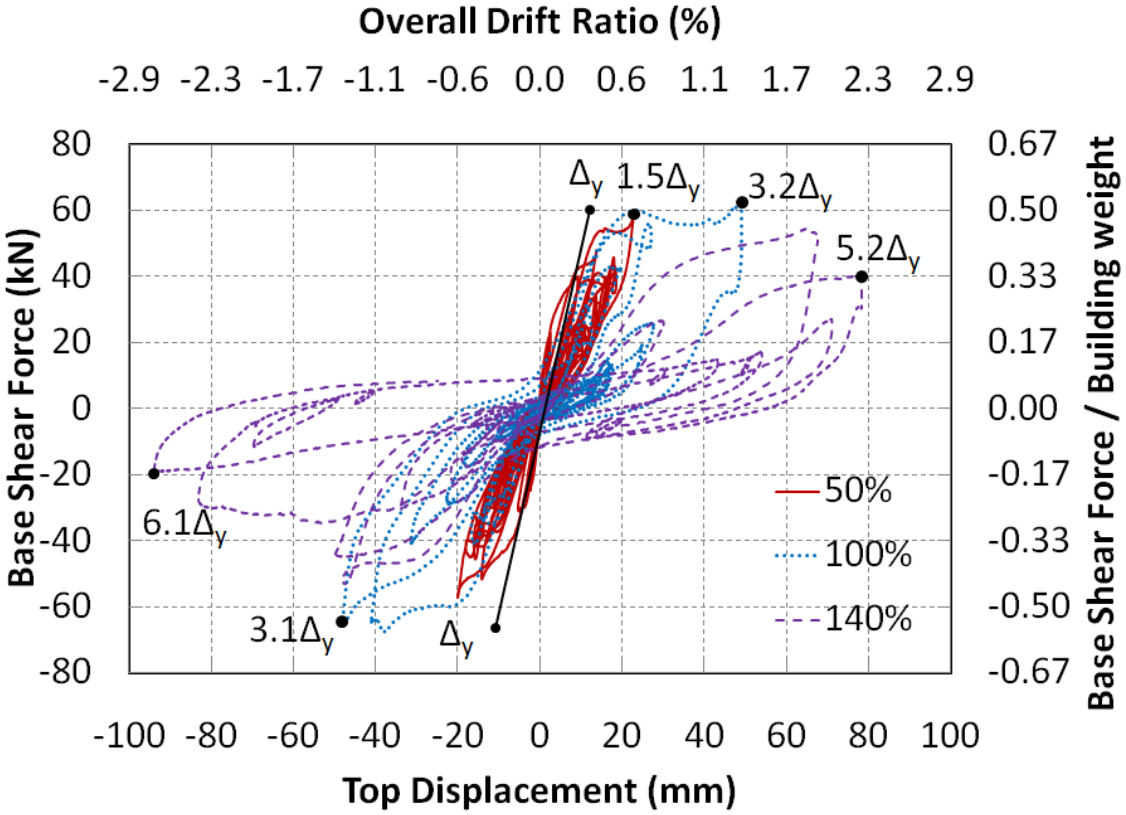

Figure 5.5 Force – Deformation Response.

In Figure 5.5 base shear versus roof displacement response of the displacement is presented. Yield displacement Δ_y (≈ 15 mm) is found by extending a line from origin and passing through a point on the initial loading curve that corresponds to 75% of the ultimate load carrying capacity. At 100% scaled experiment reached to its base shear capacity without any significant lateral strength drop at a displacement ductility of 3. At 140% scaled experiment lateral strength dropped about 30% of its maximum strength at a displacement of about 6 times its yield displacement.

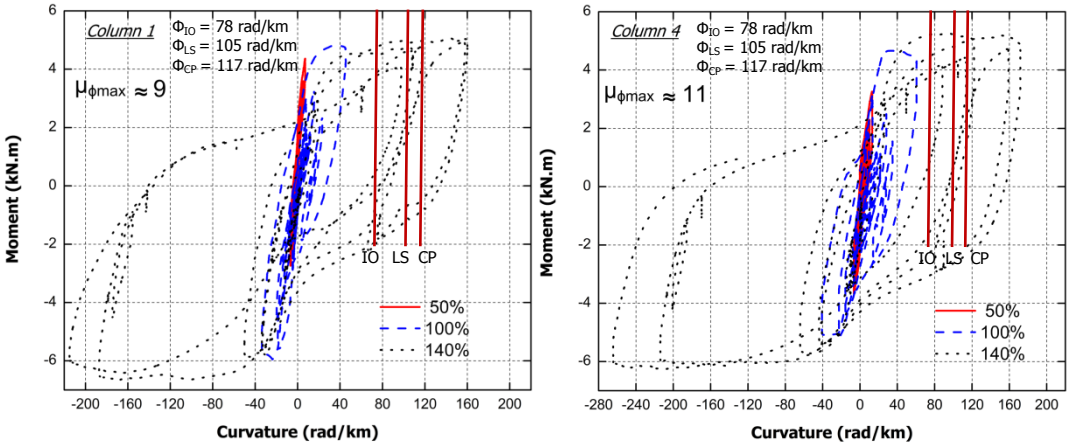

Figure 5.6 Moment – Curvature Diagrams of Column 1 and 4.

Moment-curvature response of columns C1 and C4 are presented in Figure 5.6. Measured column demands indicate plastic hinging of column bases experiencing a maximum curvature ductility demand of about 9 for column 1 and 11 for column 4. However, no significant loss of column lateral load carrying capacity was observed. Corresponding curvatures for immediate occupancy (ϕ_{IO}), life safety (ϕ_{LS}) and collapse prevention (ϕ_{CP}) according to TEC 2007 are also presented in Figure 5.6.

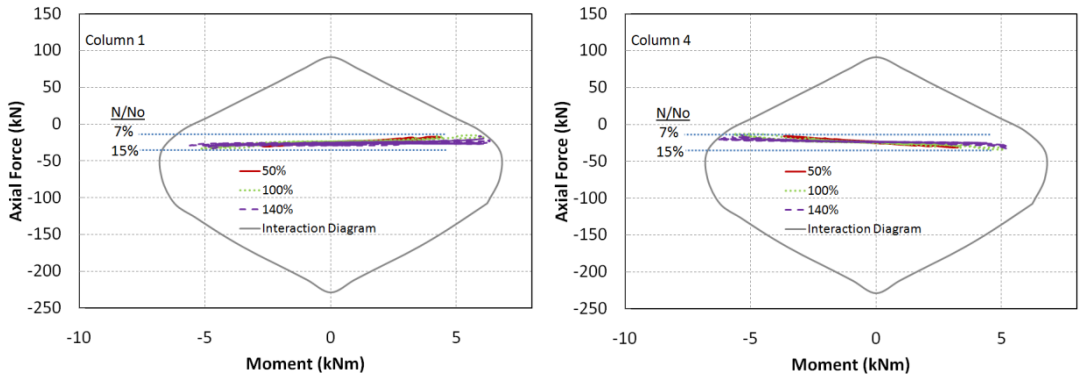

Figure 5.7 Moment Interaction Response of Column 1 and 4 (Response 2000).

Variation of axial force on columns 1 and 4 are shown in Figure 5.7. Axial force / axial force capacity was between 7-15 % on both columns.

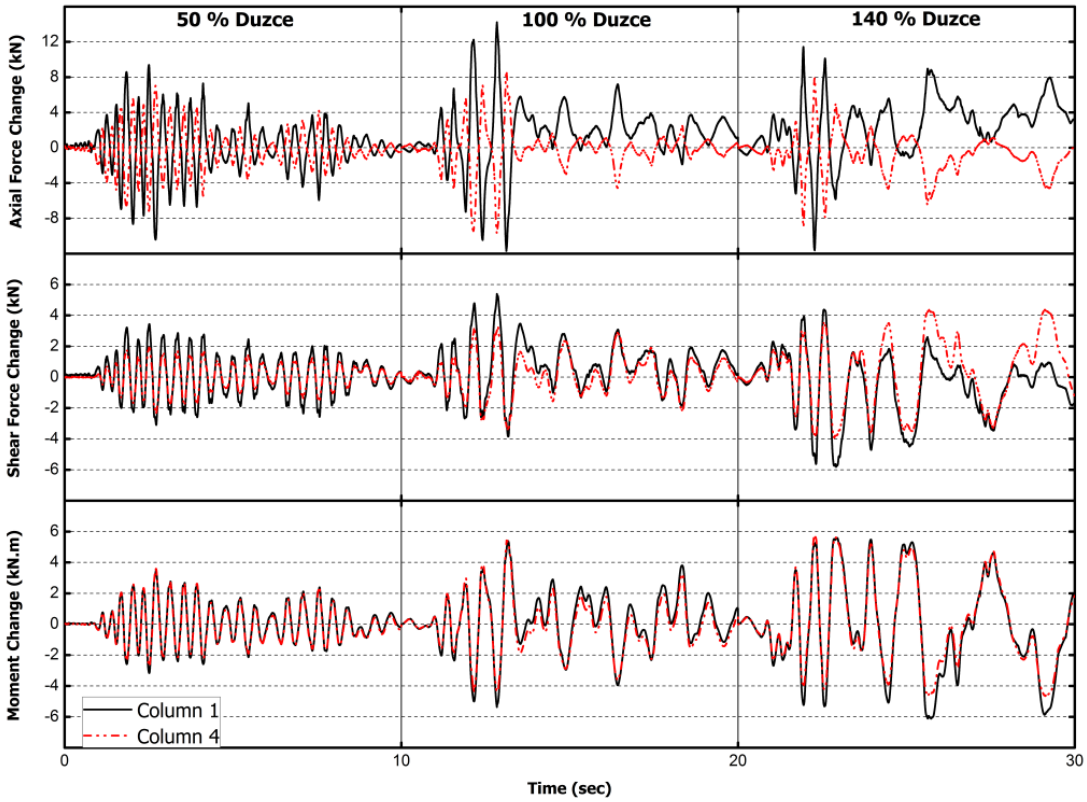

Figure 5.8 Time histories of axial, shear and moment forces change.

Force transducer readings are evaluated and following results are shown on Figure 5.8 and Figure 5.9. In Figure 5.8 change in axial, shear and moment forces during all scaled experiments are plotted. It can be easily observed that change in axial forces for exterior columns designated as 'Column 1' and 'Column 4' are reverse of each other due to overturning during experiments. Maximum changes for axial forces are 14.2 kN for tension at column 1 and -9.6 kN for compression at column 4. Maximum shear forces changes are observed at 140% scaled Duzce ground motion experiment; -5.8 kN for column 1 and 4.4 kN for column 4. The reason why maximum shear force changes for columns 1 and 4 are obtained at 140% scaled experiment is the failure of the infill wall and interior columns. Consequently, maximum changes of moment forces are obtained at the same phases of the

experiments as shear force changes. Peak changes of moment force for column 1 & 4 are -6.1 kN.m and 5.7 kN.m, respectively.

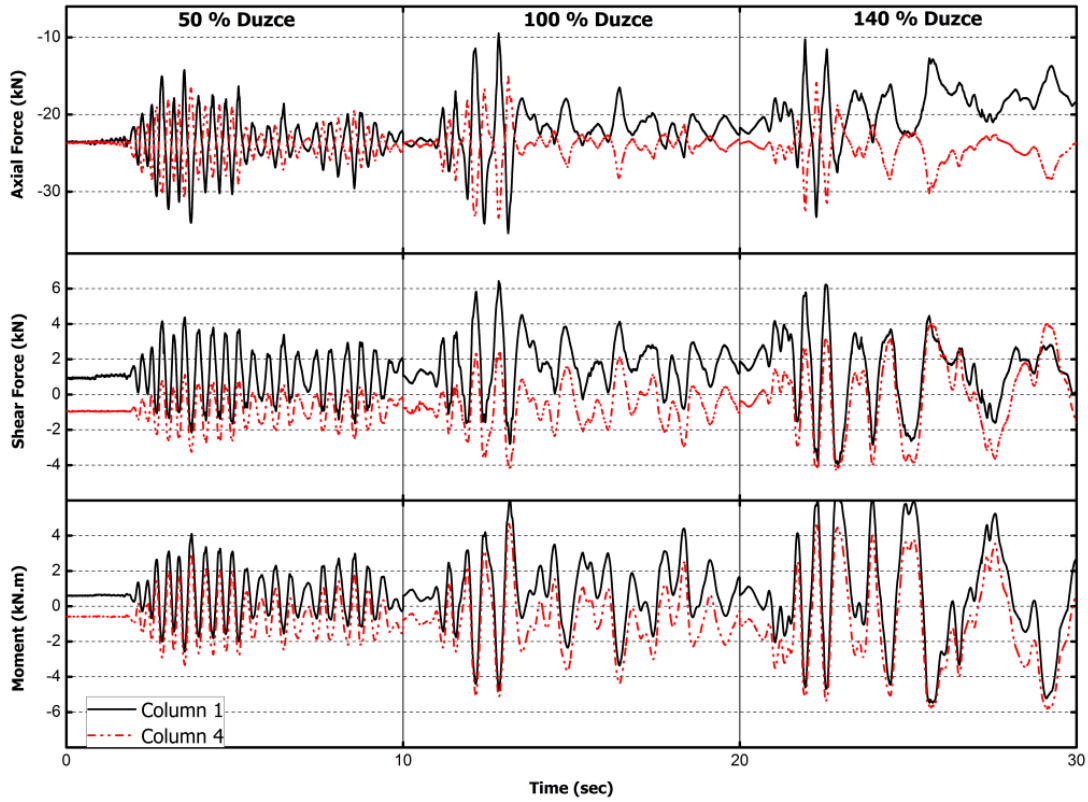

Figure 5.9 Time histories of axial, shear and moment forces.

Aforementioned force transducer readings are shown in Figure 5.9. At the time axial compression force is increasing on column 1, axial force on the column 4 is decreasing due to overturning. Shear forces on columns 1 and 4 have similar behaviors as expected. Sectional analyses show that moment capacity of the columns is about 6 kN.m. As it can be easily seen from Figure 5.9 plastic hinging of the columns 1 and 4 occurred at 100% scaled experiment.

Column bases curvatures are measured by means of LVDTs (see chapter 4). According to Figure 5.10, exterior columns did not experience any significant damage whereas interior columns had visually minor damage at 50% scaled experiment. Diagonal cracking on infill wall resulted increase in curvature values for both interior and exterior columns significantly at 100% scaled experiment. After failure of the infill wall at 140% scaled test, peak curvatures are observed.

Maximum values of curvatures are 215, 123, 390 and 264 rad/km for columns 1, 2, 3 and 4 respectively.

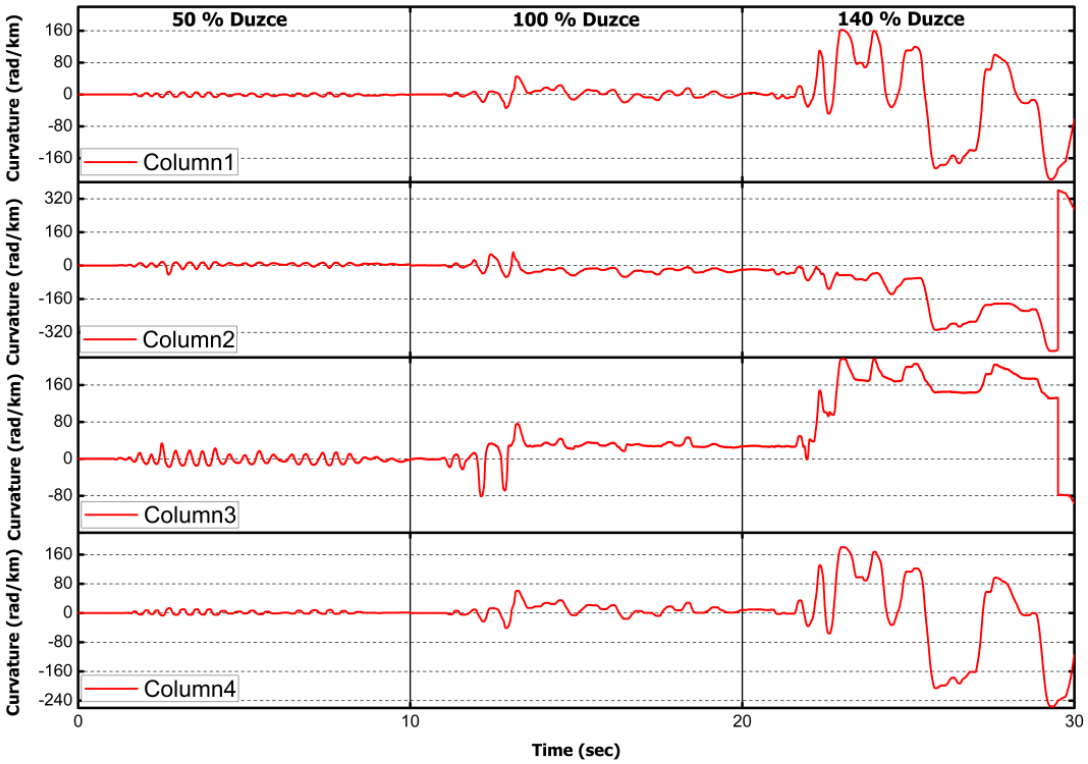

Figure 5.10 Time histories of curvatures at column bases.

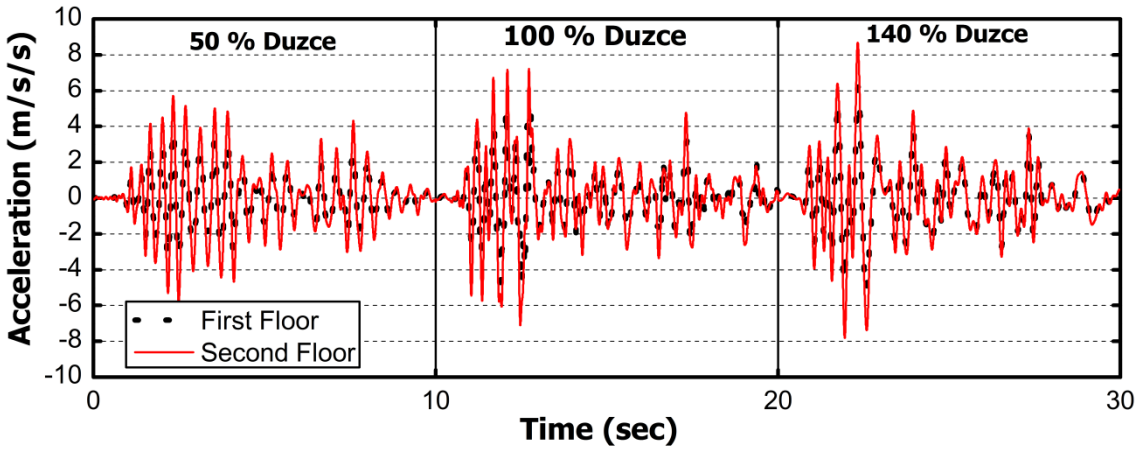

Figure 5.11 Floor Accelerations.

While drift demand is an important indication of damage state of the structure, the floor acceleration response is another important factor that might be considered since it affects the response of nonstructural elements and occupants of a building. Figure 5.11 presents the floor accelerations obtained from the experiments during whole excitation. The maximum floor acceleration observed was equal to 5.71 m/s^2 (~0.58g) for the 50% Duzce motion. The maximum floor accelerations for 100% Duzce motion was 7.22 m/s^2 (~0.74g) but after the first three seconds, the floor accelerations were much smaller, the maximum being 4 m/s^2. At 140% Duzce motion peak floor acceleration was 8.68 m/s^2 (~0.87g).

Time dependent dynamic properties, namely period and equivalent viscous damping, of the test frame are determined according to the procedure proposed by Molina et. al. (1999).

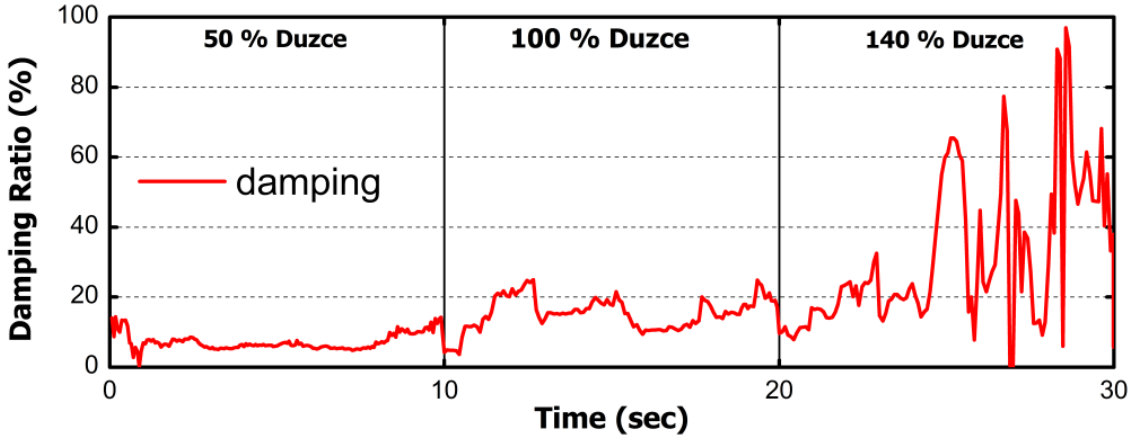

Figure 5.12 Identified Damping Ratio.

Figure 5.12 presents the variation of damping ratio of the first mode in time for test specimen. At 50% Duzce motion, maximum damping ratio was around 14%. Peak damping ratio at full scale Duzce motion was ~25%. Damping ratio reached up to ~90% at 140% Duzce motion.

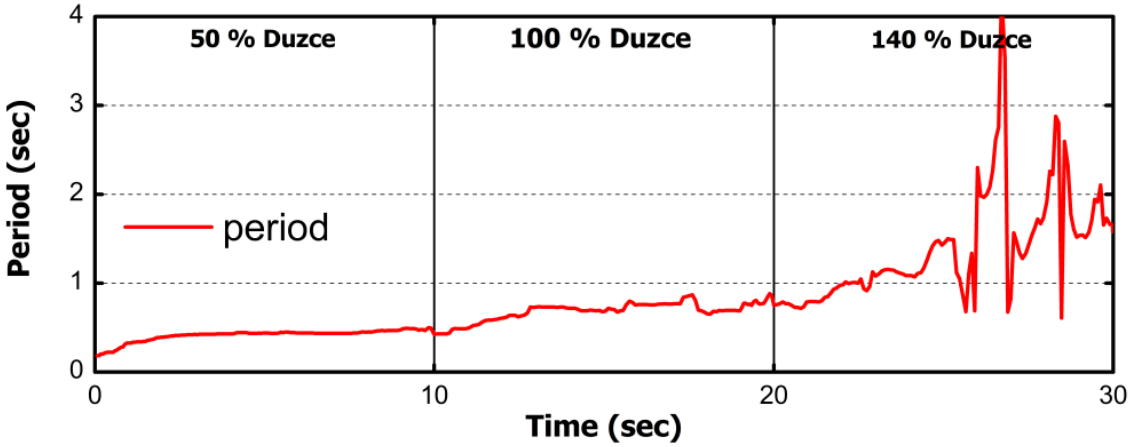

Figure 5.13 Identified Period of the Test Specimen.

Initial period of the test specimen was 0.17 seconds (Figure 5.13). At the end of the 50% Duzce motion, after some minor damages occurred on the

structure, test structure's period increased to 0.43 seconds. Full scale Duzce motion ended with a period of 0.75 seconds.

In Figure 5.14 inter-story drift ratios and observed damage states are presented. Photos are correlated with specific points at time history of inter-story drift ratios. At point A, flexural cracks on interior columns and interface cracks between infill wall and surrounding columns at first floor were observed. At point B, spalling of concrete and longitudinal bar buckling took place. At point C, compression strut formation was clearly seen. At point D, two bar buckling regions were observed. At final state of the experiments global buckling of the first floor interior columns and failure of infill wall occurred. Table 5.1 summarizes the global and local parameters obtained during whole ground motions.

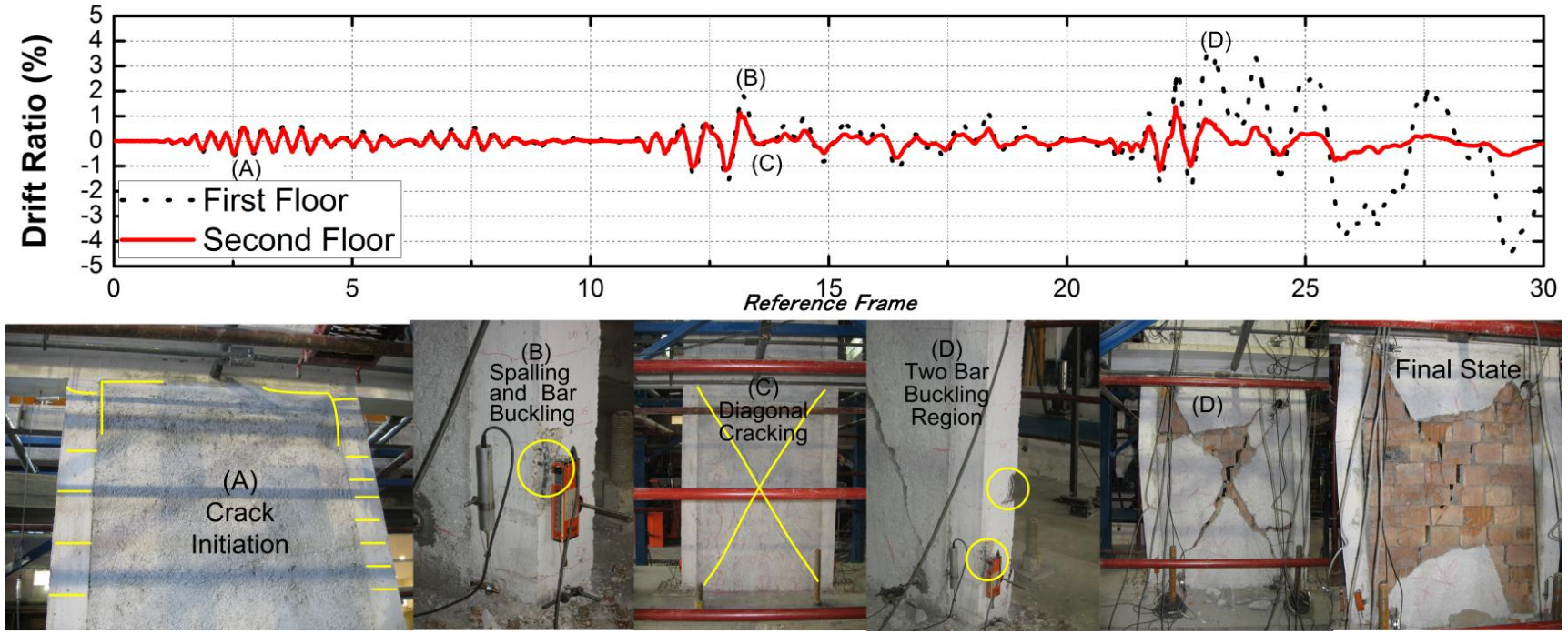

Figure 5.14 Drift Ratio and Observed Damage

Table 5.1 Summary of Results

Ground Motion	Maximum Displacement Demand (mm)		Maximum Interstory Drift Ratio (%)		Maximum Story Base Shear Force (kN)		Column Plastic Rotation Demands			
	1st Story	2nd Story	1st Story	2nd Story	1st Story	2nd Story	θ_{p1} $\mu_{\phi 1}$	θ_{p2} $\mu_{\phi 2}$	θ_{p3} $\mu_{\phi 3}$	θ_{p4} $\mu_{\phi 4}$
50% Duzce	15	23	0.7	0.6	60.4	27.6	0 0.3	0.003 1.9	0.001 1.5	0 0.6
100% Duzce	35	49	1.8	1.1	67.9	58.2	0.004 2.0	0.006 2.8	0.008 3.5	0.006 2.6
140% Duzce	85.3	93.8	4.5	1.4	54.5	52.9	0.038 9.4	0.055 16.9	0.025 8.3	0.036 11.5

*: Plastic rotation is calculated as θ_p = Gauge Length (Ultimate Curvature – Yield Curvature) where Gauge Length is 150mm

**: Curvature Ductility is calculated as μ_Φ = Ultimate Curvature / Yield Curvature

5.2. SUMMARY AND DISCUSSION OF TEST RESULTS

Experimental results of inter-story drift ratio (or simply drift ratio obtained as the difference of floor displacement divided by the floor height) versus time are presented in Figures 5.3 for the three ground motion scale levels. Important damage events are shown with pictures and marked on the time history response in Figure 5.14. Base shear versus roof displacement response of the specimen is presented in Figure 5.5. Experimentally obtained moment-curvature response and variations of axial force-moment along with the interaction diagram of columns for exterior columns named as C1 and C4 are presented in Figure 5.7. Table 5.1 presents the summary of test results based on obtained measurements and observations.

50% Duzce motion resulted in cracks at maximum moment regions of the first story columns. In addition, interface cracks were observed at the infill wall-frame boundaries indicating the separation of the infill walls along one diagonal. Infill wall mainly contributed to the load carrying capacity by the compression strut action judged from the closing of previously formed interface cracks around the region under compression. Besides such cracking, no other significant damage was observed. Maximum roof displacement for this ground motion was about 23 mm,

resulting in inter-story drift ratios of about 0.7% and 0.6% at the first and second stories, respectively. Figure 5.5 indicates that significant stiffness reduction took place prior to the beginning of the second test. Maximum base shear capacity measured in this test was about 68 kN. Column base curvature measurements indicate that exterior columns did not experience any longitudinal steel yielding. On the other hand, interior columns had minor plastic rotation demands (Table 5.1). Based on the observed damage and measurements the test structure has experienced minor damage and remains functional without any significant repair effort. Based on measured demand parameters and judgment of the observed damage state, immediate occupancy level damage criterion is satisfied.

Afterwards, the same frame was tested with 100% scaled Duzce motion. In this ground motion scale, 50 mm maximum top displacement was observed which resulted in a maximum inter story drift ratio of 1.8 % and 1.1 % at first and second stories, respectively. Two important damage events were observed for this ground motion level:

1) Concrete crushing at column base of interior columns followed by longitudinal bar buckling.

2) Significant diagonal cracking along the diagonals of the first story infill wall.

Figure 5.5 indicates that the frame sustained its base shear capacity (67.9 kN) without any significant strength drop up to a displacement ductility of about 3. Same graph shows that the hysteretic behavior was severely pinched due to opening and closing of diagonal cracks on the first story infill wall. Exterior columns reached to their moment carrying capacity and experienced a curvature ductility of about 2. The maximum plastic rotation demand at the column base was about 0.01. The results indicate that for this earthquake level, structural elements experienced some yielding and nonstructural elements sustained significant cracking while remaining intact. The structure was capable of withstanding the deformation demands without any significant drop of lateral strength and could be occupied after strengthening if needed. Hence, the structure satisfies the life safety performance criterion based on engineering judgment.

Finally, 140% Duzce was applied on the test structure to observe the final damage state. A maximum top displacement of 94 mm was measured

corresponding to a 4.5% maximum inter-story drift ratio in the first story. First story plastic mechanism (i.e. formation of a soft story) was observed, where the second story sustained drift levels not exceeding 1.4 %. Lateral strength of the frame degraded to about 30% of its maximum strength at a displacement ductility demand of about 6. Loss of significant lateral strength was mainly due to the distress observed in the first story infill wall (Figure 5.5). Extended diagonal cracking and separation of plaster from infill wall surface was observed. Measured column demands (Table 5.1) indicated that plastic hinging of column bases demanded a maximum curvature ductility of about 17. As the infill wall was distorted due to large crack openings, damage on the interior columns shifted upwards (Figure 5.14). Longitudinal bar buckling was observed both in top and bottom plastic hinges of the interior columns. Results show that the test frame is unsafe for occupancy purposes and can be labeled to be at the collapse state (although no gravity collapse took place) due to the following reasons:

1) The infill wall is susceptible to out of plane collapse for any out of plane disturbance.

2) Lateral strength has significantly deteriorated.

3) Repair is not possible due significant damage in the structural and non-structural elements.

4) A stability problem arise as the longitudinal bar buckling is observed.

Figure 5.7 presents the variation of axial force with bending moment at exterior column bases. The axial load level due to gravity loads on the columns was determined as 10% and 22% for the exterior and interior column axial load carrying capacities, respectively. The axial load varied between 7 to 15% of the axial load carrying capacity of the exterior columns during the tests. The test frame had a lateral load carrying capacity ratio (lateral load divided by building weight) of about 0.5. This capacity was maintained in the first two tests. Upon failure of the infill wall at a maximum inter-story drift ratio of about 1.5% in one direction, lateral load capacity ratio rapidly dropped to about 0.17 in the first few seconds of the 140% Duzce. This capacity ratio is similar to that of the bare frame, which was about 35% of the test structure. Hence, we observe that presence of the infill wall was effective

up to an overall drift ratio of about 1.2% (corresponding interstory drift ratio was about 1.5%), beyond which, bare frame behavior governed the response.

CHAPTER 6

FIBER REINFORCED POLYMERS (FRP) RETROFITTED FRAME

6.1. TEST RESULTS

First and second floor displacements are gathered by means of the data acquisition system. Time history of both floor displacements is plotted (Figure 6.1). At 50% scaled experiment, maximum displacements for first and second floors followed a ratio of 0.57:1 as the ratio of first floor to total height. Peak displacements at this level of test for the first and second floors were 2.15 mm and 3.95 mm, respectively. Full scaled Duzce ground motion showed nearly the same ratio of displacement ratio. Maximum first floor displacement was 13 mm whereas peak tip displacement was 21.81 mm. Upon FRP anchorage failure and scale of the excitation, displacements yielded higher values at 140% ground motion compared to preceding experiments. Displacements reached to 42 mm and 71.8 mm for first and second floors, respectively.

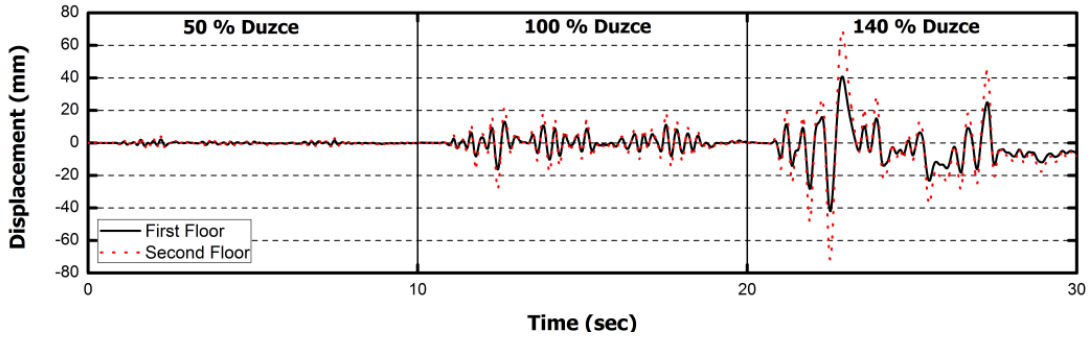

Figure 6.1 Time history of floor displacements.

Inter-story drift ratio (IDR) is calculated as relative floor displacement divided by floor height.. Time history of IDRs is drawn in Figure 6.2 for all scales of ground motions. As small displacements (2~3 mm) occurred at 50% Duzce ground motion, IDRs were around 0.1%. IDRs remained below 1% at full scaled ground motion. Maximum IDRs were observed at 140% ground motion. IDRs at first and second floors were 2% and 1.9% at peak, respectively.

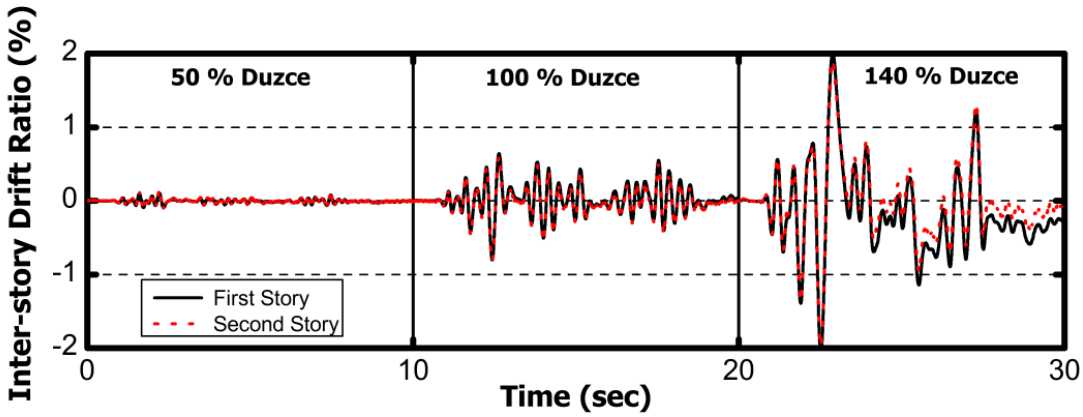

Figure 6.2 Time history of inter-story drift ratios.

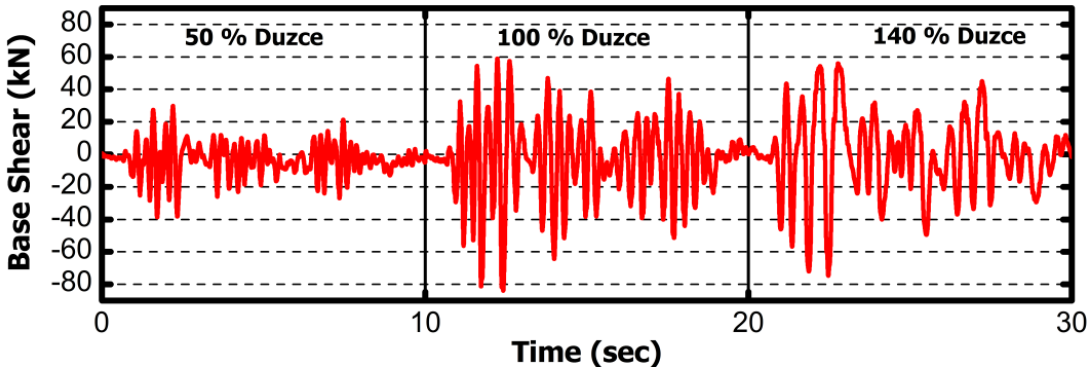

Figure 6.3 Time history of base shear.

Based on Figure 6.3, maximum base shear of the retrofitted test specimen was around 40 kN at 50% scaled experiment. Test frame reached to its capacity;

~84 kN at 100% scaled experiment. After failure of the base FRP anchorages, decrease in the base shear is observed at 140% scaled experiment. Maximum base shear at 140% scaled test was around 55 kN.

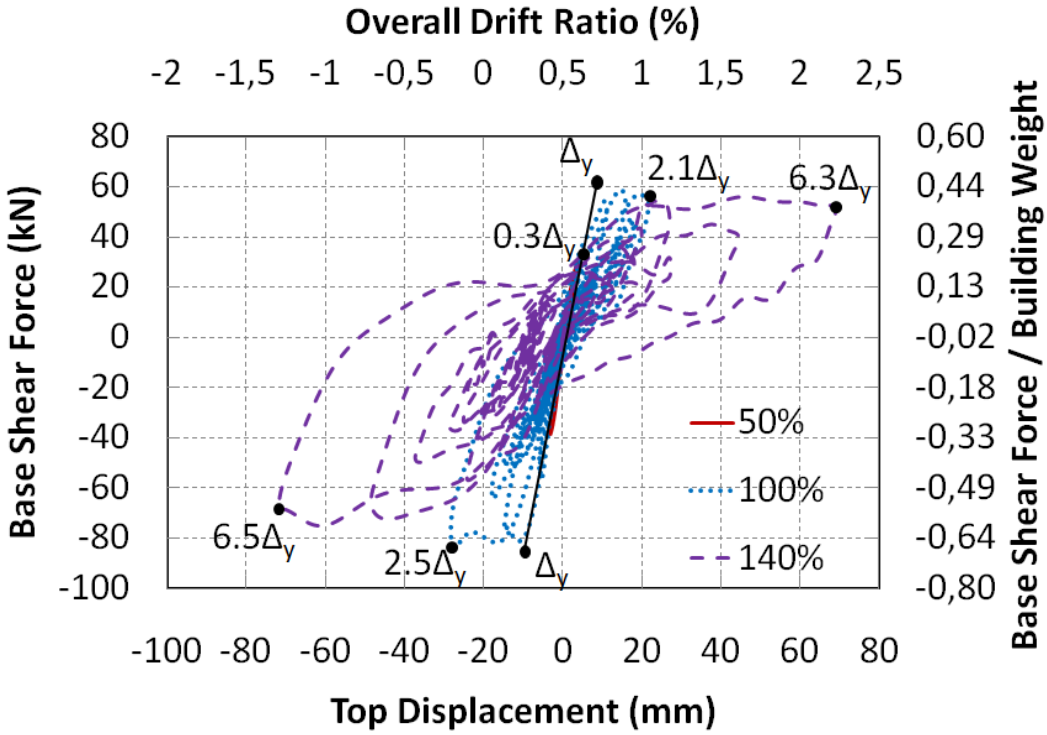

Figure 6.4 Force – Deformation Response.

In Figure 6.4 base shear versus roof displacement response is presented. Yield displacement, Δ_y ($\approx$ 12 mm) is found by extending a line from origin and passing through a point on the initial loading curve that corresponds to 75% of the ultimate load carrying capacity. At 100% scaled specimen reached to its base shear capacity without any significant lateral strength drop at a displacement ductility level of 2. At 140% ground motion FRP retrofitted frame was nearly capable of retaining its lateral strength. Lateral strength decreased about 88% of its maximum strength at a displacement of about 6.5 times its yield displacement.

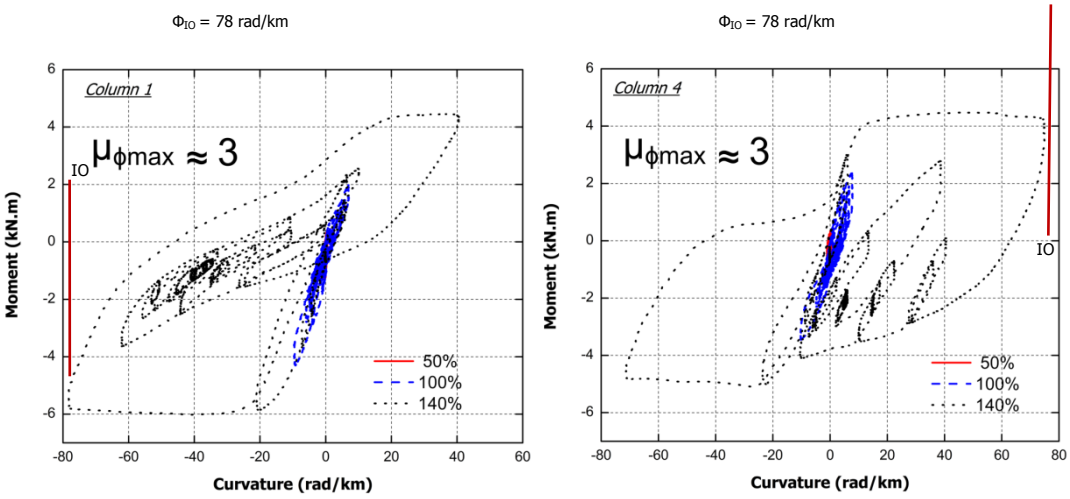

Figure 6.5 Moment – Curvature Diagrams of Column 1 and 4.

Moment-curvature response of columns C1 and C4 are presented in Figure 6.5. Measured column demands indicate plastic hinging of column bases experiencing a maximum curvature ductility demand of about 3 for exterior columns. However, no significant loss of column lateral load carrying capacity was observed.

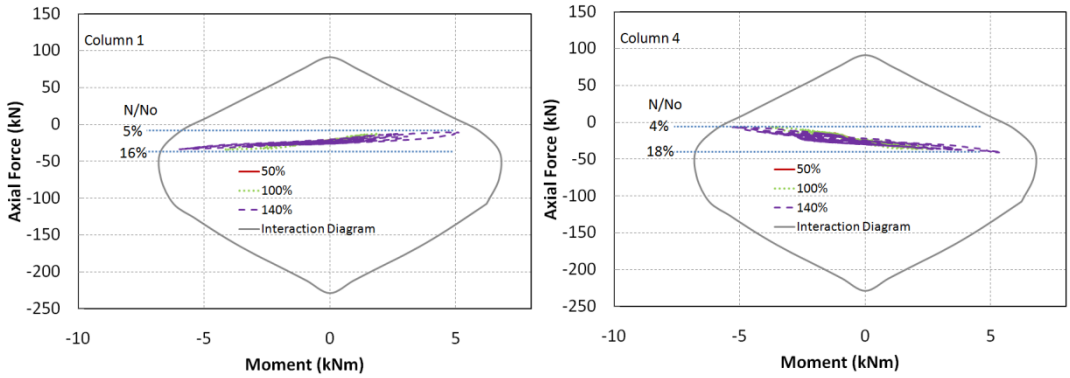

Figure 6.6 Moment Interaction Response of Column 1 and 4.

Variation of axial force on columns 1 and 4 are shown in Figure 6.6. Axial force / axial force capacity was between 5-16 % for column 1 and 4-18 % for column 4.

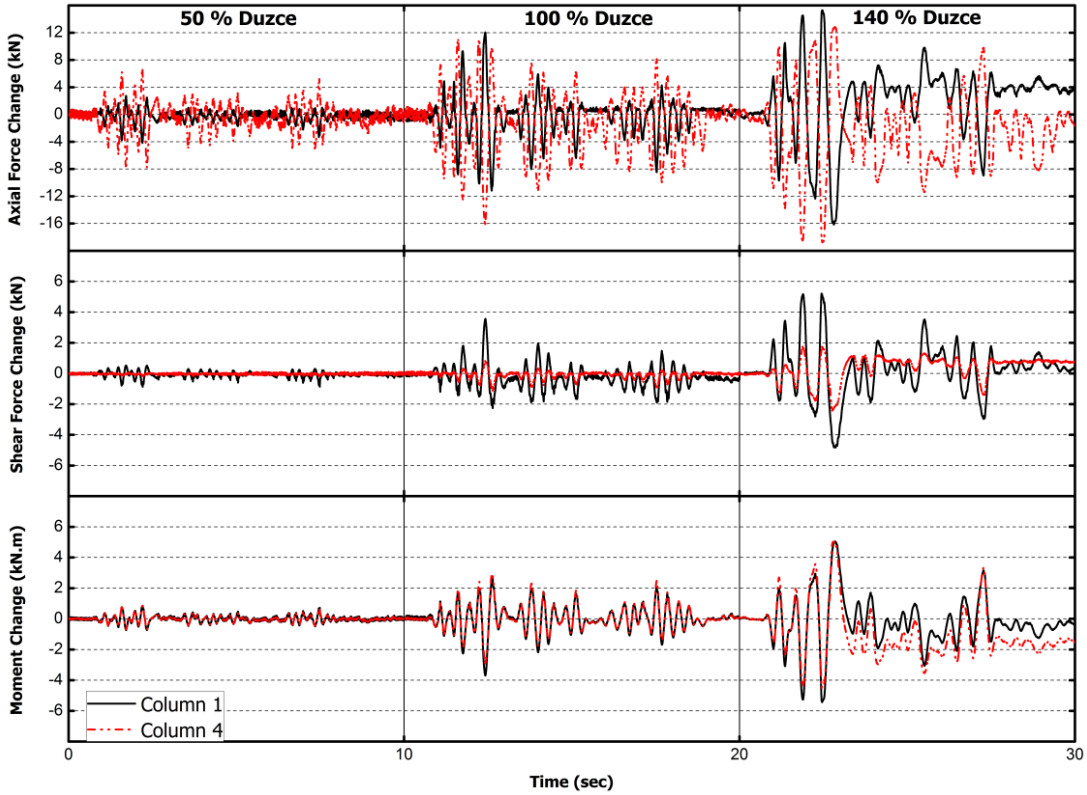

Figure 6.7 Time histories of axial, shear and moment force changes.

Force transduce readings are collected as mV / V. These readings are evaluated by a pre-determined matrix. This matrix was calibrated and converted mV / V data to axial, shear, and moment forces. In Figure 6.7 change in axial, shear and moment forces during all scaled experiments are plotted. It can be easily observed that change in axial forces for exterior columns designated as 'Column 1' and 'Column 4' are reverse of each other. This situation is an indicator of overturning effect during experiments. Maximum changes for axial forces are 16.1 kN for tension at column 1 and 18.8 kN for tension at column 4. Maximum shear forces changes are observed at 140% scaled Duzce ground motion experiment; 5.2 kN for column 1 and -2.4 kN for column 4. The reason why maximum shear force changes for columns 1 and 4 are obtained at 140% scaled experiment is the failure of base FRP anchorage on one side. Consequently, maximum changes of moment forces are obtained at the same phases of the experiments as shear force changes.

Peak changes of moment force for column 1 & 4 are -5.4 kN.m and 5.0 kN.m, respectively.

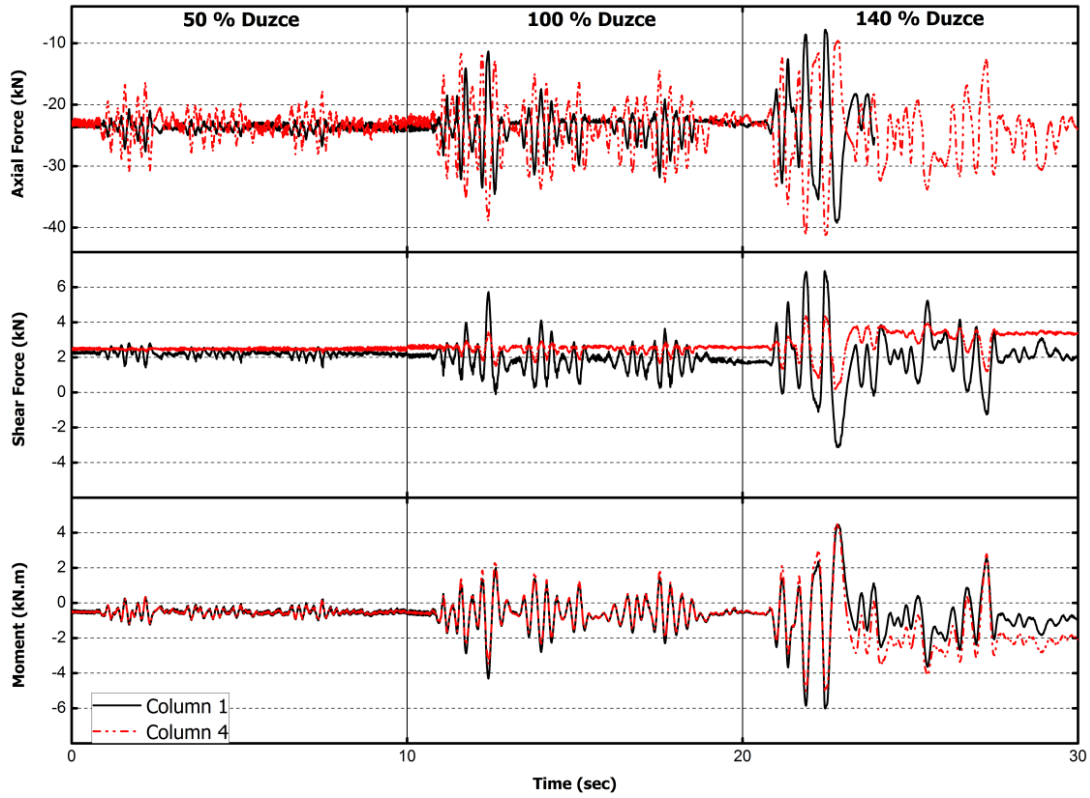

Figure 6.8 Time histories of axial, shear and moment forces.

Aforementioned force transducer readings are shown in Figure 6.8. Shear forces on columns 1 and 4 have similar behaviors as expected. Sectional analyses show that moment capacity of the columns is about 6 kN.m. As it can be easily seen from Figure 6.8, plastic hinging of the columns 1 and 4 occurred at 140% scaled experiment.

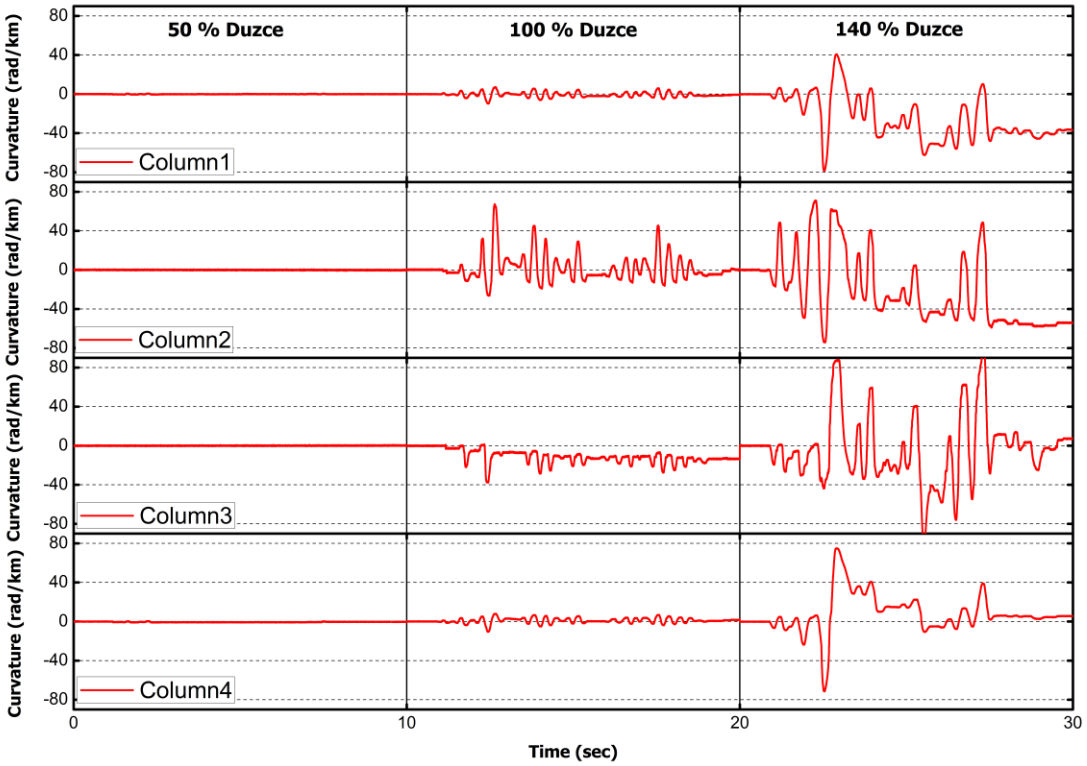

Figure 6.9 Time histories of curvatures at column bases.

Column bases curvatures are measured by means of LVDTs (see chapter 4). Exterior and interior columns did not experience any significant damage at 50% scaled experiment (Figure 6.9). Interior column curvature values increased significantly at 100% scaled experiment. Upon failure of base FRP anchorages at 140% scaled test, peak curvatures are observed. Maximum values of curvatures are 74, 78, 99 and 71 rad/km for columns 1, 2, 3 and 4 respectively.

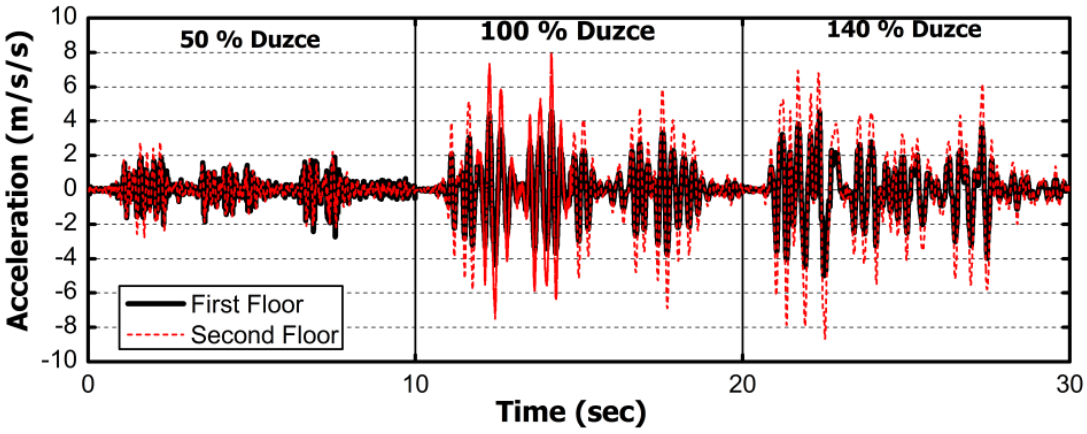

Figure 6.10 Floor Accelerations.

Figure 6.10 presents the floor accelerations obtained from the FRP retrofitted experiments during the complete motion. The maximum floor acceleration observed was equal to 2.78m/s^2 (~0.28g) for the 50% Duzce motion. The maximum floor acceleration ,7.59 m/s^2 (~0.76g), for 100% Duzce motion occurred at the fourteenth second but the accelerations were around 0.5g throughout the whole 100% Duzce motion. At 140% Duzce motion peak floor acceleration was 8.66 m/s^2 (~0.87g).

Figure 6.11 presents the variation of damping ratio of the first mode in time for test specimen. At 50% Duzce motion, maximum damping ratio was around 32%. Peak damping ratio at full scale Duzce motion was ~29%. Damping ratio reached up to ~63% at 140% Duzce motion.

Initial period of the test specimen was 0.15 seconds (Figure 6.12). At the end of the 50% Duzce motion, after some minor damages experienced on the structure, test structure's period increased to 0.18 seconds. Full scale Duzce motion ended up with a period of 0.30 seconds.

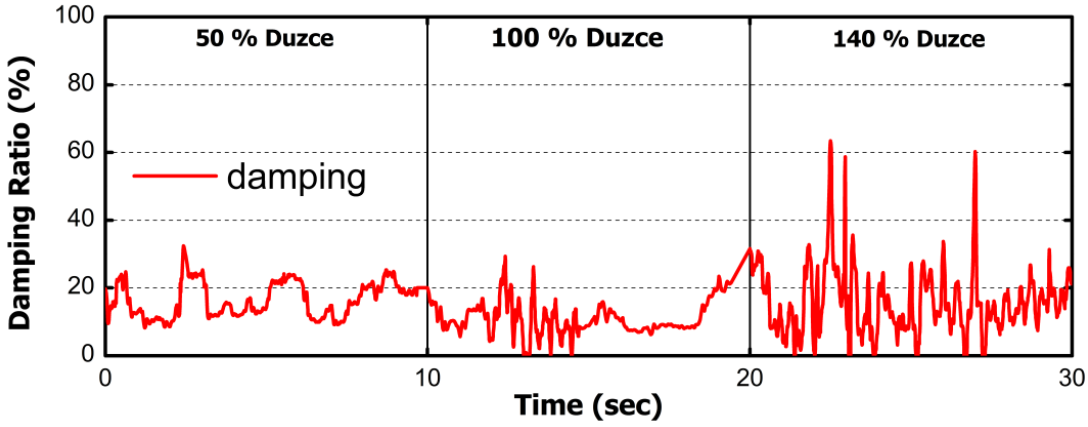

Figure 6.11 Identified Damping Ratio.

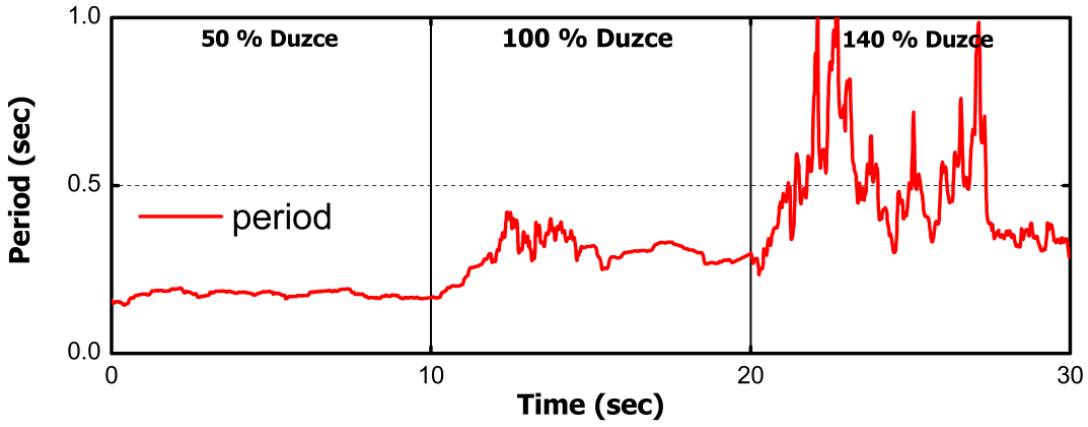

Figure 6.12 Identified Period of the Test Specimen.

In Figure 6.13 inter-story drift ratios and observed damages states are presented. Photos are matched with specific points at time history of inter-story drift ratios. At point A, flexural crack inition on interior columns and at first floor was observed. At point B, base FRP anchorage slip took place. At point C, failure of base FRP anchorages was clearly seen. Final state of the experiemnts is also presented in Figure 6.13. A brief summary of test results are tabulated in Table 6.1.

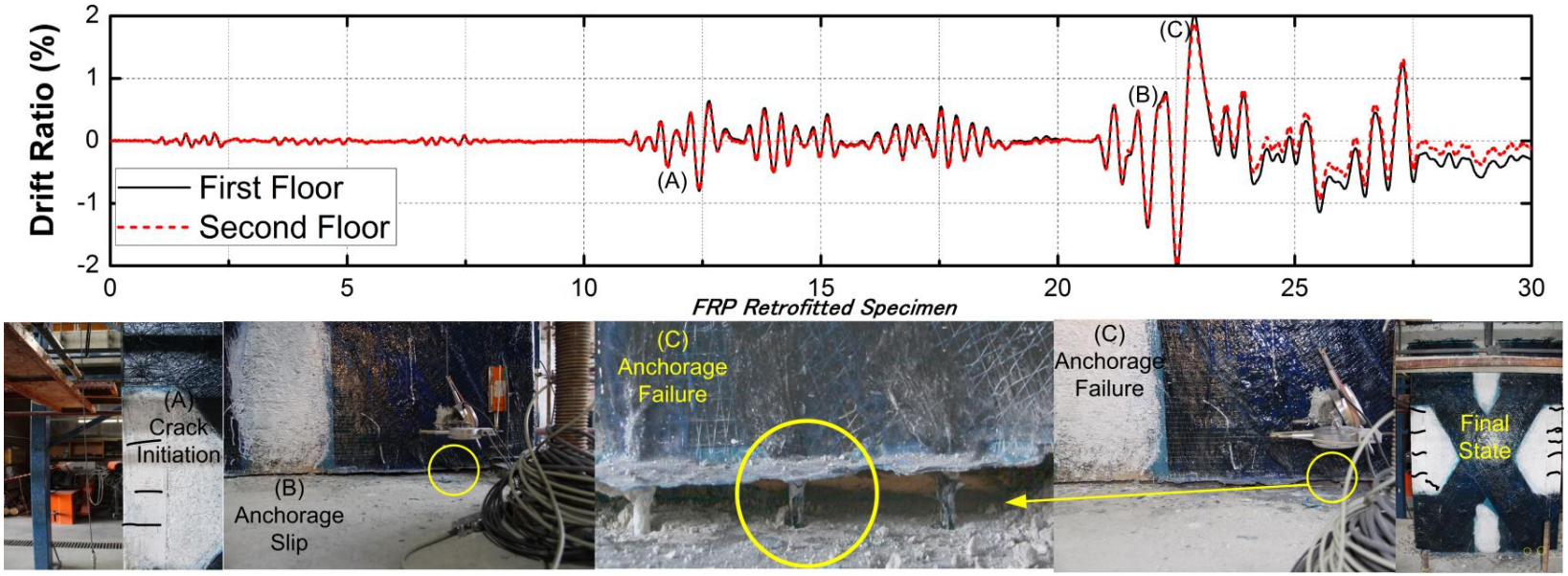

Figure 6.13 Drift Ratio and Observed Damage

Table 6.1 Summary of Results.

Ground Motion	Maximum Displacement Demand (mm)		Maximum Interstory DriftRatio (%)		Maximum Story Base Shear Force (kN)		Column Plastic Rotation Demands			
	1st Story	2nd Story	1st Story	2nd Story	1st Story	2nd Story	θ_{p1} $\mu_{\phi 1}$	θ_{p2} $\mu_{\phi 2}$	θ_{p3} $\mu_{\phi 3}$	θ_{p4} $\mu_{\phi 4}$
50% Duzce	2.2	4	0.1	0.1	38.7	26.5	0 0.03	0 0.05	0 0.04	0 0.05
100% Duzce	16.3	28.2	0.8	0.8	83.9	57.9	0 0.42	0.006 2.93	0.002 1.64	0 0.46
140% Duzce	42	71.8	2.1	2.0	74.8	53.7	0.008 3.41	0.007 3.22	0.011 4.29	0.008 3.1

*: Plastic rotation is calculated as θ_p = Gauge Length (Ultimate Curvature – Yield Curvature) where Gauge Length is 150mm

**: Curvature Ductility is calculated as μ_Φ = Ultimate Curvature / Yield Curvature

6.2. SUMMARY AND DISCUSSION OF TEST RESULTS

Experimental results of inter-story drift ratio versus time are presented in Figures 6.13 for the three ground motion scale levels. Important damage events are shown with pictures and marked on the time history response in Figure 6.13. Base shear versus roof displacement response of the specimen is presented in Figure 6.4. Experimentally obtained moment-curvature response and variations of axial force-moment along with the interaction diagram of columns for exterior columns named as C1 and C4 are presented in Figure 6.6. Table 6.1 presents the summary of test results based on obtained measurements and observations.

50% Duzce motion resulted in flexural cracks at interior columns of the first story columns. No additional significant damage was observed at this scaled ground motion. Maximum roof displacement for this ground motion was about 4 mm, resulting in inter-story drift ratios of about 0.1% for both stories. Figure 6.4 indicates that no significant stiffness deterioration took place prior to the beginning of the second test. Maximum base shear capacity measured in this test was about 84 kN. Column base curvature measurements indicate that interior and exterior columns did not experience any longitudinal steel yielding. As a result, all columns had no plastic rotation demands (Table 6.1). Based on the observed damage and measurements, the test structure has experienced minor damage and remained

functional without any need of repairs. Based on measured demand parameters and judgment of the observed damage state, immediate occupancy level damage criterion is satisfied.

Afterwards, the same frame was tested with 100% scaled Duzce motion. In this ground motion scale, 50 mm maximum top displacement was observed which resulted in a maximum inter story drift ratio of 0.8% for both stories. Two important damage events were observed for this ground motion level:

1) Base FRP anchorage slip

2) Specimen exhibited lift off from the foundation due to the extension/slip of FRP dowels.

Figure 6.4 indicates that the frame sustained its base shear capacity (83.9 kN) without any significant strength drop up to a displacement ductility of about 2.5. Same graph shows that the hysteretic behavior was pinched due to extension/slip of FRP dowels at base. The maximum plastic rotation demand at the column base was about 0.006. The structure was capable of withstanding the deformation demands without any significant loss of lateral strength and can be occupied without any needs of repair. Hence, the structure satisfies the life safety performance criterion based on engineering judgement.

Finally, 140% Duzce ground motion was applied on the test structure to observe the final damage state. A maximum top displacement of 71.8 mm was measured corresponding to a 2.1% maximum inter-story drift ratio in the first story, where the second story sustained drift levels not exceeding 2.0 %. Lateral strength of the frame degraded to about 88% of its maximum strength at a displacement ductility demand of about 6.5. Retrofitted specimen exhibited limited damage, the most important event being the pull-out of FRP dowels at the base. The infill wall remained intact and was not susceptible to out of plane failure.

Figure 6.9 presents the variation of axial force with bending moment at exterior column bases. The axial load level due to gravity loads on the columns was determined as 10% and 22% for the exterior and interior column, respectively. The axial load varied between 5 to 16% and 4 to 18% of the axial load carrying capacity column 1 and column 4, respectively. The test frame had a lateral load carrying capacity ratio (lateral load divided by building weight) of about 0.64. This capacity was maintained in the second test. Although failure of FRP anchorages at the base

at 140% Duzce ground motion occured, the capacity ratio did not dropped significantly.

CHAPTER 7

PRECAST CONCRETE PANEL RETROFITTED FRAME

7.1. TEST RESULTS

Time history of both floor displacements is plotted (Figure 7.1). At 50% scaled experiment, peak displacements for first and second floors were 1.9 mm and 4.2 mm, respectively. Maximum first floor displacement was 14.3 mm whereas peak tip displacement was 26.4 mm. Following the damages on concrete panels and longitudinal bar buckling, displacements showed higher values at 140% ground motion compared to preceding experiments. Displacements reached to 28.2 mm and 48.8 mm for first and second floors, respectively.

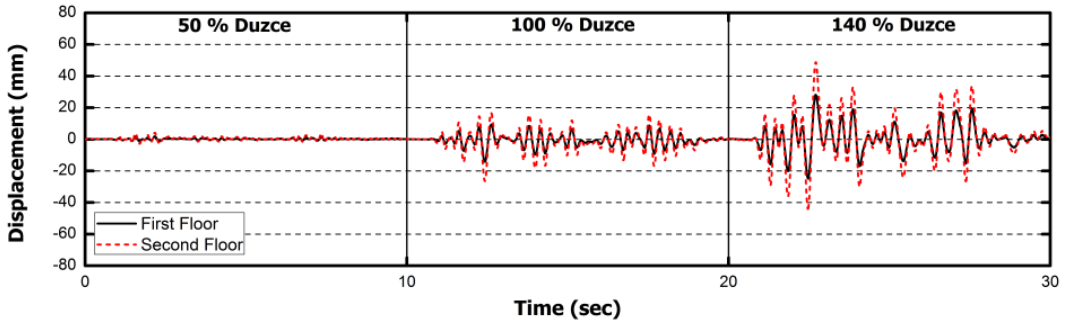

Figure 7.1 Time history of floor displacements.

Time history of IDRs is drawn in Figure 7.2 for all scales of ground motions. At 50% Duzce ground motion, IDRs were around 0.1%. IDRs at full scaled ground motion for first and second floors were 0.7% and 0.8%, respectively. Maximum

IDRs were observed at 140% ground motion. IDRs at first and second floors were around 1.4% at peak.

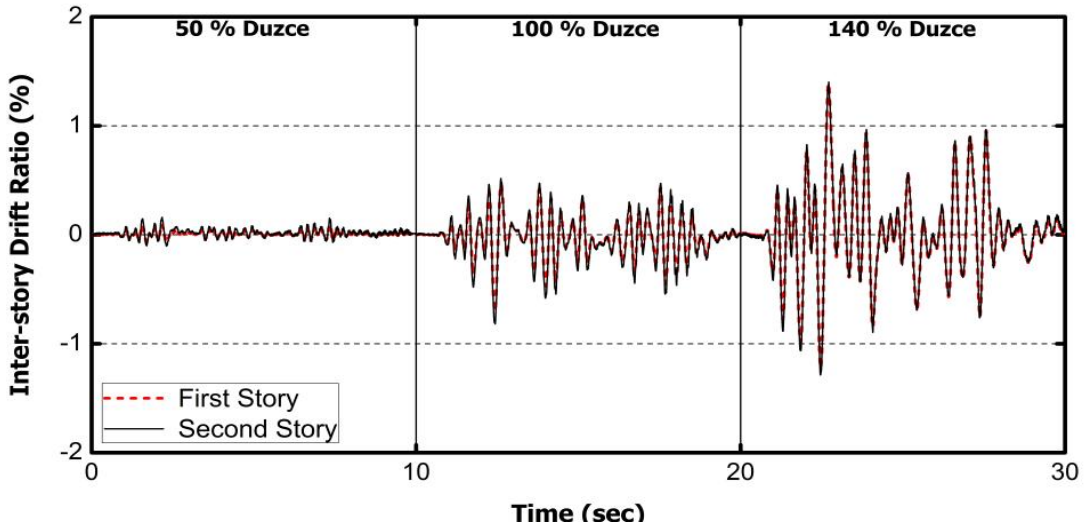

Figure 7.2 Time history of inter-story drift ratios.

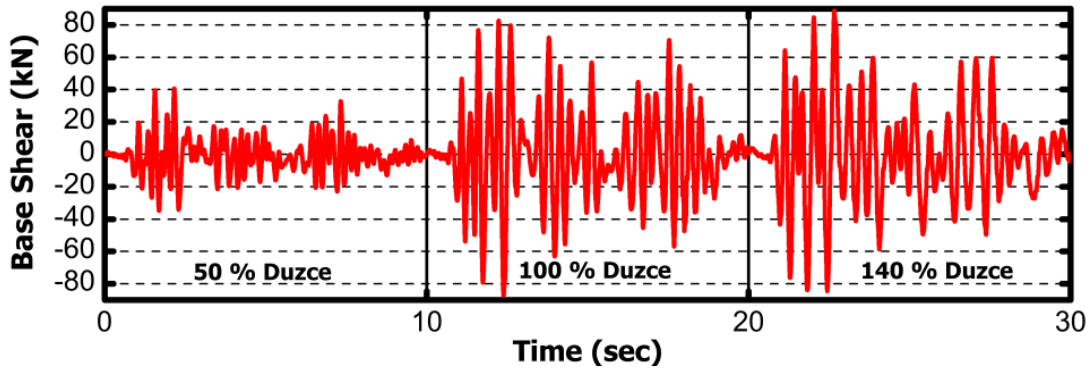

Figure 7.3 Time history of base shear.

Based on Figure 7.3, maximum base shear of the PCP retrofitted test specimen was around 40 kN at 50% scaled experiment. Test frame reached to its capacity; ~88 kN at 100% scaled experiment. Maximum base shear at 140% scaled test was also around 88 kN.

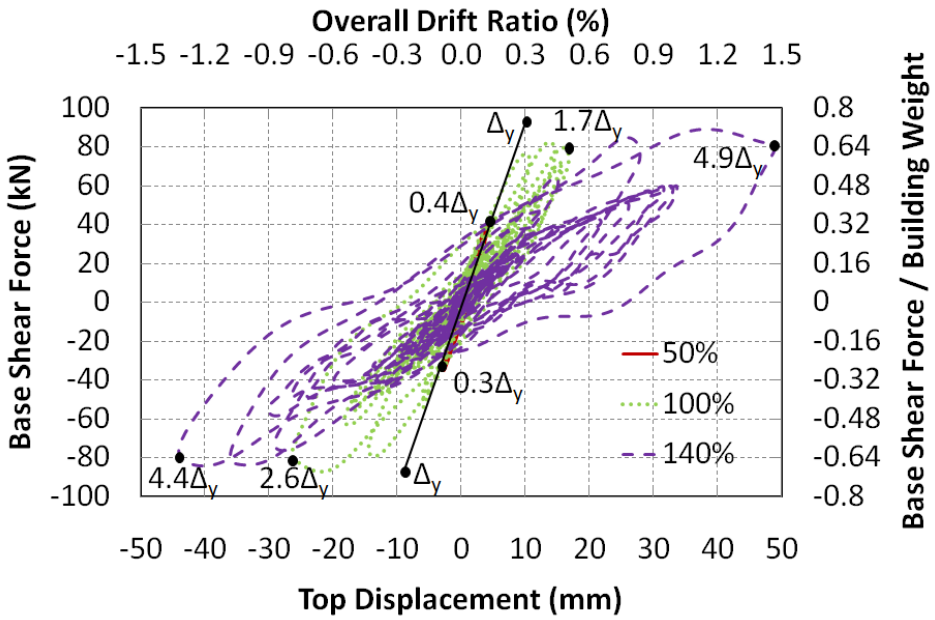

Figure 7.4 Force – Deformation Response

In Figure 7.4 base shear versus roof displacement response is presented. Δ_y (≈ 11 mm) is found by extending a line from origin and passing through a point on the initial loading curve that corresponds to 75% of the ultimate load carrying capacity. At 100% scaled specimen reached to its base shear capacity without any significant lateral strength drop at a displacement ductility of 2.6. At 140% ground motion PCP retrofitted frame was capable of retaining its lateral strength. No drop at lateral strength was observed at a displacement ductility of 5.

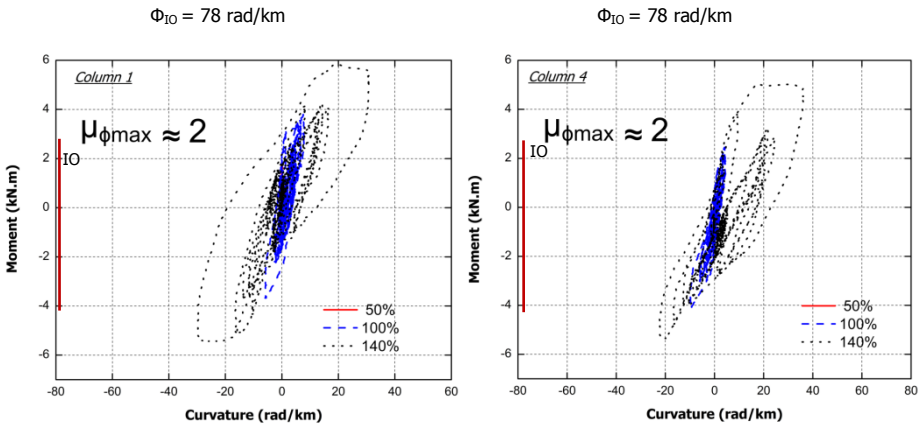

Figure 7.5 Moment – Curvature Diagrams of Column 1 and 4.

Moment-curvature response of columns C1 and C4 are presented in Figure 7.5. Measured column demands indicate plastic hinging of column bases experiencing a maximum curvature ductility demand of about 2 for exterior columns. However, no significant loss of column lateral load carrying capacity was observed.

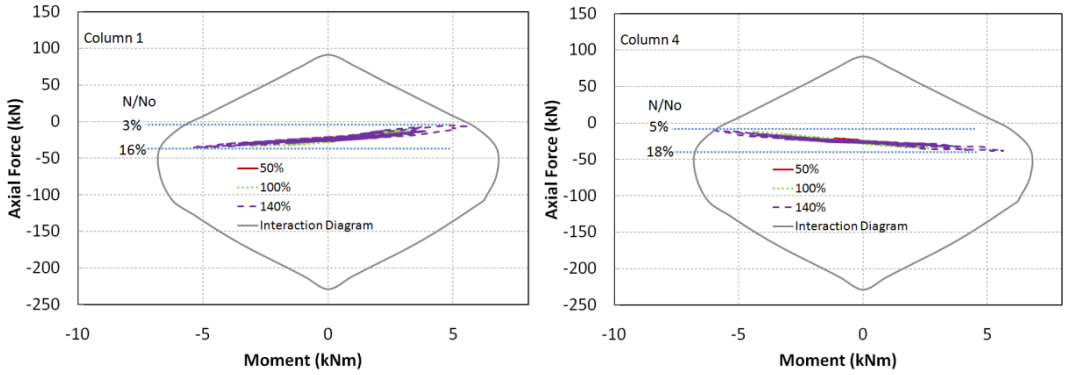

Figure 7.6 Moment Interaction Response of Column 1 and 4.

Variation of axial force on columns 1 and 4 are shown in Figure 7.6. Axial force / axial force capacity was between 3-16 % for column 1 and 5-18 % for column 4.

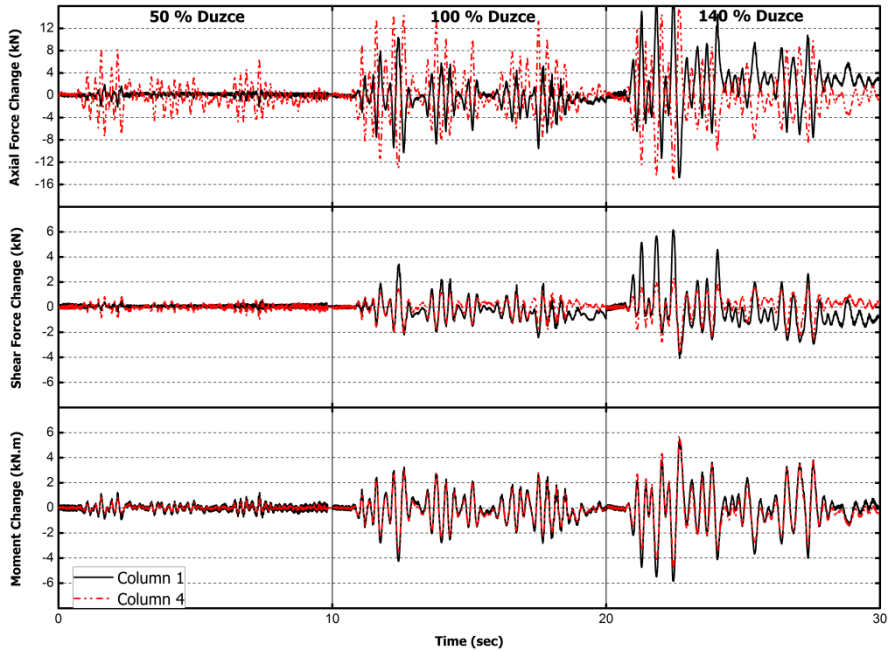

Figure 7.7 Time histories of axial, shear and moment forces change.

In Figure 7.7 change in axial, shear and moment forces during all scaled experiments are plotted. It can be easily observed that change in axial forces for exterior columns designated as 'Column 1' and 'Column 4' are reverse of each other. This situation is an indicator of overturning during experiments. Maximum changes for axial forces are 18.6 kN for compression at column 1 and 15.3 kN for compression at column 4. Maximum shear forces changes are observed at 140% scaled Duzce ground motion experiment; 6.1 kN for column 1 and -3.6 kN for column 4. Consequently, maximum changes of moment forces are obtained at the same phases of the experiments as shear force changes. Peak changes of moment force for column 1 & 4 are -5.8 kN.m and 5.7 kN.m, respectively.

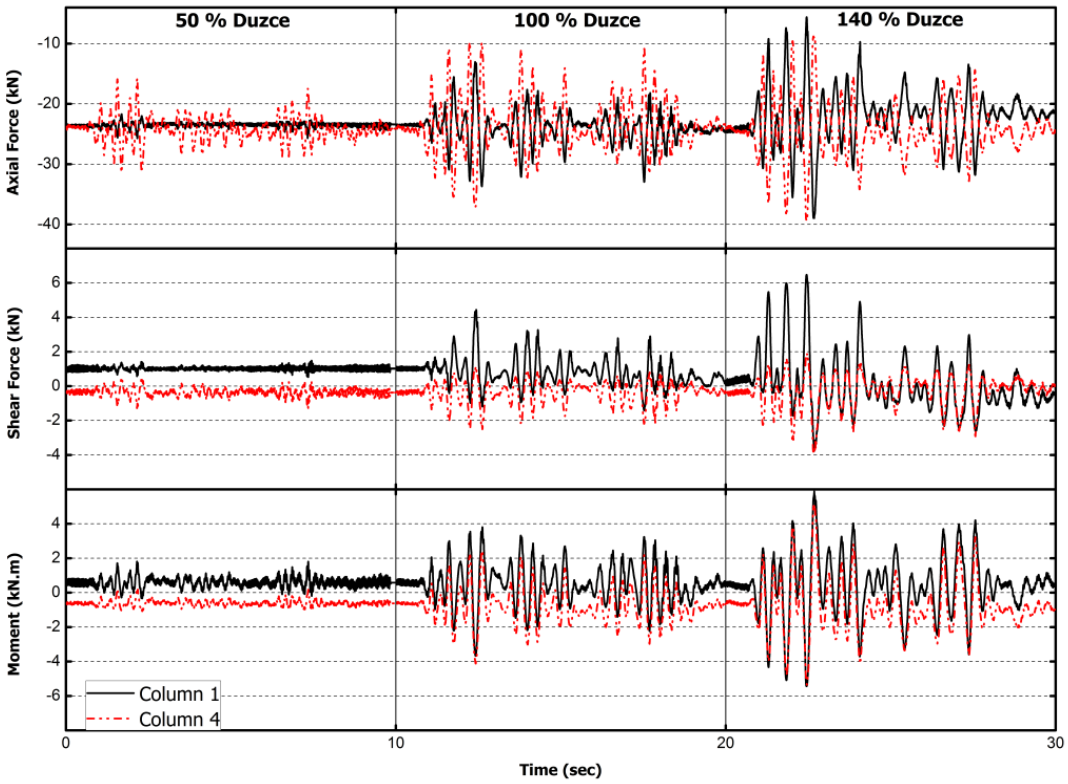

Figure 7.8 Time histories of axial, shear and moment forces.

Total axial, shear and moment forces time histories are shown in Figure 7.8. At the time axial compression force is increasing on column 1, axial force on the column 4 is decreasing due to overturning. Shear forces on columns 1 and 4 have similar behaviors as expected.

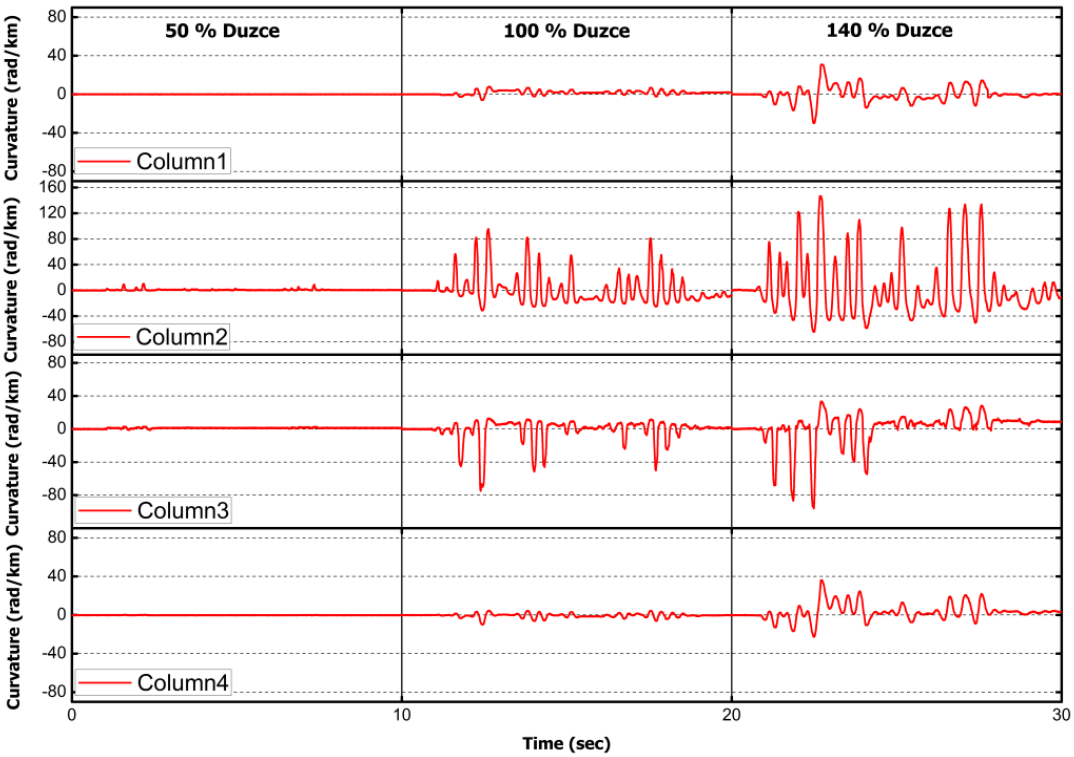

Figure 7.9 Time histories of curvatures at column bases.

Column bases curvatures during all ground motions are shown in Figure 7.9. Exterior and interior columns did not experience any significant damage at 50% scaled experiment. Interior column curvature values increased significantly at 100% scaled experiment. Upon cracks on precast concrete at first floor at 140% scaled test, peak curvatures are observed. Maximum values of curvatures are 30, 146, 96 and 36 rad/km for columns 1, 2, 3 and 4 respectively.

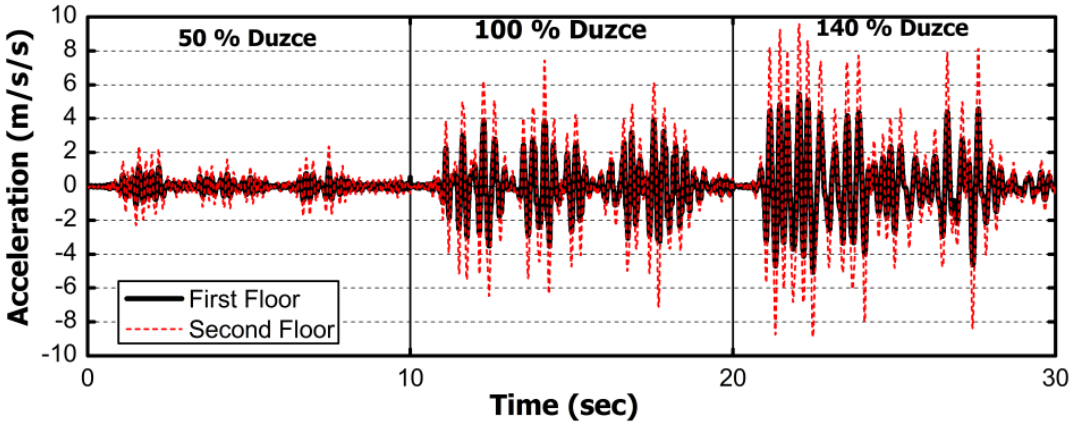

Figure 7.10 Floor Accelerations.

Figure 7.10 presents the floor accelerations obtained from the PCP retrofitted experiments during the complete motion. The maximum floor acceleration observed was equal to 2.38m/s^2 (~0.24g) for the 50% Duzce motion. The maximum floor acceleration was 7.42 m/s^2 (~0.74g) for 100% Duzce motion. At 140% Duzce motion peak floor acceleration was 9.59 m/s^2 (~0.96g).

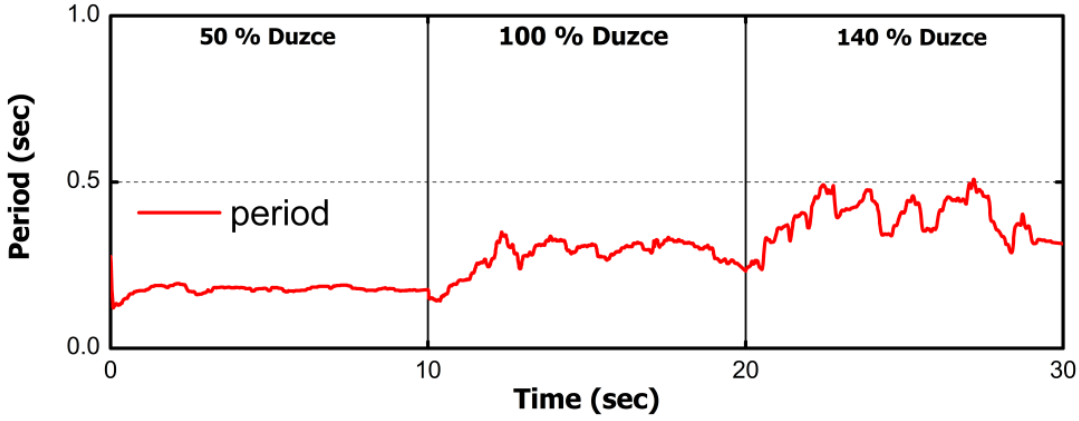

Figure 7.11 Identified Period of the Test Specimen.

Initial period of the test specimen was 0.13 seconds. At the end of the 50% Duzce motion, after some minor damages occurred on the structure, test structure's period increased to 0.18 seconds. Full scale Duzce motion ended with a period of 0.26 seconds (Figure 7.12).

In Figure 7.13 inter-story drift ratios and observed damages are presented. Photos are correlated with specific points at time history of inter-story drift ratios. At point A, flexural crack initiation on interior columns and at first floor was observed. At point B, crack pattern of the first story precast concrete panels is presented. At point C, longitudinal bar buckling was observed at interior column. At point D, two bar buckling regions was observed at one of the exterior columns. Final state of the experiments is also presented in Figure 7.13. A brief summary of test results are presented in Table 7.1.

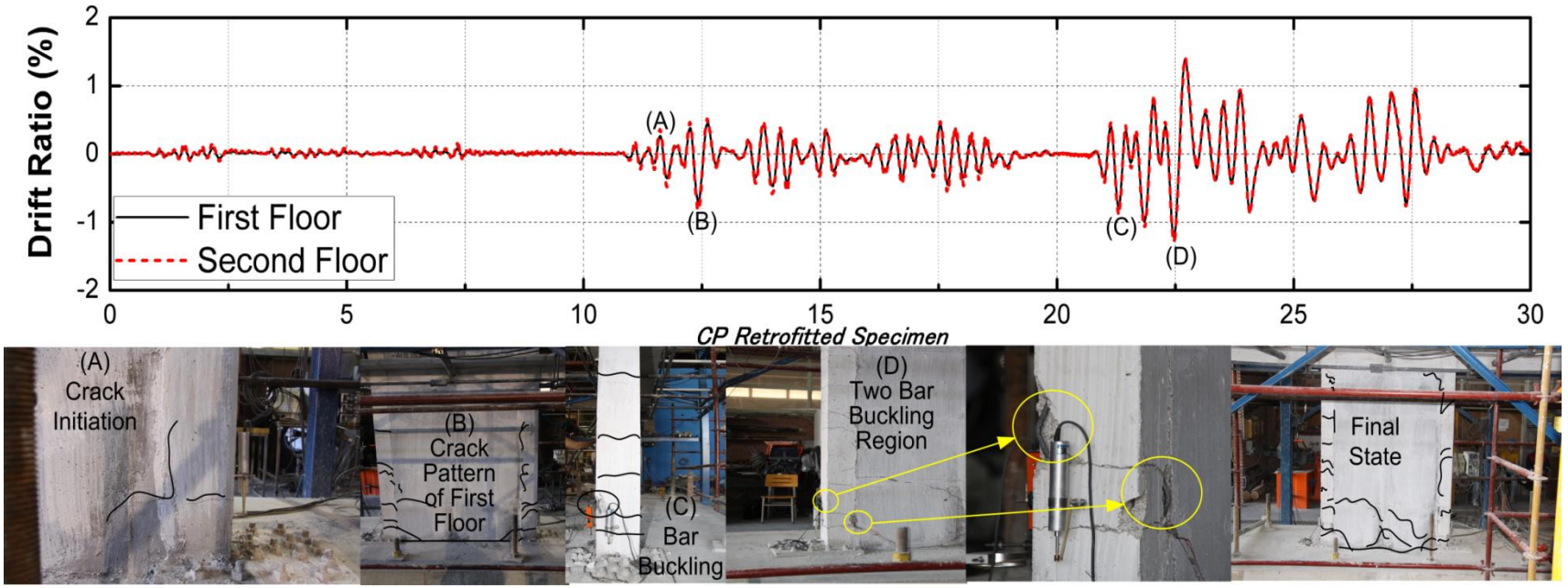

Figure 7.13 Drift Ratio and Observed Damage

Table 7.1 Summary of Results

Ground Motion	Maximum Displacement Demand (mm)		Maximum Interstory Drift Ratio (%)		Maximum Story Base Shear Force (kN)		Column Plastic Rotation Demands			
	1st Story	2nd Story	1st Story	2nd Story	1st Story	2nd Story	θ_{p1} $\mu_{\phi 1}$	θ_{p2} $\mu_{\phi 2}$	θ_{p3} $\mu_{\phi 3}$	θ_{p4} $\mu_{\phi 4}$
50% Duzce	1.9	4.1	0.1	0.1	40.2	26.2	0 0.02	0 0.4	0 0.1	0 0.03
100% Duzce	14.3	26.4	0.4	0.5	87.2	59.2	0 0.3	0.01 3.7	0.007 2.9	0 0.4
140% Duzce	28.2	48.8	1.4	1.4	88.9	60.9	0.001 1.3	0.02 5.6	0.01 3.7	0.002 1.6

*: Plastic rotation is calculated as θ_p = Gauge Length (Ultimate Curvature – Yield Curvature) where Gauge Length is 150mm

**: Curvature Ductility is calculated as μ_Φ = Ultimate Curvature / Yield Curvature

7.2. SUMMARY AND DISCUSSION OF TEST RESULTS

Experimental results of inter-story drift ratio (or simply drift ratio obtained as the difference of floor displacement divided by the floor height) versus time are presented in Figures 7.13 for the three ground motion scale levels. Important damage events are shown with pictures and marked on the time history response in Figure 7.13. Base shear versus roof displacement response of the specimen is presented in Figure 7.4. Experimentally obtained moment-curvature response and variations of axial force-moment along with the interaction diagram of columns for exterior columns named as C1 and C4 are presented in Figure 7.6. Table 7.1 presents the summary of test results based on obtained measurements and observations.

50% Duzce motion resulted in flexural cracks at interior columns of the first story columns. No additional significant damage was observed at this scaled ground motion. Maximum roof displacement for this ground motion was about 4 mm, resulting in inter-story drift ratios of about 0.1% for both stories. Figure 7.4indicates that no significant stiffness deterioration took place prior to the beginning of the second test. Maximum base shear capacity measured in this test was about 40 kN. Column base curvature measurements indicate that interior and exterior columns did not experience any longitudinal steel yielding. As a result, all columns had no

plastic rotation demands (Table 7.1). Based on the observed damage and measurements the test structure has experienced minor damage and remains functional without any need of repairs. Based on measured demand parameters and judgment of the observed damage state, immediate occupancy level damage criterion is satisfied.

Afterwards, the same frame was tested with 100% scaled Duzce motion. In this ground motion scale, 26 mm maximum top displacement was observed which resulted in a maximum inter story drift ratio of 0.4% for first floor and 0.5% for second floor. Crack at potential hinging zones at exterior columns and crack initiation on concrete panels at base level were the important damage events observed for this ground motion level.

Figure 7.4 indicates that the frame sustained its base shear capacity (~87 kN) without any drop up to a displacement ductility of about 2.6. The maximum plastic rotation demand at the column base was about 0.01. The structure was capable of withstanding the deformation demands without any significant drop of lateral strength and can be occupied without any needs of repair. Hence, the structure satisfies the life safety performance criterion based on engineering judgment.

Finally, 140% Duzce was applied on the test structure to observe the final damage state. A maximum top displacement of 48.8 mm was measured corresponding to a 1.4% maximum inter-story drift ratio for first and second floors. No lateral strength degradation of the frame was observed at a displacement ductility demand of about 4.4. Retrofitted specimen exhibited limited damage, the most important event being the cracks on the concrete panels and longutidinal bar buckling at interior columns. The infill wall remained intact and was not susceptible to out of plane failure.

Figure 7.9 presents the variation of axial force with bending moment at exterior column bases. The axial load level due to gravity loads on the columns was determined as 10% and 22% for the exterior and interior column axial load carrying capacities, respectively. The axial load varied between 3 to 16% and 5 to 18% of the axial load carrying capacity column 1 and column 4, respectively. The test frame had a lateral load carrying capacity ratio (lateral load divided by building weight) of about 0.65. This capacity was maintained in the second test. Although severe cracks

on concrete panel at third of the first floor and longitudinal bar buckling at exterior columns at 140% Duzce ground motion occured, the capacity ratio did not dropped.

CHAPTER 8

REINFORCED CONCRETE INFILL WALL RETROFITTED FRAME

8.1. TEST RESULTS

Time history of both floor displacements is plotted (Figure 8.1). At 50% scaled experiment, peak displacements for first and second floors were 0.8 mm and 1.4 mm, respectively. Maximum first floor displacement was 1.9 mm whereas peak tip displacement was 3.5 mm at full Duzce ground motion. Displacements reached to 14.9 mm and 26.1 mm for first and second floors, respectively.

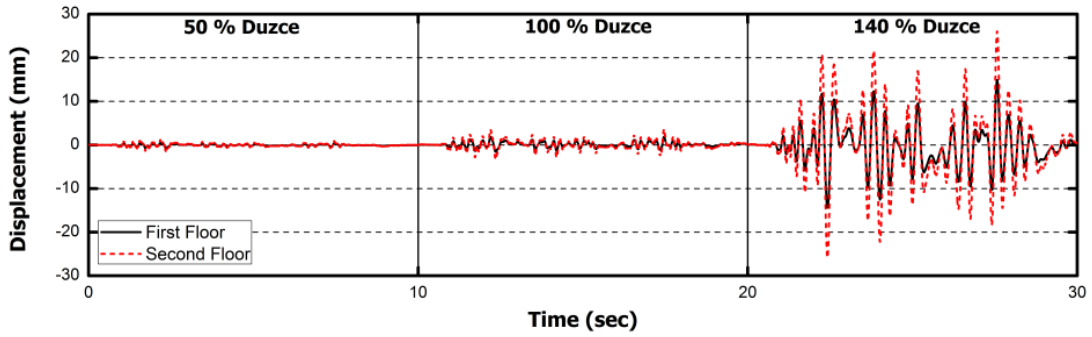

Figure 8.1 Time history of floor displacements.

Time history of IDRs is drawn in Figure 8.2 for all scales of ground motions. At 50% Duzce ground motion, IDRs were around 0.04%. IDRs at full scaled ground motion for first and second floors were 0.09% and 0.11%, respectively. Maximum IDRs were observed at 140% ground motion. IDRs at first and second floors were around 0.75% at peak.

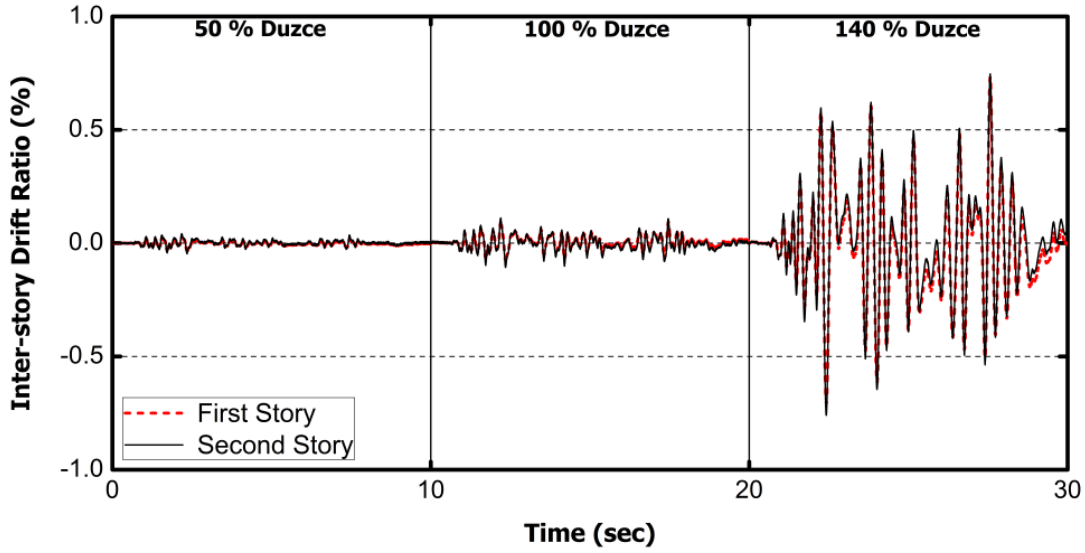

Figure 8.2 Time history of inter-story drift ratios.

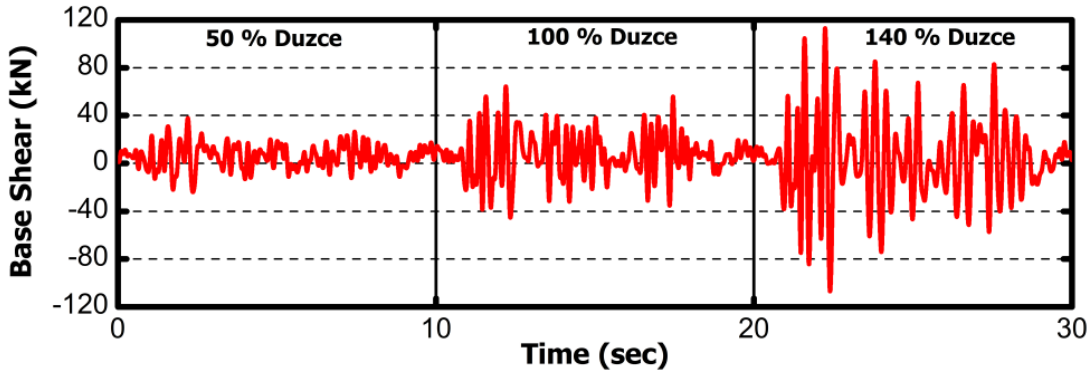

Figure 8.3 Time history of base shear.

Based on Figure 8.3, maximum base shear of the reinforced concrete infill wall retrofitted test specimen was around 40 kN at 50% scaled experiment. At 100% scaled experiment, base shear increased to 65 kN. Test frame reached to its base shear capacity at 140% scaled test; ~115 kN.

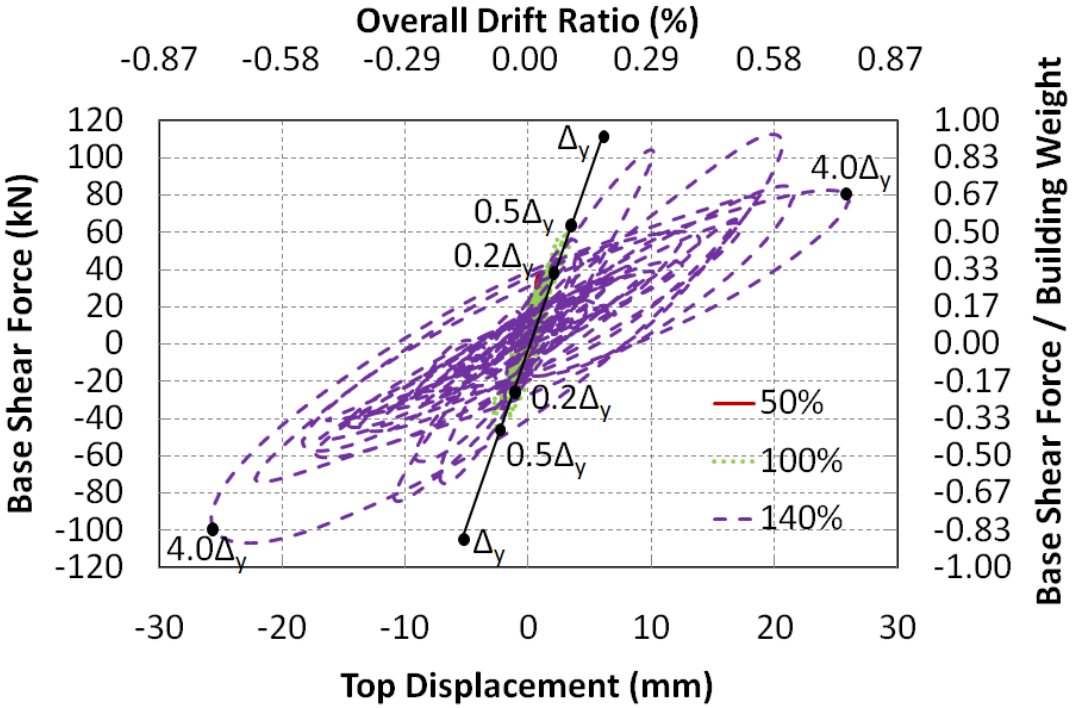

Figure 8.4 Force – Deformation Response.

In Figure 8.4 base shear versus roof displacement response is presented. Δ_y (≈ 6.5 mm) is found by extending a line from origin and passing through a point on the initial loading curve that corresponds to 75% of the ultimate load carrying capacity. At 140% ground motion reinforced concrete infill wall retrofitted frame reached to its base shear capacity. No significant drop at lateral strength was observed at a displacement ductility of 4.

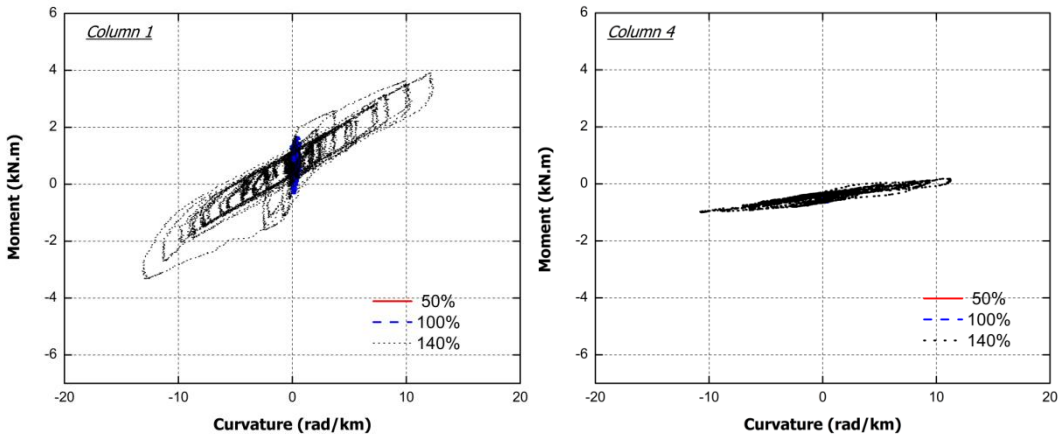

Figure 8.5 Moment – Curvature Diagrams of Column 1 and 4.

Moment-curvature response of columns C1 and C4 are presented in Figure 8.5. Measured column demands indicate that no plastic hinging of the exterior columns was observed. There was also no visual plastic hinging at the bases of the exterior columns.

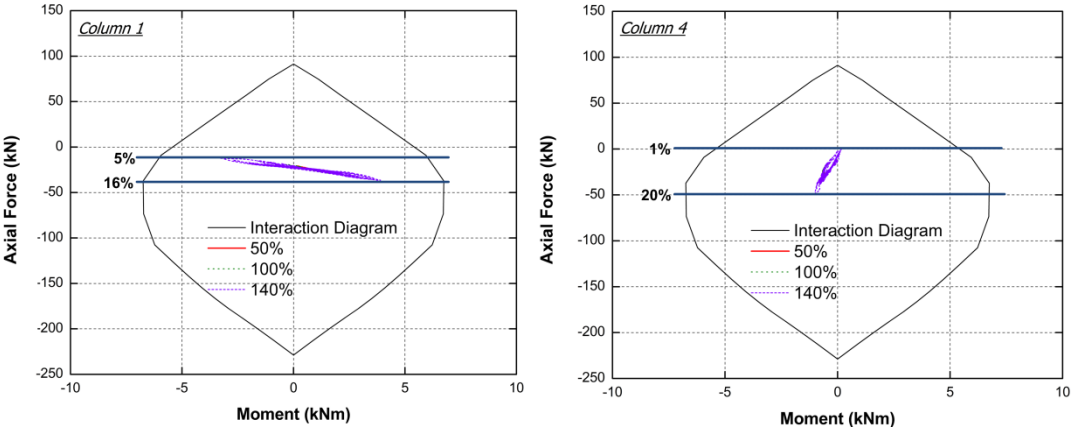

Figure 8.6 Moment Interaction Response of Column 1 and 4

Variation of axial force on columns 1 and 4 are shown in Figure 8.7. Axial force / axial force capacity was between 5-16 % for column 1 and 1-20 % for column 4.

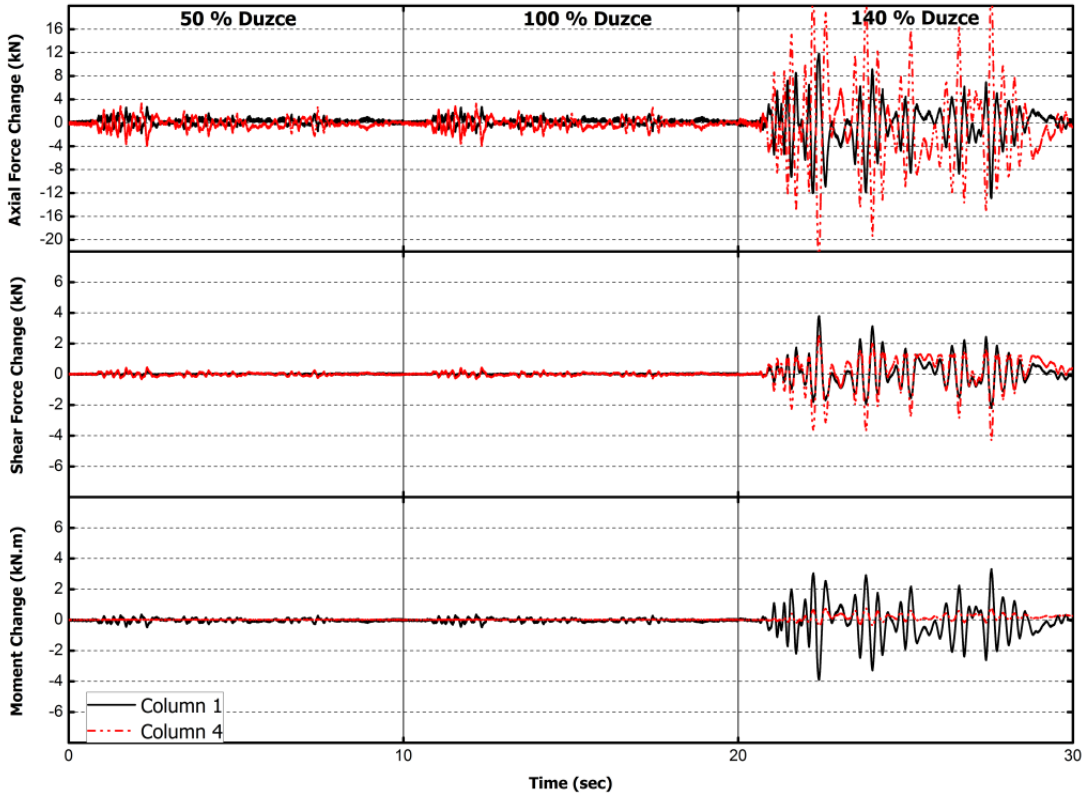

Figure 8.7 Time histories of axial, shear and moment forces change.

In Figure 8.7 change in axial, shear and moment forces during all scaled experiments are plotted. It can be easily observed that change in axial forces for exterior columns designated as 'Column 1' and 'Column 4' are reverse of each other. This situation is an indicator of overturning during experiments. Evaluation of force transducer under column 4 was somehow problematic and resulted in misreading. However, transducer under column was capable of getting data during all experiments. Maximum change of axial, shear and moment forces for column 1 were 12.9 kN, 3.8 kN and 3.9 kNm, respectively.

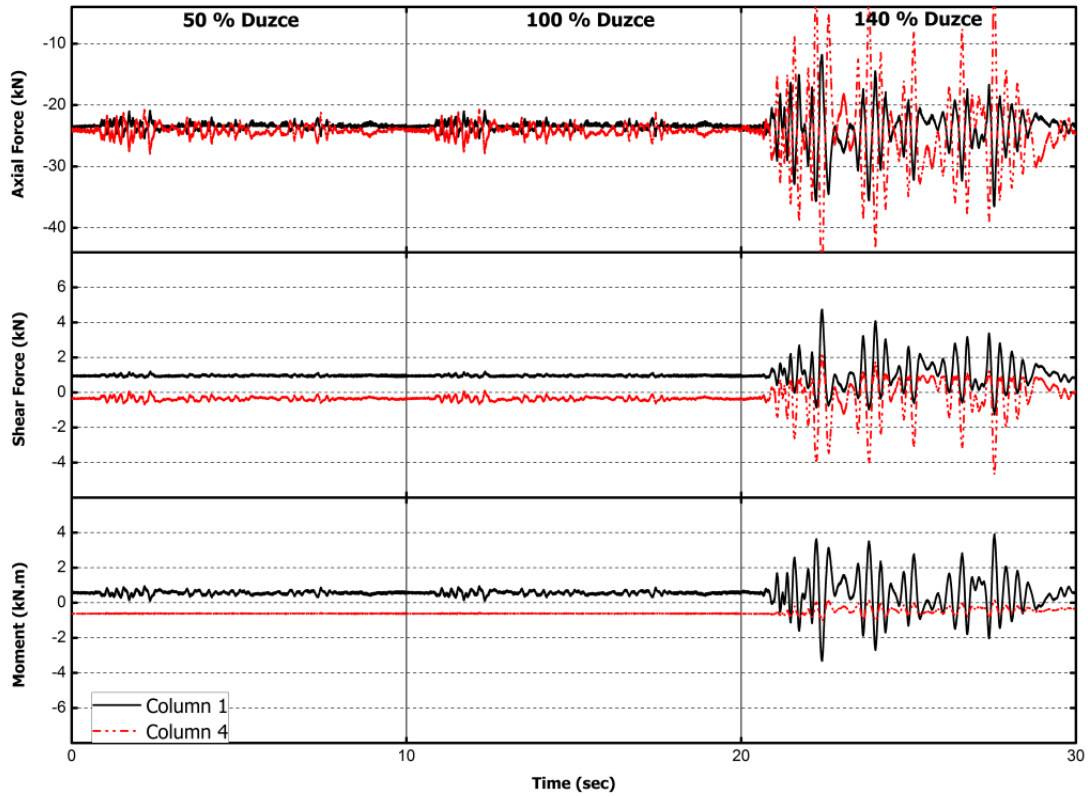

Figure 8.8 Time histories of axial, shear and moment forces.

Total axial, shear and moment forces time histories are shown in Figure 8.8. At the time axial compression force is increasing on column 1, axial force on the column 4 is decreasing due to overturning. Peak values of axial, shear and moment forces were observed at 140% scaled experiment; 36 kN, 4.7 kN and 3.9 kNm.

Column bases curvatures during all ground motions are shown in Figure 8.9. All columns did not experience any yielding until 140% experiment. At 140% ground motion, interior columns yielded. Maximum values of curvatures are 60 and 40 rad/km for columns 2 and 3, respectively.

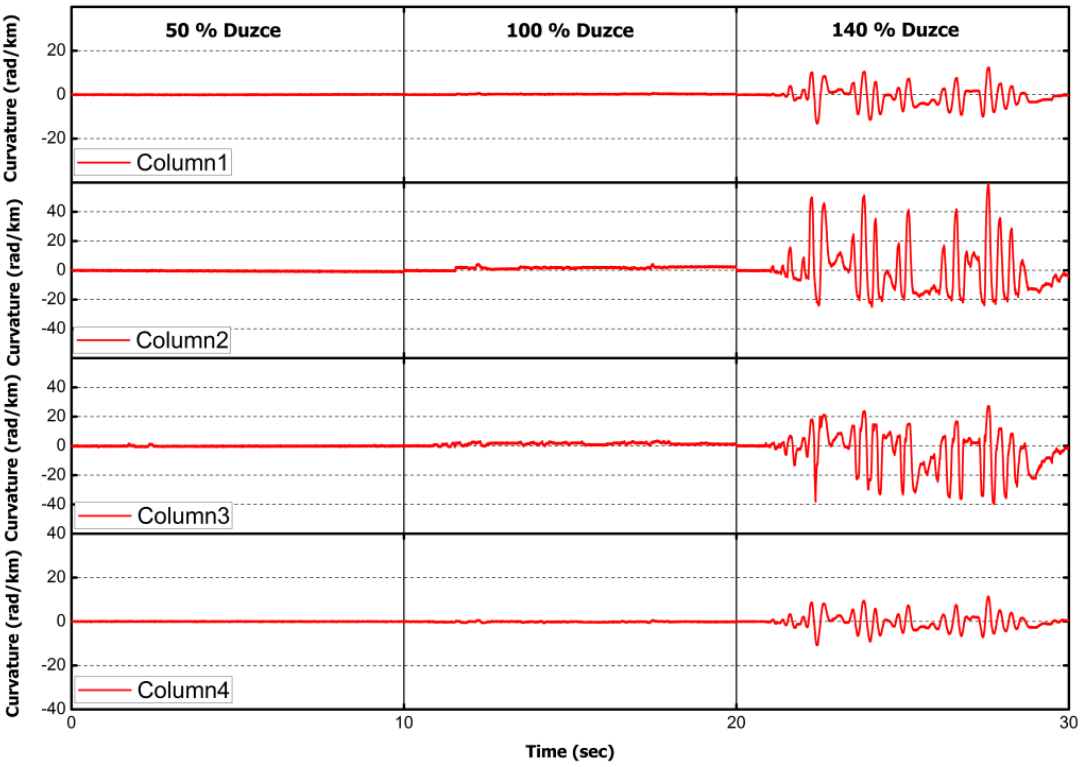

Figure 8.9 Time histories of curvatures at column bases.

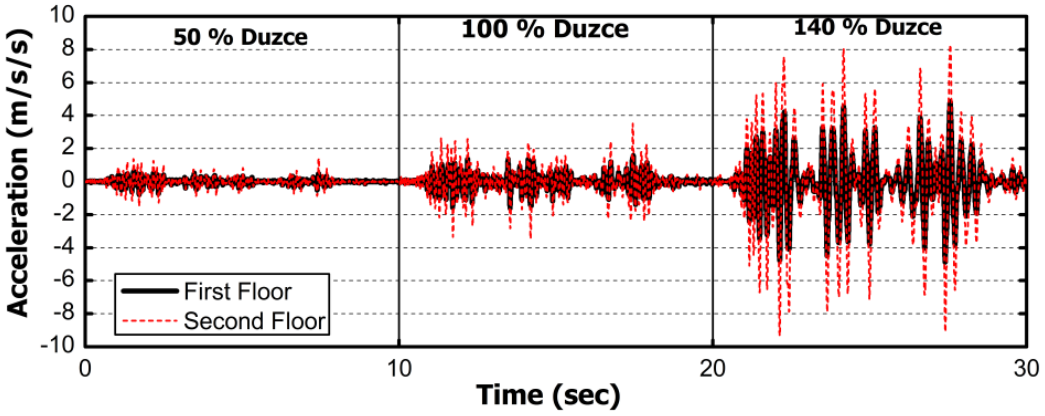

Figure 8.10 Floor Accelerations

Figure 8.10 presents the floor accelerations obtained from the reinforced concrete infill wall retrofitted experiments during the complete motion. The maximum floor acceleration observed was equal to 1.49 m/s^2 (~0.15g) for the 50%

Duzce motion. The maximum floor acceleration was 3.52 m/s^2 (~0.35g) for 100% Duzce motion. At 140% Duzce motion peak floor acceleration was 9.34 m/s^2 (~0.93g).

Initial period of the test specimen was 0.1 seconds. At the beginning of 100% scaled Duzce motion, period of the system was 0.11 seconds. Full scale Duzce motion ended with a period of 0.14 seconds (Figure 8.11).

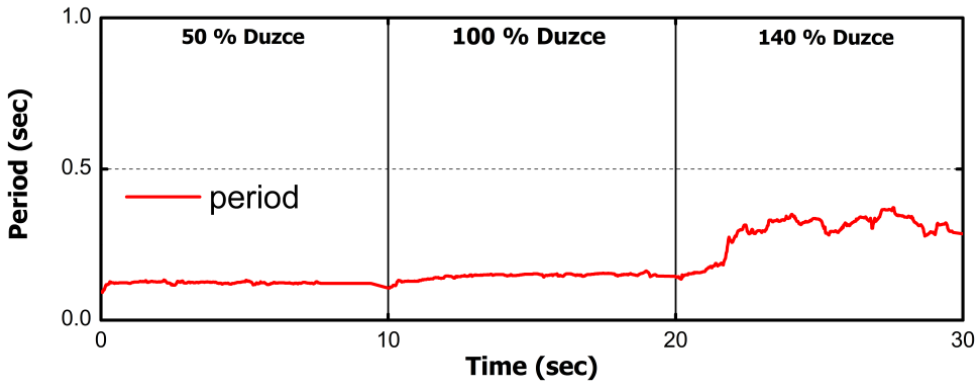

Figure 8.11 Identified Period of the Test Specimen.

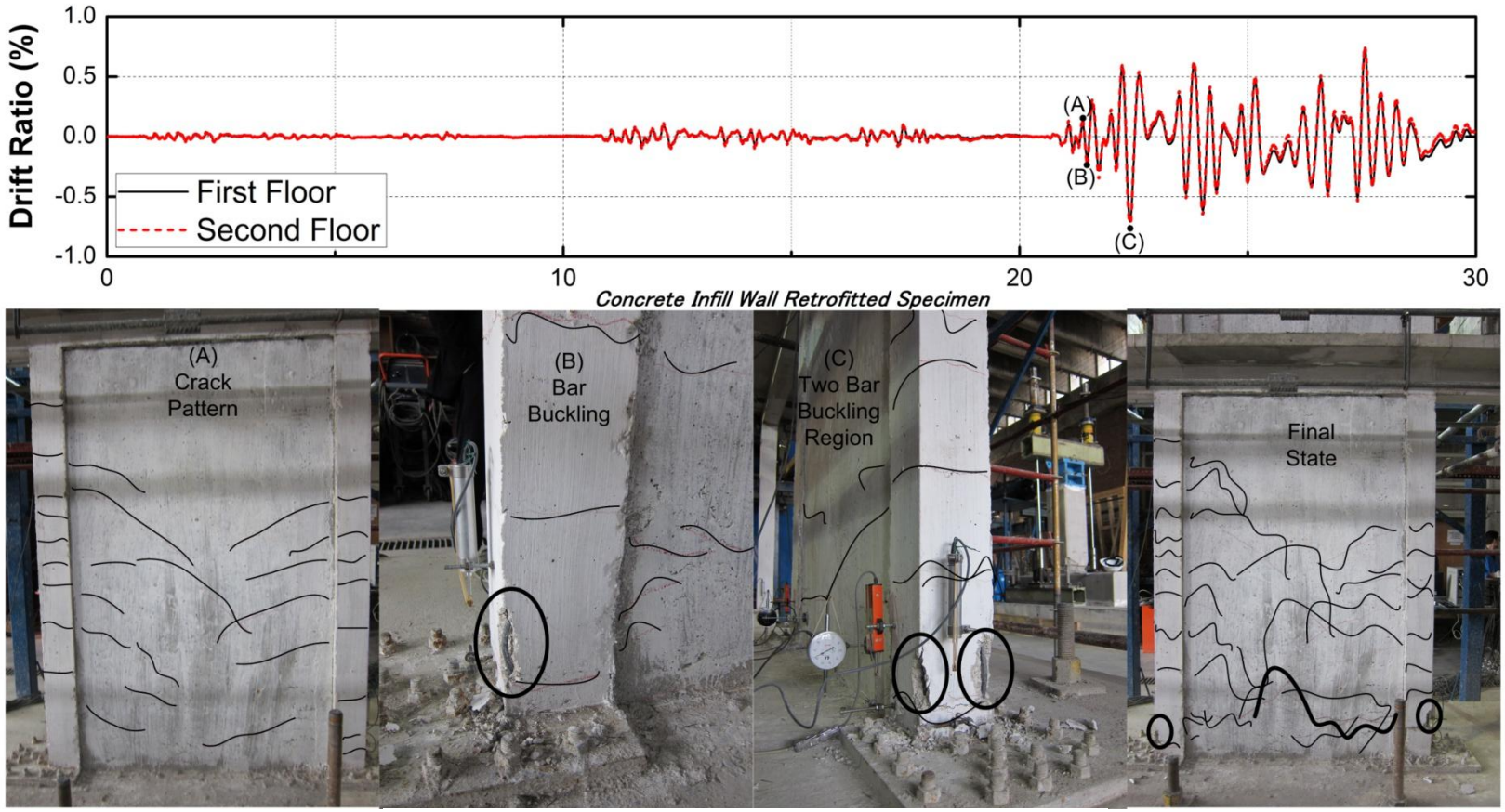

Figure 8.12 Drift Ratio and Observed Damage

In Figure 8.12 inter-story drift ratios and observed damages are presented. Photos are correlated with specific points at time history of inter-story drift ratios. At point A, crack pattern of first story reinforced concrete infill wall is presented. At point B, longitudinal bar buckling was observed. At point C, two longitudinal bar buckling region was observed. Final state of the experiments is also presented in Figure 8.13. A brief summary of test results are presented in Table 8.1.

Table 8.1 Summary of Results

Ground Motion	**Maximum Displacement Demand (mm)**		**Maximum Interstory Drift Ratio (%)**		**Maximum Story Base Shear Force (kN)**		**Column Plastic Rotation Demands**			
	1st Story	**2nd Story**	**1st Story**	**2nd Story**	**1st Story**	**2nd Story**	θ_{p1} $\mu_{\phi 1}$	θ_{p2} $\mu_{\phi 2}$	θ_{p3} $\mu_{\phi 3}$	θ_{p4} $\mu_{\phi 4}$
50% Duzce	0.8	1.4	0.04	0.04	40.2	21	0 0.02	0 0.06	0 0.06	0 0.02
100% Duzce	1.9	3.5	0.09	0.11	65	45	0 0.04	0 0.17	0 0.14	0 0.04
140% Duzce	14.9	26.1	0.75	0.75	115	49	0 0.6	0.005 2.2	0.002 1.5	0 0.5

*: Plastic rotation is calculated as θ_p = Gauge Length (Ultimate Curvature – Yield Curvature) where Gauge Length is 150mm

**: Curvature Ductility is calculated as μ_Φ = Ultimate Curvature / Yield Curvature

8.2. SUMMARY AND DISCUSSION OF TEST RESULTS

Experimental results of inter-story drift ratio (or simply drift ratio obtained as the difference of floor displacement divided by the floor height) versus time are presented in Figures 8.12 for the three ground motion scale levels. Important damage events are shown with pictures and marked on the time history response in Figure 8.2 Base shear versus roof displacement response of the specimen is presented in Figure 8.4. Experimentally obtained moment-curvature response and variations of axial force-moment along with the interaction diagram of columns for exterior columns named as C1 and C4 are presented in Figure 8.6. Table 8.1

presents the summary of test results based on obtained measurements and observations.

50% Duzce motion resulted in no significant damage for reinforced concrete infill wall retrofitted specimen. Maximum roof displacement for this ground motion was about 1.4 mm, resulting in inter-story drift ratios of about 0.04% for both stories. Maximum base shear capacity measured was about 40 kN at 50% Duzce ground motion. Column base curvature measurements indicate that interior and exterior columns did not experience any longitudinal steel yielding. As a result, all columns had no plastic rotation demands (Table 8.1). Based on the observed damage and measurements the test structure has experienced no significant damage and remains functional without any need of repairs. Based on measured demand parameters and judgment of the observed damage state, immediate occupancy level damage criterion is satisfied.

Afterwards, the same frame was tested with 100% scaled Duzce motion. In this ground motion scale, 3.5 mm maximum top displacement was observed which resulted in a maximum inter story drift ratio of 0.09% for first floor and 0.11% for second floor. No significant damage was observed in this experiment.

Finally, 140% Duzce was applied on the test structure to observe the final damage state. A maximum top displacement of 26.1 mm was measured corresponding to a 0.75% maximum inter-story drift ratio for first and second floors. The maximum plastic rotation demand at the column base was about 0.005. The structure was capable of withstanding the deformation demands and can be occupied without any needs of repair. Hence, the structure satisfies the life safety performance criterion based on engineering judgment.

Retrofitted specimen exhibited limited damage, the most important event being the cracks on the reinforced concrete infill wall and longitudinal bar buckling at interior columns. The specimen was capable of withstanding vertical loads under lateral loading.

Figure 8.9 presents the variation of axial force with bending moment at exterior column bases. The axial load level due to gravity loads on the columns was determined as 10% and 22% for the exterior and interior column axial load carrying capacities, respectively. The axial load varied between 5 to 16% and 1 to 20% of the axial load carrying capacity column 1 and column 4, respectively. The test frame

had a lateral load carrying capacity ratio (lateral load divided by building weight) of about 0.96. This capacity was maintained in the third test.

CHAPTER 9

COMPARISONS OF DIFFERENT RETROFIT TECHNIQUES

9.1. INTRODUCTION

The traditional approach of adding reinforced concrete infill walls is the most commonly chosen alternative for current seismic retrofit applications in Turkey. However, the construction work involved for this retrofit scheme is extremely demanding. Furthermore, it results in lengthened retrofit time and necessitates relocating the occupants. In order to overcome these shortcomings, alternative retrofit schemes by utilizing the presence of substantial amount of infill walls can be quite efficient. In order to rely on these infill walls for collapse prevention during an earthquake, they need to be intervened. Two rehabilitation methods namely use of fiber reinforced polymer (FRP) and precast panels integrated on the infill walls were developed at Middle East Technical University (Baran 2005, Özcebe et. al. 2005, Binici et. al. 2007). In this way, it was aimed to provide a wider range of retrofit alternatives at the service of practicing engineers for seismic hazard mitigation studies. Later these retrofit methods were included as possible retrofitting techniques in the Turkish Earthquake Code (TEC 2007), perhaps in a slightly premature manner due to the fact that design proposals were based solely on quasi-static cyclic testing.

9.2. EXPERIMENTAL RESULTS

Displacement time histories of all four specimens were presented in Figure 9.1. Maximum displacement values of both floors at each ground motion, namely 50%, 100% and 140%, were preseneted as tables on the graphs. The inter-story drift ratios and the pictures of the observed damage in time for the three different

ground motion scales are shown in Figure 9.2 for the four specimens. All specimens experienced minor damage during the 50% ground motion level. For the reference specimen, formation of interface cracks between the infill wall and the boundary frame elements was the most important observed damage. The maximum drift ratio achieved for the reference specimen was about 0.7% for this ground motion level whereas this value was only about 0.1% for the FRP and CP retrofitted specimens and 0.04% for reinforced concrete infill walls. Reference, FRP and CP specimens exhibited significant inelastic deformations for the 100% Duzce ground motion. The damage for the reference frame was significant diagonal cracking of the infill wall and initiation of cover spalling in column base plastic hinge regions. On the other hand, FRP retrofitted specimen exhibited rocking displacements due to extension/slip of FRP dowels. CP retrofitted specimen had interface cracks along with some inclined cracks extending from the neighboring columns. Whereas, reinforced concrete infill wall retrofitted specimen was resulted with no significant damage at this ground motion scale. The maximum interstory drift ratio demand decreased from about 1.7% for the reference specimen to about 0.8%, 0.5% and 0.1% for the FRP, CP and reinforced concrete infill wall retrofitted specimens, respectively. Final ground motion scale level (140%) brought the reference frame to a near collapse state. Plaster on the infill wall completely detached and the infill wall became vulnerable to out of plane collapse. The contribution of the infill wall completely diminished at 140% Duzce ground motion. Interior columns of the frame were severely damaged with visible longitudinal bar buckling.

A soft story mechanism was formed following the failure of the infill wall. This resulted in a 4.2% drift ratio of the first story, whereas the second story drift ratio was only about 1.3%. For the same ground motion FRP retrofitted specimen exhibited limited damage, the most important event being the slip of FRP dowels at the base. Despite anchor failure, FRP cross bracing enabled the wall to remain intact and contribute to lateral strength significantly. PCP retrofitted specimen, on the other hand, experienced severe cracking at wall-column interfaces. Reinforced concrete infill wall retrofitted specimen exhibited longitudinal bar buckling at the interior columns. The inclined cracks on the wall surfaces propagated from the columns to the wall base. FRP and PCP retrofitted specimens sustained maximum inter-story drift ratios of less than or equal to about 2%. On the other hand,

reinforced concrete infill wall retrofitted specimen experienced drift ratios less than or equal to 0.75%.

Envelope curves of all the specimens are shown in Figure 9.3. The curves shown in this figure are the demand envelopes. It should be noted that the larger the drift demand, the larger the damage. The demand envelopes of the reference frame, and specimens FRP and PCP showed considerable plasticity, indicating that these specimens had experience substantial amount of damage. Whereas the RC infill wall retrofitted specimen survived the 140% Duzce ground motion by displaying a nearly elastic behavior. In same figure the overall drift ratios were also shown. As can be seen from the figure the drift demand of RC infill wall specimen is nearly one third of the drift demand of reference specimen. This difference becomes less pronounced in the case of FRP and PCP specimens.

In the case of Reference frame, the lateral strength dropped about 30% of its maximum strength at a displacement of about 6 times its yield displacement. The FRP retrofitted frame was capable of sustaining its lateral strength while a cumulative damage built up due to rocking mechanism. Lateral strength decreased about 88% of its maximum strength at a displacement of about 6.5 times its yield displacement. At 140% scaled test, PCP retrofitted frame was capable of retaining its lateral strength. A slight drop at lateral strength was observed at a displacement ductility of 5. Reinforced concrete infill wall, however, responded the 50 percent and 100 percent Duzce motions in elastic mode. During 140 percent Duzce motion due to buckling of the longitudinal steel of the boundary columns on both sides of the wall a strength drop of approximately 30 percent of the peak resistance was observed in one direction. The observed damage in other parts of the structure was visibly less as compared to specimens FRP and PCP.

The first floor exterior column base moment curvature relationships are shown in Figure 9.4. Column base curvatures indicated that neither of the exterior columns of all four specimens experienced longitudinal bar yielding at 50% and 100% ground motion. Measured column demands indicate plastic hinging of column bases experiencing a maximum curvature ductility demand of about 9 and 11 for at reference frame, 3 at FRP retrofitted specimen, 2 at PCP retrofitted specimen at 140% ground motion. No longitudinal bar yielding of exterior columns was observed at reinforced concrete infill wall retrofitted specimen.

Base shear time histories of all specimens were presented in Figure 9.5. Maximum base shear forces at each ground motion, namely 50%, 100% and 140%, were presented as tables on the graphs.

Identified period variations are presented in Figure 9.6. Initial periods of the test specimens were presented in tables in the figure.

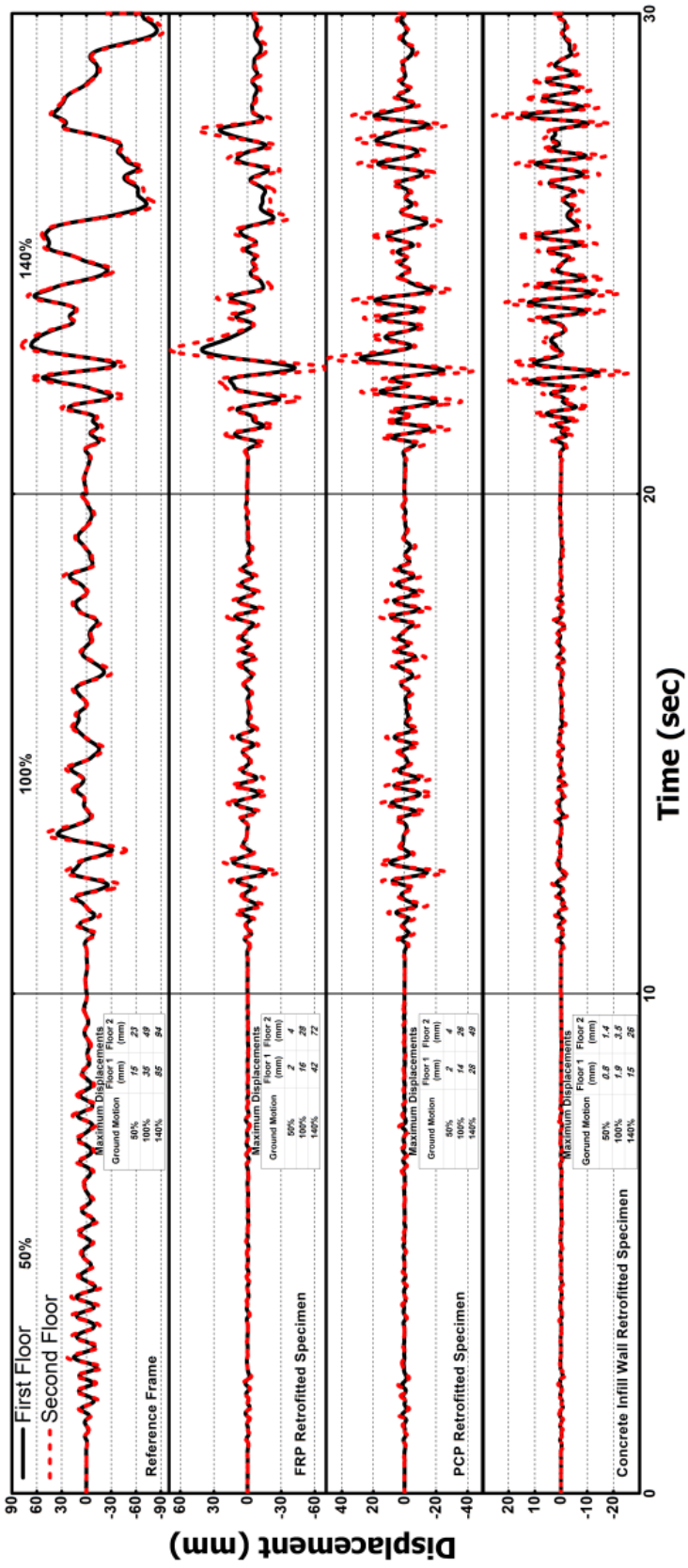

Figure 9.1 Displacement time histories of all specimens

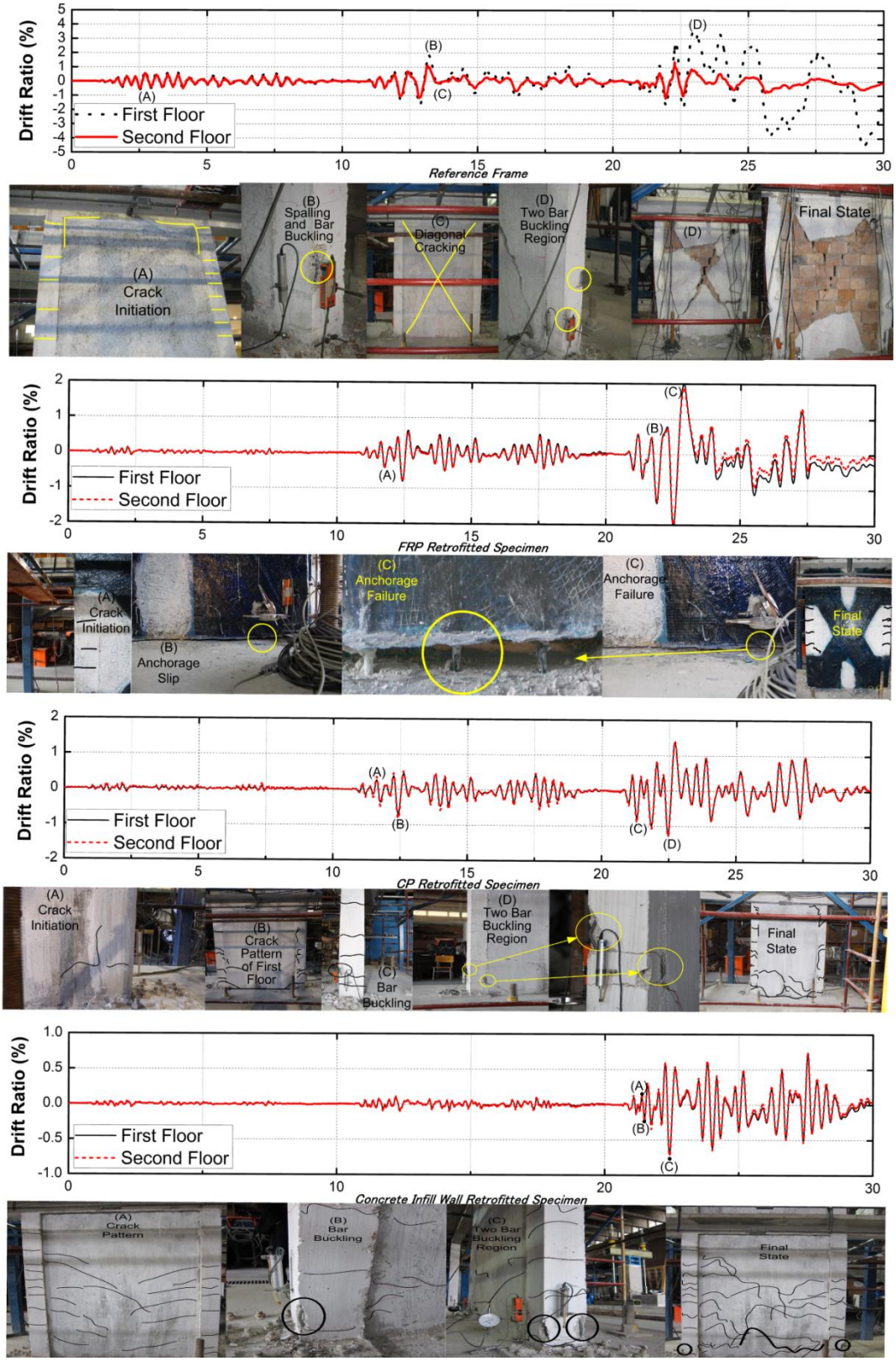

Figure 9.2 Drift Ratio and Observed Damage of Test Specimens

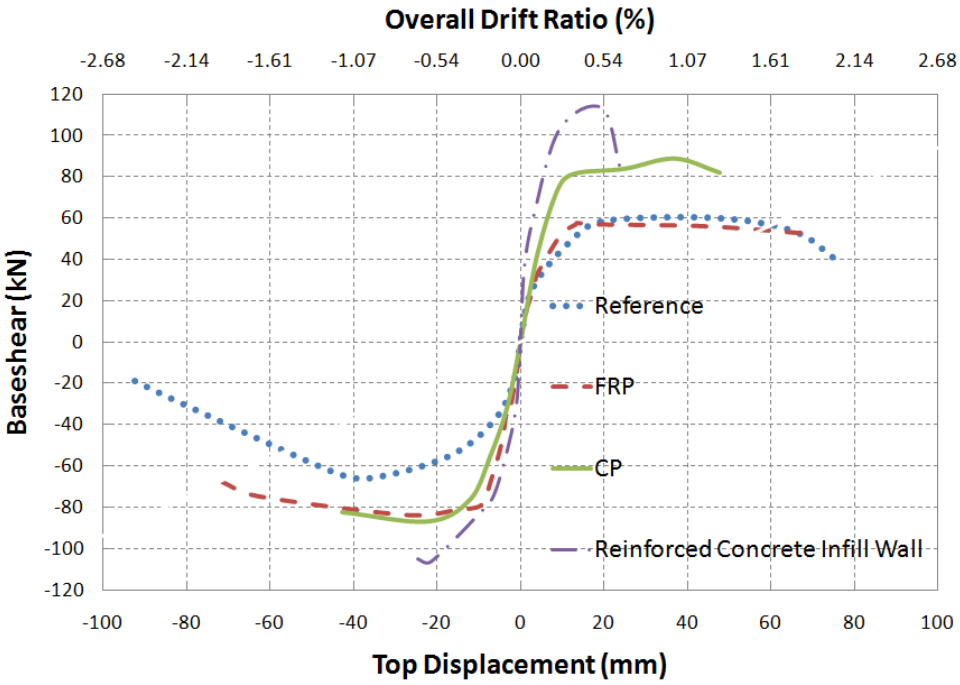

Figure 9.3 Demand Envelope Curves of Test Specimens

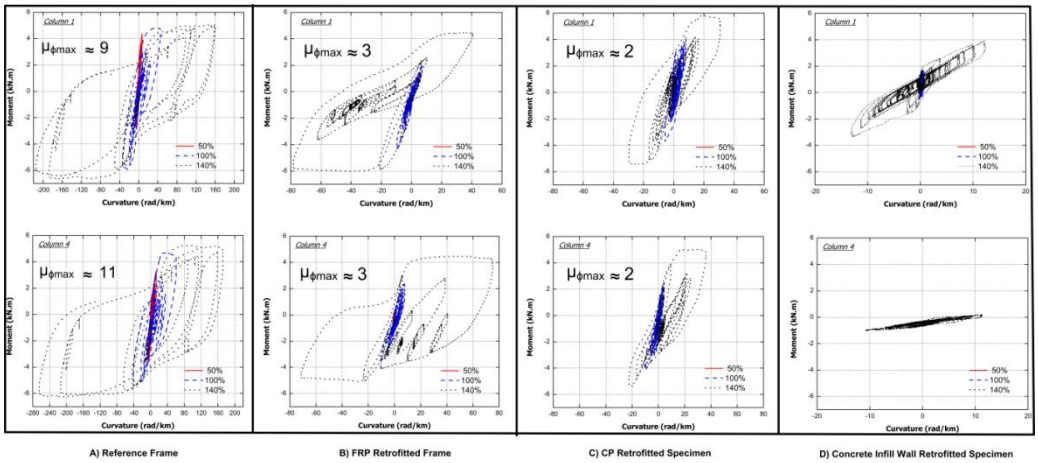

Figure 9.4 Measured Moment Curvature Response of Exterior Columns

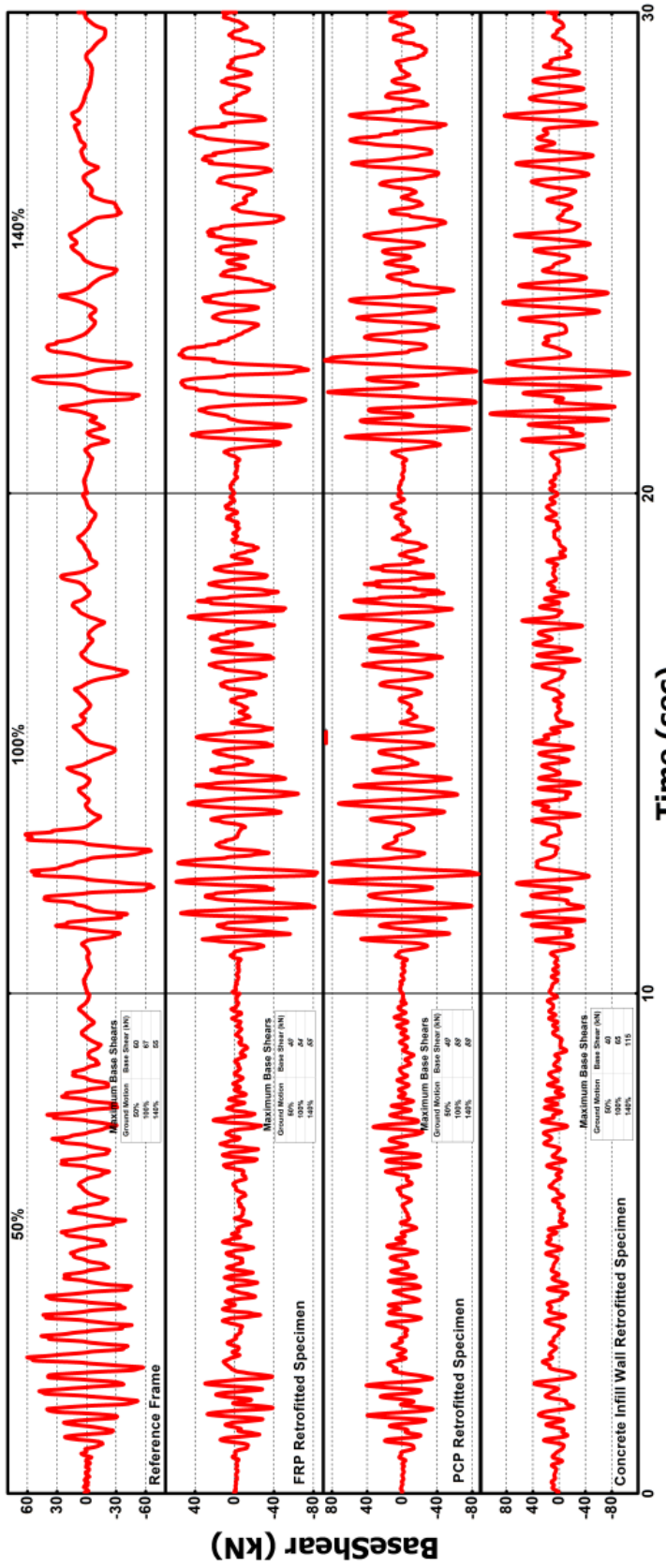

Figure 9.5 Base shear time histories of all specimens

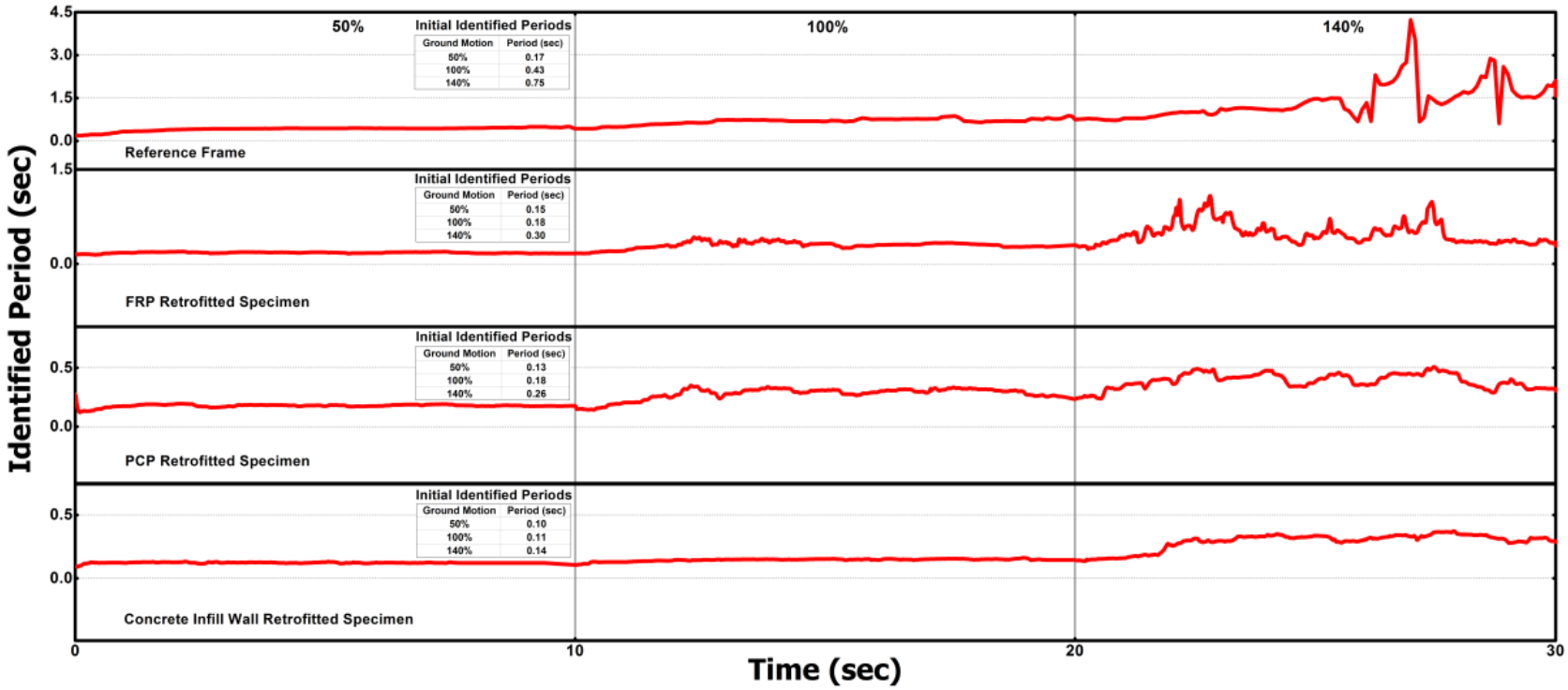

Figure 9.6 Initial Period Time Histories of All Specimens

CHAPTER 10

CONCLUSION

10.1. GENERAL

A total of four ½ scaled, three-bay and two story concrete frames were tested by employing pseudo-dynamic testing. The frames had the common deficiencies observed in building stock in Turkey. One of the test frames was used as reference specimen and no strengthening scheme was employed. Three different retrofitting methods were utilized in the other three specimens. Two of these were non-invasive and occupant friendly retrofit schemes suggested in the Turkish Earthquake Code, namely use of Fiber Reinforced Polymers (FRPs) and precast concrete panels integrated on the HCT infills and the last one was adding of reinforced concrete infill walls.

10.2. CONCLUSIONS

- The three level scale Duzce ground motions (50%, 100% and 140%), resulted in approximately minimum damage, moderate damage, and severe damage states for all experimentally tested frames.
- The PCP and reinforced concrete infill wall application resulted in a reduced displacement ductility demand. FRP retrofitted specimen on the other hand was more beneficial in terms of keeping the wall intact and dissipating the energy through a rocking mechanism.
- Infill wall contribution to the lateral strength was about 65%. Upon failure of the infill wall at about 1% overall and 2% interstory drift ratio, formation of a first story was observed at Reference Frame. Severe strength degradation and out of plane collapse susceptibility of the HCT infills along

with significant damage on the interior columns at the end of tests indicate the role of infills on deciding the final state of the structure.

- FRP retrofitted specimen exhibited strength degradation as a result of anchor slip which indicates the importance of anchors in a FRP strengthening application.

- Capacity of the PCP retrofitted specimen was obtained soon after significant diagonal cracking was observed at the lower third of the specimen. PCP retrofitted specimen was observed to withstand a displacement ductility demand of 5 without any significant strength drop. Hence, it is believed it can safely be employed limiting the inter-story drift demands.

- Reinforced concrete infill wall retrofitted specimen had increased stiffness. This retrofit scheme showed increased lateral forces than other retrofitted specimens with a displacement ductility demand of 4.

- Identified period variations showed that sudden pulses in the period-time curves were good indicators of physical damage. Among all frames, the one with reinforced concrete infill wall retrofit exhibited the most stable period variation due to better control of drift deformations and maintenance of lateral strength.

- The highest floor acceleration was observed in the reference frame for low level ground motion demand. On the other hand floor acceleration demands at 100% and 140% Duzce ground motions were similar for all specimens. Hence retrofitting of the specimens did not amplify the floor accelerations offering a serviceable structure.

REFERENCES

Akin E., Ozcebe G. and Ersoy U. (2009). "Strengthening of Brick Infilled Reinforced Concrete (RC) Frames with Carbon Fiber Reinforced Polymers (CFRP) Sheets" Seismic Risk Assessment and Retrofitting with special emphasis on existing low rise structures, edited by Ilki A., Karadogan F., Pala S. and Yuksel E, Springer Netherlands, pp. 367-386.

Aktan H.M. (1986). "Pseudo-dynamic testing of structures.", Journal of Engineering Mechanics, Vol. 112, pp. 183-190.

Albert, M. L., Elwi, A. E., and Cheng, J. J. (2001). "Strengthening of unreinforced masonry walls using FRPs." J. Compos. Constr., 5(2), 76–84.

Altin, S., Ersoy U., Tankut T. (1992). "Hysteretic Response of Reinforced Concrete Infill Walls", ASCE, Journal of Structural Engineering, Vol 118, No. 8, pp. 2133-2150

Aoyama, H., Kate, D., Katsurnata, H., Hosokawa, Y. (1984). "Strength and Behavior of Postcast Shear Walls for Strengthening of Existing Reinforced Concrete Buildings" List of Manuscripts Submitted to Eighth WCEE in San Francisco 7/1984, Aoyama Laboratory, Department of Architecture, University of Tokyo, Hongo, Bunkyo-ku, Tokyo 113, Japan.

Baran, M. (2005). "Precast Concrete Panel Reinforced Infill Walls for Seismic Strengthening of Reinforced Concrete Framed Structures", A Doctor of Philosophy Thesis in Civil Engineering, Middle East Technical University, Ankara, Turkey.

Binici B., Ozcebe G. and Ozcelik R. (2007). "Analysis and design of FRP composites for seismic retrofit of infill walls in reinforced concrete frames", Composites Part B: Eng 38 (5–6), 575–583.

Biskinis, D. and Fardis, M. N. (2009). "Upgrading of Resistance and Cyclic Deformation Capacity of Deficient Concrete Columns." *Seismic Risk Assessment and Retrofitting* edite by Ilki A., Karadogan F., Pala S. and Yuksel E., Springer Netherland, pp. 307-328.

Bursi,O.S., Shing, P.B. (1996). "Evaluation of Some Implicit Time-Stepping Algorithms for Pseudodynamic Tests", Earthquake Engineering and Structural Dynamics, Vol. 25, pp. 333-355.

Canbay E., Ersoy U., Tankut T. (2004). " A Three-Component Force Transducer for RC Structural Testing." Engineering Structures, 26, pp. 257-265.

Canbay, E., Ersoy, U., and Ozcebe, G. (2003), Contribution of RC infills to the seismic behavior of structural systems, ACI STRUCTURAL JOURNAL 100 (5), pp. 637–643.

Chang, S. (2002). "Explicit Pseudodynamic Algorithm with Unconditional Stability", Journal of Engineering Mechanics, ASCE, Vol. 128, No. 9, pp. 935-947.

Darby, A.P., Blakeborough, A., Williams, M.S. (1999). "Real-Time Substructure Tests Using Hydraulic Actuator", Journal of Engineering Mechanics, ASCE, Vol. 125, No. 10, pp. 1133-1139.

Di Ludovico M., Prota A., Manfredi G. and Cosenza E. (2008). "Seismic Strengthening of an Under- Designed RC Structure with FRP" Earthquake Engineering and Structural Dynamics, 37, 141-162.

Ehsani, M. R., Saadatmanesh, H., and Velazquez-Dimas, J. I. (1999). "Behavior of retrofitted URM walls under simulated earthquake loading." J. Compos. Constr., 3(3), 134–142.

Erdem, I., Akyuz, U., Ersoy, U. and Ozcebe, U. (2003). "A Comparative Study on the Strengthening of Frames" Seismic Assessment and Rehabilitation of Existing Buildings, edited by Wasti S.T., Ozcebe G., pp. 305-334.

Frosch R, Li W, Jirsa J and Kreger M. (1996). "Retrofit of non-ductile moment-resisting frames using precast infill wall panels." Earthquake Spectra (12), 741-760.

Frosch, R.J., Jirsa, J. O., Kreger, M. E. (2003) "Experimental Response of a Precast Infill Wall System", Seismic Assessment and Rehabilitation of Existing Buildings Edited by Wasti S.T. and Ozcebe G., Vol. 29, pp.383- 406.

Hamilton III, H. R., Holberg, A., Caspersen, J., and Dolan, C. W. (1999)."Strengthening concrete masonry with fiber reinforced polymers."4th Int. Symp. on Fiber Reinforced Polymer (FRP) for Reinforced Concrete Structures, ACI SP-188, Baltimore, 1103–1115.

Jirsa, J.O. and Kreger, M. (1989). "Recent Research on Repair and Strengthening of Reinforced Concrete Structures," Proceedings, ASCE Structures Congress, Vol. 1.

Julio, E. N. B. S., and Branco, F.A.B., and Silva, V. D. (2005). "Reinforced concrete jacketing interface influence on monotonic loading response." *ACI Struct. J.,* 102(2), 252-257.

Kalkan, E. and Gulkan, P. (2004). "Site-dependent spectra derived from ground motions records in Turkey, Earthquake Spectra, 20(4), 1111-1138.

Laursen, P. T., Seible, F., Hegermier, G. A., and Innamorato, D. (1995). "Seismic retrofit and repair of masonry walls with carbon overlays." Non-metallica (FRP) Reinforcement for Concrete Structures, Rilem.

Mahin, S.A., Shing, P.B. (1985). "Pseudodynamic Method for Seismic Testing", Journal of the Structural Engineering, ASCE, Vol. 111, No. 7 , pp. 1482-1503.

Mahin, S.A., Shing, P.B., Thewalt, C.R. Sz Hanson, R.D. (1989). "Pseudodynamic test method: current status and future directions." J. Struct. Engng115, pp. 2113-2128.

Miller J.T., Reaveley L.D. (1996). "Historic hotel Utah remodel and seismic upgrade." Seismic Rehabilitation of Concrete Structures, edited by Sabnis G.M., Shroff A.C., Khan, L.F.,SP-160, American Concrete Institute, Farmington Hills, MI, pp. 115–145.

Molina F. J., P. Pegon and G. Verzeletti (1999). "Time-domain identification from seismic pseudodynamic test results on civil engineering specimens." 2nd International Conference on Identification in Engineering Systems, University of Wales, Swansea.

Nakashima, M. (1985a). "Part 1: Relationship between Integration Time Interval and Response Stability in Pseudo Dynamic Testing", Journal of Structural and Construction Engineering, Transactions of AIJ, No. 353, pp. 29-34.

Nakashima, M. (1985b). "Part 2: Relationship between Integration Time Interval and Accuracy of Displacement, Velocity, and Acceleration Responses in Pseudo Dynamic Testing", Journal of Structural and Construction Engineering, Transactions of AIJ, No. 358, pp. 35-40.

Nakashima, M., Kaminosono, T., Ishida, M, Ando, K. (1990). "Integration Techniques for Substructure Pseudo Dynamic Test", 4th US National Conference on Earthquake Engineering, Palm Springs CA.

Nakashima, M., Kato, H., Takaoka, E. (1992). "Development of Real-Time Pseudo Dynamic Testing", Earthquake Engineering and Structural Dynamics, Vol. 21, pp. 79-92.

Ozcan O., Binici B. and Ozcebe G. (2008). "Improving seismic performance of deficient reinforced concrete columns with carbon fiber-reinforced polymers.", *Eng Struct* 30 (6), pp. 1632–1646.

Ozcebe G., Ersoy U., Tankut T., Erduran E., Keskin R.S., Mertol H.C. (2003). "Strengthening of brick-infilled RC frames with CFRP." TUBITAK 536, Structural Engineering Research Unit Report, No. 2003-01; p. 67.

Pantelides, C. P., Gergely, J., Reaveley, L. D., and Volnyy, V. A. (1999). "Retrofit of RC bridge pier with CFRP advanced composites." *J. Struct. Eng.,* 125(10), 1094-1099.

Peek, R., Yi, W. H. (1990). "Error Analysis for Pseudodynamic Test Method. I: Analysis", Journal of Engineering Mechanics, Vol. 116, No. 7, pp. 1618-1637.

Schwegler, G. (1995). "Masonry construction strengthened with fiber composites in seismically endangered zones." 10th European Conference on Earth Engineering, pp. 2299-2303.

Shan, B., Xiao, Y., and Guo,Y. (2006). "Residual performance of FRP-retrofitted RC columns after being subjected to cyclic loading damage." /. *Compos. Constr.,* 10(4), 304-312.

Shing, P. B., Mahin, S. A. (1987). "Cumulative Experimental Errors in Pseudodynamic Tests", Earthquake Engineering and Structural Dynamics, Vol. 15, pp. 409-424.

Shing, P. B., Vannan, M.T. (1991). "Implicit Time Integration for Pseudodynamic Tests: Convergence and Energy Dissipation", Earthquake Engineering and Structural Dynamics, Vol. 20, pp. 809-819.

Sonuvar, M. O., Ozcebe, G. and Ersoy U. (2004). "Rehabilitation of Reinforced Concrete Frames with Reinforced Concrete Infills", ACI, Struct J 101 (4), pp. 494-500.

Takanashi k., Udagawa K., Seki M., Okada T. and Tanaka H. (1975). "Nonlinear earthquake response analysis of structures by a computer-actuator on-line system." Bull. Earthquake resist. Struct. Res. Center, Tokyo, Japan.

Tankut, T., Ersoy, U., Ozcebe, G., Baran, M. and Okuyucu, D. (2005)."In Service Seismic Strengthening of RC Framed Structures" Seismic Assessment and Rehabilitation of Existing Buildings, International Closing Workshop, NATO Project SfP 977231,Istanbul, Turkey.

Tumialan, J. G. (2001). "Strengthening of masonry structures with FRP composites." Doctoral dissertation, Univ. of Missouri-Rolla, Rolla, Mo.

Turk, A. M. (1998). "Rehabilitation of Reinforced Reinforced concrete infill walls", A Doctor of Philosophy Thesis in Civil Engineering, Bogazici University, Istanbul, Turkey.

Elkhoraibi, T., and Mosalam K.M., 2007. "Towards error-free hybrid simulation using mixed variables." *Earthquake Engineering & Structural Dynamics*, 36(11), 1497-1522.

Bertero, V.V., Aktan, A.E., Charney, F.A: and Sause, R. (1984). "Earthquake simulation tests and associated studies of a 1/5th-scale model of a 7-story R/C frame-wall test structure." Report No. UCB/EERC-84/05, University of California, Berkeley, 180p.

APPENDIX A

IDENTIFICATION OF DYNAMIC PARAMETERS

Time dependent dynamic properties, namely period and equivalent viscous damping, of the test frames are determined according to the procedure proposed by Molina et. al. (1999). Accordingly, at any time step, *T*, measured restoring force $r(n)$, can be expressed as:

$$\begin{bmatrix} \mathbf{u}^T(n) & \mathbf{v}^T(n) & \mathbf{1} \end{bmatrix} \cdot \begin{bmatrix} \mathbf{K}^T \\ \mathbf{C}^T \\ \mathbf{o}^T \end{bmatrix} = \mathbf{r}^T(n) \qquad (1)$$

Where K and C are the 2x2 secant stiffness and damping matrices, u and v are the displacement and velocities at floor levels, and o is an equilibrium constant. It can easily be shown that Equation 1 can be solved for K and C using the data obtained at N time intervals as long as $N > 2 \cdot ndof + 1$. By selecting a time window containing steps not less than N, least square solutions is obtained for K and C. Following, Maisa and Silva (1997), one can then extract the frequency and damping coefficient from:

$$s\begin{bmatrix} \mathbf{C} & \mathbf{M} \\ \mathbf{M} & 0 \end{bmatrix}\mathbf{v} + \begin{bmatrix} \mathbf{K} & \mathbf{0} \\ \mathbf{0} & -\mathbf{M} \end{bmatrix}\mathbf{v} = \mathbf{0} \qquad (2)$$

where $s_i, s_i^* = \omega_i(\varsigma_i \pm j\sqrt{1-\varsigma_i^2})$ $\qquad j^2=-1$ $\qquad (3)$

In Equation 3, ω_i is the natural frequency and ζ_i is the equivalent damping ratio (or simply damping ratio) at i^{th} mode.